

R. V. COLLEGE OF ENGINEERING, BENGALURU - 560059

(Autonomous Institution Affiliated to VTU, Belagavi)



A Project Report On

**DESIGN, FABRICATION AND TESTING OF TWIN
VERTICAL AXIS WIND TURBINES**

Submitted by

ADITYA S N

PANEENDRA BHAT P

PRATIK V NAYAK

1RV11ME009

1RV11ME072

1RV11ME078

Under the Guidance of

M S Krupashankara

Professor

Dept. of Mechanical Engineering

R.V. College of Engineering

Bengaluru – 560059

In partial fulfillment for the award of degree

of

Bachelor of Engineering

in

MECHANICAL ENGINEERING

2015

This project was sponsored by Karnataka State Council for Science and Technology (KSCST),

Indian Institute of Science Campus, Bengaluru - 560012



R. V. COLLEGE OF ENGINEERING, BENGALURU 560059

(Autonomous Institution Affiliated to VTU, Belagavi)

DEPARTMENT OF MECHANICAL ENGINEERING



CERTIFICATE

Certified that the project work titled “**DESIGN, FABRICATION AND TESTING OF TWIN VERTICAL AXIS WIND TURBINES**”, is a work carried out by **Aditya S N (1RV11ME009)**, **Paneendra Bhat P (1RV11ME072)**, **Pratik V Nayak (1RV11ME078)** who are the bonafide students of R.V. College of Engineering, Bengaluru, in partial fulfillment for the award of degree of **Bachelor of Engineering in Mechanical Engineering** of Visvesvaraya Technological University, Belagavi during the year **2014-2015**. It is certified that all corrections/ suggestions indicated for the internal assessment have been incorporated in the report deposited in the departmental library. The project report has been approved as it satisfies the academic requirements in respect of project work prescribed by the institution for the said degree.

M S Krupashankara
Professor,
Dept. of Mechanical Engg.

Dr. R S Kulkarni
Professor and Head,
Dept. of Mechanical Engg.

Dr. B S Satyanarayana
Principal, R.V.C.E

External viva

Name of Examiners

Signature with date

1)

2)



Karnataka State Council for Science and Technology
Indian Institute of Science Campus, Bengaluru - 560 012

Telephone: 080-23341652, 23348848, 23348849 ♦ Telefax: 080-23348840
Email: office@kscst.iisc.ernet.in, office@kscst.org.in ♦ Website: www.kscst.iisc.ernet.in, www.kscst.org.in

Dr. S. G. Sreekanteswara Swamy
Fellow & Principal Investigator - SPP

12th March 2015

Ref: 7.1.03/SPP/1018

The Principal
RV College Of Engineering,
Mysore Road, R V Vidyanikethan Post,
Bengaluru - 560 059.



Dear Sir,

Sub : Sanction of Student Project - 38th Series: Year 2014-2015

Your Project Proposal Reference No. : **38S0899**

Ref : Your Project Proposal entitled "**LOW COST VERTICAL AXIS DUAL WIND TURBINES FOR REMOTE VILLAGES**"

I am happy to inform that your project proposal referred above, has been approved by the Secretary, KSCST for "Student Project Programme - 38th Series" and has been sanctioned with a budgetary break-up as detailed below:

Student / s	Mr. Paneendra Bhat P. and others	Budget	Amount (Rs)
		Materials/Consumables	7,000.00
Guide/s	Prof. Krupashankara M.S.	Labor	-
		Travel	-
Department	Mechanical Engineering	Miscellaneous	500.00
		Report	500.00
		TOTAL	8,000.00
Rupees	EIGHT THOUSAND	ZERO HUNDRED	

The following are the guidelines to carryout the project work :

- The project should be performed based on the objectives of the proposal sent by you.
- The project should be completed in all respects and one copy of the hardbound report along with softcopy of the full report in a CD (.pdf format) should be submitted to KSCST.
- Any change in the project title and objectives, etc., or students is liable to rejection of the project and the amount sanctioned needs to be returned to KSCST.
- Please quote your **project sanction reference number printed above** in all your future correspondences.
- Important:** After completing the project, 2 to 3 page write-up (synopsis) needs to be sent by e-mail [spp@kscst.iisc.ernet.in] and should include following :

- Title of the project
- Name of the College & Department
- Name of the students & Guide(s)
- Keywords

To,
RV M.S.
RV College of Engineering
26/3/15

38S0899

- 5) Introduction / background
(with specific reference to the project, work done earlier, etc) - about 20 lines
- 6) Objectives (about 10 lines)
- 7) Methodology (about 20 lines)
(materials, methods, details of work carried out, including drawings, diagrams etc)
- 8) Results and Conclusions
(about 20 lines with specific reference to work carried out)
- 9) Scope for future work (about 20 lines).

(Note: The write-up (Synopsis) should be sent with the approval of project guide. The softcopy of the write-up, in MS Word format, should be sent by e-mail (spp@kscst.iisc.ernet.in). In your e-mail, please also include project proposal reference number and title of the project.)

e) Projects selected for Seminar / Exhibition will be awarded.

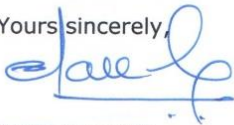
The sanctioned amount will be sent separately by our Accounts Department.

The sponsored projects evaluation will be held in the Nodal Centre and the details of the nodal centre will be intimated shortly.

Please visit our website for further announcements / information and for any clarifications please email to spp@kscst.iisc.ernet.in

Thanking you and with best regards,

Yours sincerely,



(SGS Swamy)

Copy to:

- 1) The Head of the Department of
Mechanical Engineering
Rv College Of Engineering,
Mysore Road, R V Vidyanikethan Post,
Bengaluru - 560 059.
- 2) Prof. Krupashankara M.S.
Department of Mechanical Engineering
Rv College Of Engineering,
Mysore Road, R V Vidyanikethan Post,
Bengaluru - 560 059.
- 3) The Finance Officer, KSCST, Bangalore

DECLARATION

We, **Aditya S N (1RV11ME009), Paneendra Bhat P (1RV11ME072) and Pratik V Nayak (1RV11ME078)**, the students of Eighth Semester B.E, **Mechanical Engineering, R.V. College of Engineering, Bengaluru** hereby declare that the project titled “**DESIGN, FABRICATION AND TESTING OF TWIN VERTICAL AXIS WIND TURBINES**” has been carried out by us and submitted in the partial fulfilment for the award of degree of Bachelor of Engineering in Mechanical Engineering. We do declare that this work has not been carried out by any other students for the award of degree in any other branch.

Place: Bengaluru

1) ADITYA S N

Date:

2) PANEENDRA BHAT P

3) PRATIK V NAYAK

ACKNOWLEDGEMENT

We take this opportunity to express our gratitude to the people who have been instrumental in the successful completion of this project. Apart from our efforts, the success of this project depends largely on the encouragement and guidelines of many others.

We are highly indebted to our project guide, **M S Krupashankara, Professor, Dept. of Mechanical Engineering, RVCE, Bengaluru** for his guidance and constant supervision as well as for providing necessary information regarding the project & also for his support in completing the project. We would also like to acknowledge the guidance and valuable suggestions received from **C S Prasad, Assistant Professor, Dept. of Mechanical Engineering, RVCE, Bengaluru.**

We are also grateful to **Dr. R S Kulkarni, Professor and Head, Mechanical Engineering Department, RVCE, Bengaluru** for the help he has provided.

We would like to express our special gratitude to **Dr. B S Satyanarayana, Principal, RVCE, Bengaluru** for providing this opportunity.

We like to thank **V Chayapathi**, Professor, Electrical and Electronics Engineering for his useful contribution to the project. We would like to express our gratitude towards all the faculty and staff at the **workshop of Mechanical Engineering Department, RVCE, Bengaluru** for their kind co-operation and encouragement which helped in completion of this project.

We would also like to thank **Karnataka State Council for Science and Technology (KSCST)** for partially funding the project and their encouragement.

Our thanks and appreciations also go to our **colleagues** in developing the project and our **parents, relatives, friends** who have willingly helped us in this endeavor.

ABSTRACT

It is estimated that the energy demand in India will reach 1640 billion units in 2020. Currently, 70% of India's energy needs are fulfilled through nonrenewable sources of energy which are rapidly depleting. Wind energy is one source of renewable energy, which can be harnessed through wind turbines. Vertical axis wind turbines offer a better alternative than horizontal axis wind turbines as they operate at low wind speeds and are ideally suited for rural areas where grid power is unavailable. A comprehensive literature review revealed that research efforts are primarily focused on improving the efficiency of Savonius type wind turbines which has self-starting characteristics. However, limited efforts have been made on aerodynamic coupling between two Savonius turbines. The objective of this work was to model twin Savonius wind turbines, working in tandem and placed in an array which can be installed in remote villages.

Simulations were performed on a Savonius turbine for different blade profiles, two and three bladed configurations, and for an array with two and three turbines using ANSYS Fluent 14.5. Five design variables namely the tip speed ratio, overlap ratio, rotor angle offset, angle between turbines and distance between turbines, were chosen and simulations were conducted using orthogonal array method to optimize the power coefficient (C_p). A regression relation was obtained using Minitab based on the simulation results.

The simulations showed that the circular blade profile had the highest dynamic torque coefficient of 0.19 compared to the other profiles. Also, the two bladed configuration had higher C_p of 0.251 than the three bladed configuration which had a C_p of 0.157. The array simulations also showed that the two turbine array was 12% more efficient than the three turbine configuration. Further, the twin turbine configuration yielded a higher C_p of 0.281 in comparison with an isolated turbine C_p of 0.251. Based on the simulation results, the turbine in the array was designed having a length of 720 mm and a diameter of 280 mm. Detailed fabrication drawings were prepared and the system was fabricated. The test results showed that each turbine of the array yielded more power than if operated in isolation.

TABLE OF CONTENTS

CERTIFICATE.....	I
KSCST SANCTION LETTER.....	II
DECLARATION.....	IV
ACKNOWLEDGEMENT.....	V
ABSTRACT.....	VI
TABLE OF CONTENTS.....	VII
LIST OF TABLES.....	XI
LIST OF FIGURES.....	XII
LIST OF SYMBOLS AND ABBREVIATIONS.....	XIV

CHAPTER 1

INTRODUCTION.....	1
1.1 Overview of the energy scenario in India.....	1
1.1.1 Non-renewable sources.....	2
1.1.2 Renewable sources.....	3
1.2 Wind energy.....	4
1.3 Wind turbines.....	6
1.3.1 Horizontal axis wind turbines.....	6
1.3.2 Vertical axis wind turbines.....	8
1.4 Savonius wind turbines.....	9
1.5 Societal relevance of the project.....	10
1.6 Literature review.....	11
1.6.1 Review on vertical axis wind turbine performance.....	11
1.6.2 Review on CFD and simulation studies on VAWTs.....	13
1.6.3 Review on vertical axis wind turbine arrays.....	15
1.6.4 Review on design of experiments and optimization techniques.....	15
1.6.5 Literature gap.....	16

1.7 Objectives	16
1.8 Methodology of the project.....	16
1.9 Organization of the report.....	17
1.10 Summary.....	18

CHAPTER 2

WIND ENERGY AND SAVONIUS WIND TURBINES.....19

2.1 Harnessing wind energy.....	19
2.2 Betz limit.....	19
2.3 Principle of working of Savonius turbine.....	20
2.4 Factors affecting power generation.....	21
2.4.1 Solidity.....	21
2.4.2 Tip speed ratio.....	21
2.4.3 Wind speed.....	22
2.4.4 Overlap ratio.....	22
2.4.5 Aspect ratio.....	23
2.5 Computational fluid dynamics.....	23
2.6 Design of experiments.....	26
2.6.1 Orthogonal arrays.....	26
2.6.2 Regression analysis.....	27
2.7 Summary.....	28

CHAPTER 3

MODELLING AND SIMULATION OF SAVONIUS WIND TURBINES.....29

3.1 Modelling of Savonius VAWT.....	29
3.1.1 Blade profile.....	29
3.1.2 Number of blades.....	30
3.1.3 Number of turbines.....	31

3.2 Simulation studies on single Savonius turbine.....	31
3.2.1 Computational domain and boundary conditions.....	32
3.2.2 Meshing.....	33
3.2.3 Setup.....	35
3.3 Comparison of power output.....	36
3.3.1 Blade profile	36
3.3.2 Number of blades.....	38
3.3.3 Turbine arrays.....	40
3.4 Modelling of twin-vertical axis wind turbines.....	46
3.4.1 Rotor angle offset.....	47
3.4.2 Angle between turbines.....	47
3.4.3 Distance between turbines.....	48
3.4.4 Tip Speed Ratio (TSR).....	48
3.4.5 Overlap ratio.....	49
3.5 Orthogonal array testing.....	49
3.6 Summary.....	51

CHAPTER 4

DESIGN AND FABRICATION OF THE TWIN VERTICAL AXIS WIND TURBINE SETUP.....	52
4.1 Turbine dimensioning	52
4.2 Assembly.....	52
4.2.1 Turbine blades.....	54
4.2.2 End plates.....	55
4.2.3 Flanges.....	55
4.2.4 Shafts.....	56
4.2.5 Gears.....	57
4.2.6 Supporting plates.....	57
4.2.7 Supporting rods.....	58

4.3 Assembly for preliminary testing.....	58
4.4 Description of the test rig.....	58
4.4.1 Axial fan.....	58
4.4.2 Loading conditions.....	59
4.4.3 Generator specifications.....	60
4.5 Cost analysis.....	61
4.6 Summary.....	61
CHAPTER 5	
RESULTS AND DISCUSSIONS.....	62
5.1 Simulation studies on single Savonius turbine.....	62
5.2 Simulation studies on Twin Vertical Axis Wind Turbines.....	64
5.3 Nonlinear regression analysis.....	65
5.3.1 Validation of the regression equation.....	66
5.4 Wind mapping.....	67
5.5 Testing of the setup.....	70
5.5.1 Measurement of the power output	70
5.6 Summary.....	71
CHAPTER 6	
CONCLUSIONS AND SCOPE FOR FUTURE WORK	72
6.1 Conclusions.....	72
6.2 Future scope of work.....	72
REFERENCES.....	73
APPENDIX.....	77

LIST OF TABLES

Table number	Title	Page number
1.1	Power generation capacity from various sources in India	2
2.1	L ₄ orthogonal array	26
3.1	Boundary conditions adopted for the simulations	33
3.2	Coefficient of torque for different blade profiles	36
3.3	Power coefficient at various tip speed ratios for two and three bladed turbine	39
3.4	Comparison of advancing inside and advancing outside turbines	42
3.5	Coefficient of power for the three turbine array	45
3.6	Optimal array settings for harnessing power from Savonius turbine	46
3.7	Parameter variables and their levels	49
3.8	L ₁₈ orthogonal array experiments	50
3.9	Results from the orthogonal array experiments	51
4.1	Axial fan specifications	59
4.2	Electrical loading components	59
4.3	Generator specifications	60
4.4	Cost analysis	61
5.1	Results from the orthogonal array experiments	64
5.2	Error comparison of quadratic and cubic regression models	66
5.3	Variables for regression equation validation	67
5.4	Regression equation validation	67
5.5	Wind mapping results	68
5.6	Mean standard deviation for various positions of the fluid flow domain	69
5.7	Measurement of power output from twin turbine system	70
5.8	Measurement of power output from single turbine (left)	70
5.9	Measurement of power output from single turbine (right)	71

LIST OF FIGURES

Figure number	Title	Page number
1.1	Comparison of Human Development Index with percapita electricity use	1
1.2	Non-renewable energy utilization in India	3
1.3	India's growth in renewable energy installed capacity	3
1.4	Renewable energy utilisation in India	4
1.5	Wind power density map of India	5
1.6	Year-wise installations of wind power capacity in India	6
1.7	Horizontal axis wind turbine	7
1.8	Vertical axis wind turbine	8
1.9	CAD models of a Savonius turbine	10
2.1	Power delivered by a wind flow through a cylinder	19
2.2	Relationship between C_p and Tip Speed Ratio for HAWT	21
2.3	Overlap ratio of a Savonius rotor	22
3.1 (a)	Triangular profile	29
3.1 (b)	Bach profile	30
3.1 (c)	Semicircular profile	30
3.2 (a)	Two bladed configuration	30
3.2 (b)	Three bladed configuration	30
3.3 (a)	Two turbine array	31
3.3 (b)	Three turbine array	31
3.4	Computational fluid domain	33
3.5	Meshing on a two bladed turbine	34
3.6	Inflation layer	35
3.7	Savonius turbine in a flow field	37
3.8	Flow impingement in a Savonius turbine	37
3.9	Two bladed configuration	38
3.10	Three bladed configuration	38
3.11	Comparison of coefficient of torque between three bladed and two bladed configuration of vertical axis wind turbine	39
3.12	Comparison of coefficient of power of two bladed and three bladed turbine at different TSRs	40
3.13	Fluid flow domain	41
3.14	Coefficient of power vs. Tip Speed Ratio for different configurations	43
3.15	Coefficient of torque vs. Tip Speed Ratio for different configurations	43

3.16	Advancing outside velocity contours	43
3.17	Advancing inside velocity contours	44
3.18	Three turbine array	45
3.19	Coefficient of power vs. Tip Speed Ratio for three turbine array	45
3.20	Coefficient of power vs. Tip Speed Ratio for two and three turbine arrays	46
3.21	Rotor angle offset	47
3.22	Angle between turbines	48
3.23	Distance between turbines	48
4.1 (a)	Front view of the T-VAWT setup	52
4.1 (b)	Isometric view of the T-VAWT	52
4.2	Twin Vertical Axis Wind Turbine (T-VAWT) assembly	54
4.3	Blade profile and end plates	55
4.4	Flanges	55
4.5	Shafts used in the assembly	56
4.6	The gearing arrangement of the assembly	57
4.7	Preliminary testing	58
4.8	Axial fan	59
4.9	Schematic and the fabricated loading circuit	60
5.1	Comparison of coefficient of power of three bladed and two bladed turbine at different tip speed ratios	62
5.2	Velocity vectors near the overlap of the two blades	63
5.3	Velocity vectors near the overlap of three blades	63
5.4	Geometry No. 3	65
5.5	Geometry No. 14	65
5.6	Wind mapping domain	68
5.7	Characteristic curve for twin turbine assembly and the single turbines	71

LIST OF SYMBOLS AND ABBREVIATIONS

Symbol/abbreviation	Description	Unit
P	Power generated by turbine	W
P_{wind}	Power available in the wind	W
ρ	Density of Air	$kg\ m^{-3}$
A	Projected area	m^2
V	Wind Velocity	$m\ s^{-1}$
\vec{P}	Pressure force vector	N
F_v	Viscous force vector	N
\vec{F}_a	Specified force vector	N
\vec{r}_{ab}	Moment arm vector	m
T	Torque generated by the turbine	$N\cdot m$
ω	Angular velocity of the turbine	$rad\ s^{-1}$
TSR	Tip Speed Ratio	-
X	Length of overlap	m
d	Diameter of turbine blade	m
H	Height of the turbine	m
D	Diameter of the turbine rotor	M
T_m	Mean torque generated by the turbine	$N\cdot m$
C_t	Coefficient of Torque	-
C_p	Coefficient of Power	-
N	Number of Blades	-
Φ	Azimuthal angle	<i>Degrees</i>
Θ	Rotor angle offset	<i>Degrees</i>
A	Angle between turbines	<i>Degrees</i>
Y	Distance between turbines	m
T_m	Mean torque	$N\cdot m$
<i>HDI</i>	Human Development Index	-
<i>GDP</i>	Gross Domestic Product	-
<i>C-WET</i>	Center for Wind Energy Technology	-
<i>MNRE</i>	Ministry of New and Renewable Energy	-
<i>NCEF</i>	National Clean Energy Fund	-
<i>HAWT</i>	Horizontal Axis Wind Turbine	-
<i>VAWT</i>	Vertical Axis Wind Turbine	-
<i>T-VAWT</i>	Twin Vertical Axis Wind Turbine	-
<i>CFD</i>	Computational Fluid Dynamics	-

INTRODUCTION

An overview of the current energy scenario in India has been provided in this chapter to emphasise the pressing need to switch to renewable sources of energy and wind energy is one such promising alternative. Different types of wind turbines which are used to harness wind energy has been introduced with a particular focus on vertical axis wind turbines. Detailed literature review and the objectives of the project are outlined as well.

1.1 Overview of the energy scenario in India

India is one of the largest economies in the world and the fourth largest consumer of energy after the USA, Russia and China [1]. The percapita consumption of energy is an index of development in a country and this can be seen in Figure 1.1 which shows the Human Development Index (HDI), calculated from the literacy rate, infant mortality rate and GDP plotted against per capita electricity consumption [2].

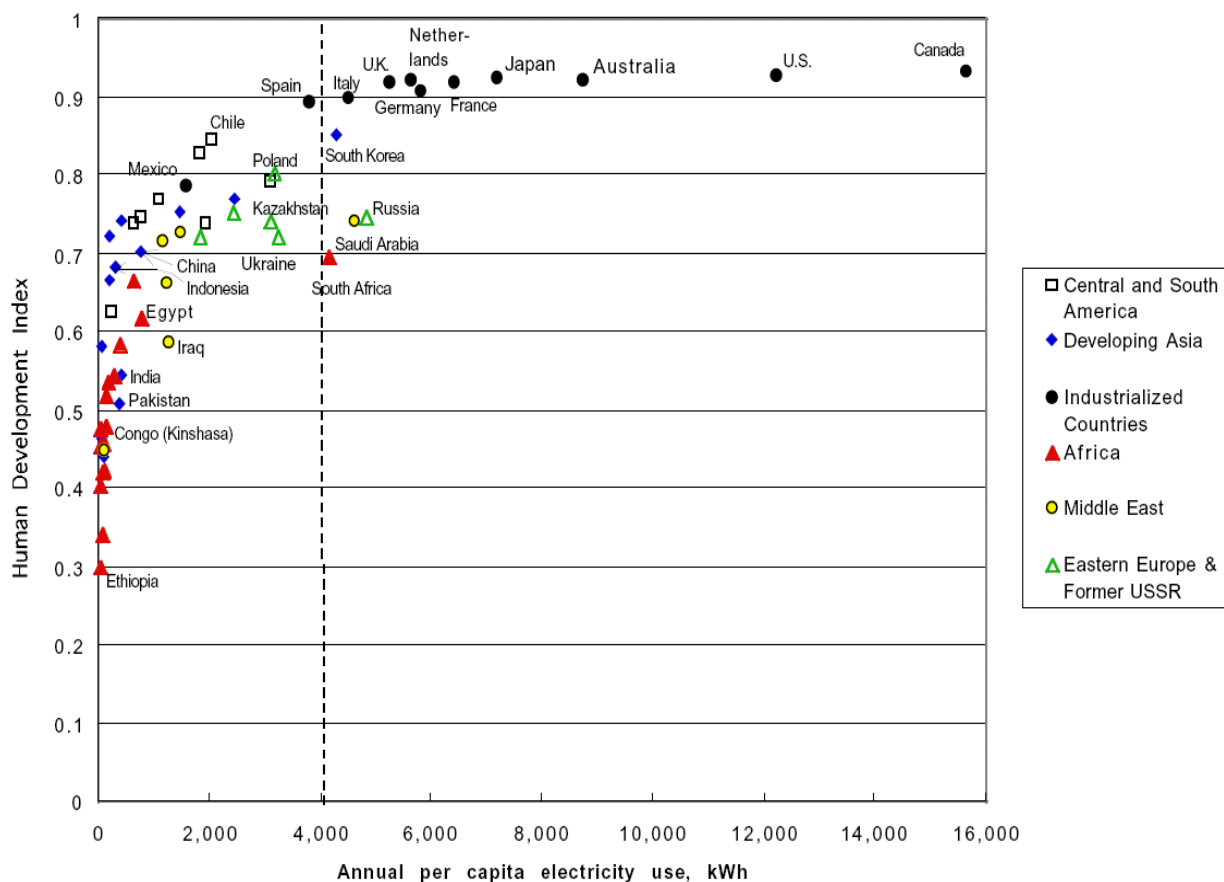


Fig. 1.1: Comparison of Human Development Index with percapita electricity use [2]

Rapid urbanisation and improved standard of living of the people will cause increase in energy demand. With Indian economy estimated to grow at 7.9% in 2015-16 and 8.2% in 2016-17, the demand is likely to grow significantly. It is estimated that the demand will reach 1640 billion units by 2020 compared to 918 billion units in 2012. The current total installed capacity in India is 260.54 GW as of 31/01/2015 [3] and the distribution among various power sectors is shown in Table 1.1.

Table 1.1: Power generation capacity from various sources in India [3]

Source		Capacity (MW)	Percentage
Thermal	Coal	156190.89	59.95
	Gas	22971.25	8.82
	Oil	1199.75	0.46
Renewable	Hydro	40867.43	15.68
	Wind	22465.03	8.62
	Solar	3062.68	1.18
	Small hydro	3990.83	1.53
	Bagasse	2648.40	1.02
	Biomass	1365.20	0.52
Nuclear		5780.00	2.22
TOTAL		260541.46	100

1.1.1 Non-renewable sources

India is relying heavily on non-renewable sources of energy like coal, natural gas and oil. Around 70% of India's energy needs are fulfilled through non-renewable sources. India has abundant supply of fossil fuels and have been exploited to produce energy. However, these non-renewable sources of energy will run out at the current rates of extraction and there is a dire need to explore renewable energy sources. The current non-renewable energy utilisation from various sources are shown in Figure 1.2

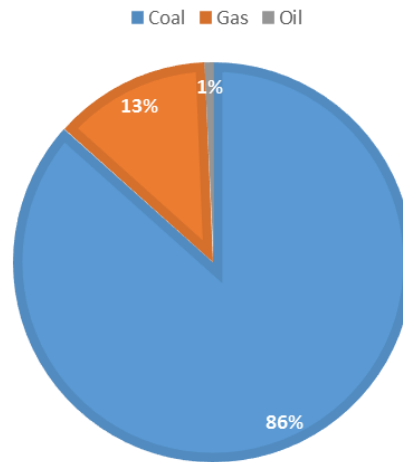


Fig. 1.2: Non-renewable energy utilisation in India [4]

1.1.2 Renewable sources

To sustain economic growth and to avoid depletion of fossil fuels, there is a need to utilise alternative sources of energy. Sustainable energy is the root of economic growth, climate stability and social equality. This need has led India to slowly adopt renewable sources and frame the required energy policies [5]. India's growth in renewable installed capacity is shown in Figure 1.3.

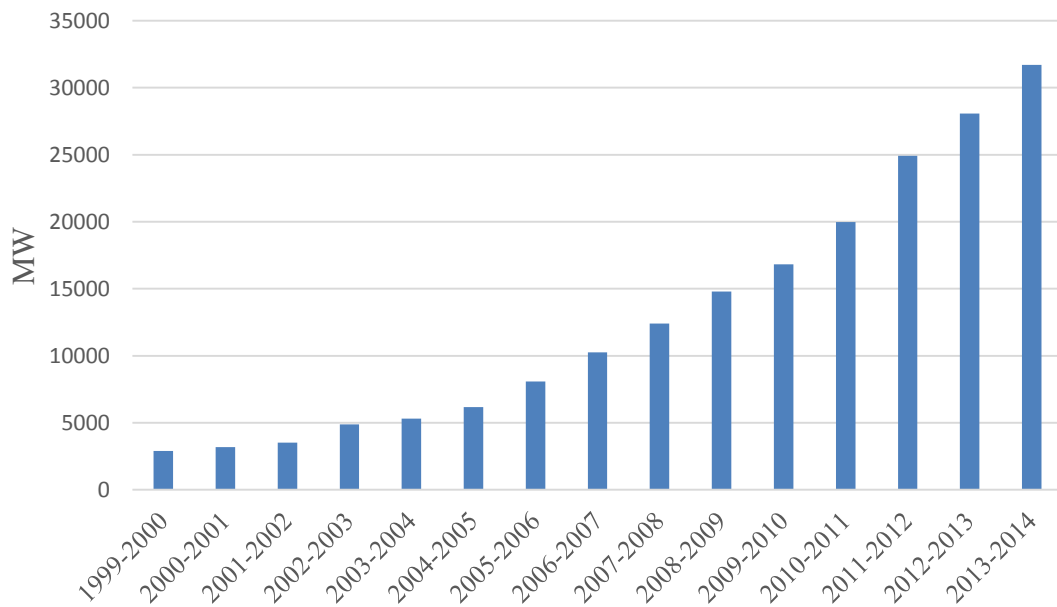


Fig. 1.3: India's growth in renewable energy installed capacity [4]

It is clear that India's progress towards maximum utilisation of renewable energy has been commendable. However, the country is lagging when compared to nations like

USA and China. With the prevailing threats of exhaustion of conventional sources of energy and global warming, it is essential to develop efficient renewable energy conversion systems. Existing systems are inefficient and expensive although recent research in this field has led to noticeable improvements. The current utilisation of various renewable energy sources have been depicted in Figure 1.4.

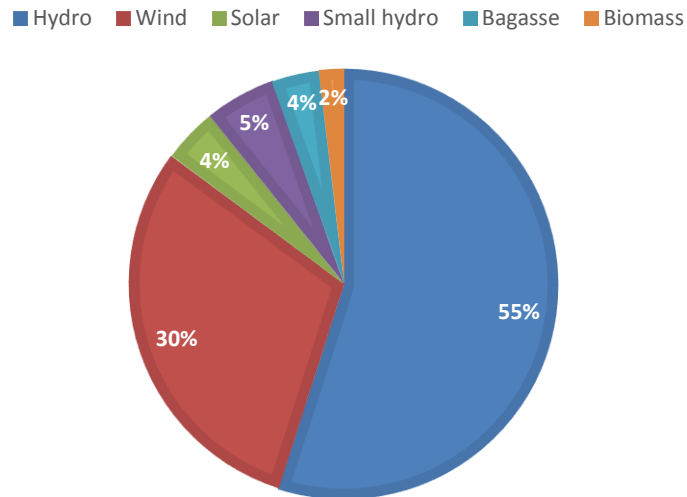


Fig. 1.4: Renewable energy utilisation in India [4]

1.2 Wind energy

One of the most promising alternative energy technologies of the future is harnessing wind energy. In India, the strong south-west monsoon (May-June), influences the wind. In October, cool dry air moves towards the ocean and during the period from November to March, wind speeds are relatively low in the country. Uniform strong winds are experienced by the Indian peninsula during the months of March-August. This is the wind scenario in the country and energy conversion devices are developed to harness the power in the wind.

The five main wind power countries are China, USA, Germany, Spain and India. 73% of the global wind capacity share is represented by these countries alone [6]. In India, as of today, 22465.03 MW of wind power has been harnessed through wind farms.

The Centre for Wind Energy Technology (C-WET) has launched Wind Resource Assessment (WRA) program in which 789 wind monitoring stations, including 87 new stations have been commissioned in 28 states and 3 Union Territories of India during the year 2012-13 [7]. The Ministry of New and Renewable Energy (MNRE) has also

taken up a new initiative for implementation of wind resource assessment in new areas with an aim to assess the realistic potential at 100 m level in 500 new stations across the country under the National Clean Energy Fund (NCEF) to be implemented through C-WET.

Tamil Nadu, Maharashtra, Gujarat, Rajasthan and Karnataka contribute 94% of total wind energy generated in the country [8]. These five states have been leaders in wind energy generation while other states like Madhya Pradesh, Rajasthan and Kerala are also increasing their capacity. Tamil Nadu has increased its capacity and shown commendable growth of 69% by upgrading the systems from 4304.5 MW in 2009 to 7275.6 MW in 2014.

Wind atlases are used to measure the on shore wind energy potential and the Indian wind atlas developed in association with RISO DTU, Denmark measures the onshore wind power potential to be 49,130 MW at a height of 50 m and 1,02,000 MW at 80 m height. Karnataka in particular has a potential of 8591 MW. Potential sites and power density at 50 m in India are shown in Figure 1.5

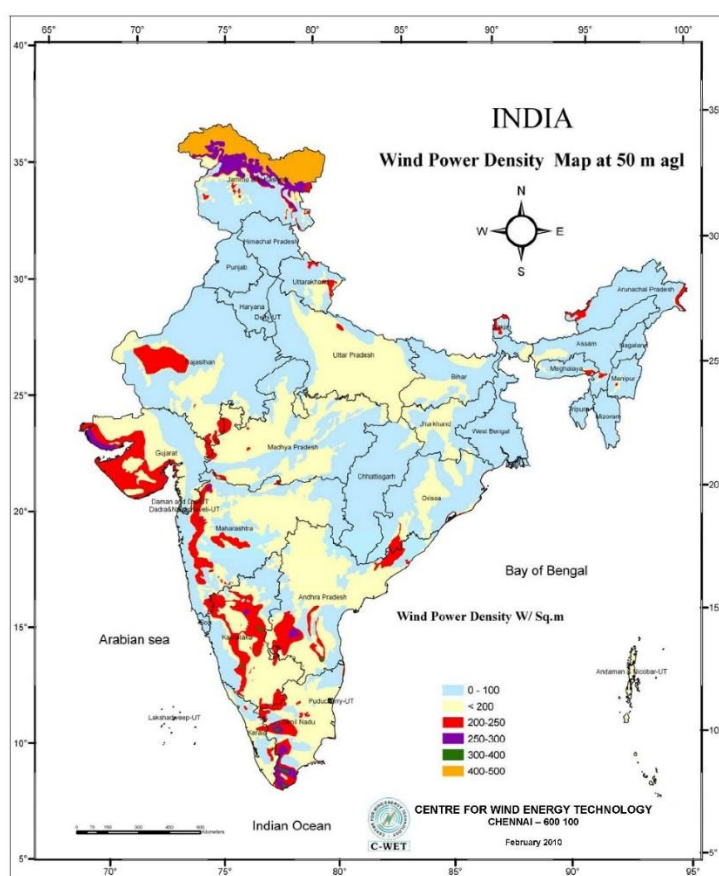


Fig. 1.5: Wind power density map of India [8]

Due to considerable advancements in wind energy research, wind power efficiency has largely increased. There have been rapid installations of wind farms over the years and the data is presented in Figure 1.6.

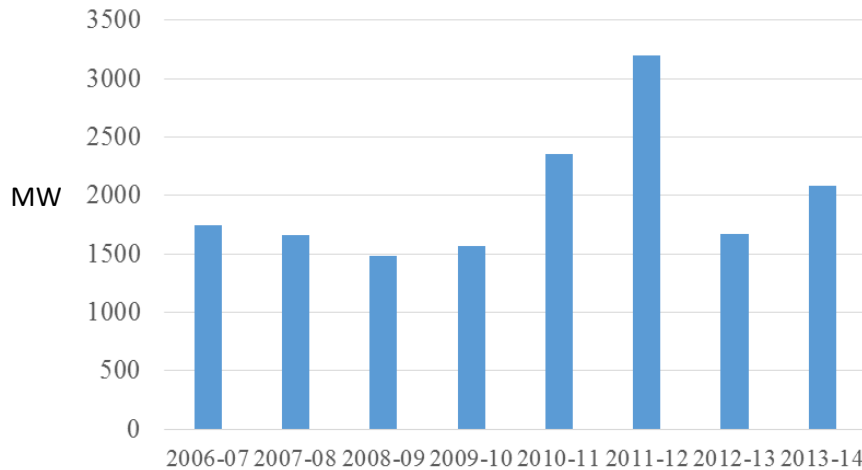


Fig. 1.6: Year-wise installation of wind power capacity (MW) in India [4]

1.3 Wind turbines

Wind turbines convert the kinetic energy in the wind into mechanical energy. While windmills utilise the mechanical energy produced, wind turbines convert this mechanical energy into electrical power.

Wind turbines are classified into two types: horizontal axis and vertical axis. A horizontal axis machine, shown in Figure 1.7, has its blades rotating on an axis parallel to the ground while a vertical axis machine, shown in Figure 1.8, has its blades rotating on an axis perpendicular to the ground. There are many available designs for both and each type has certain advantages and disadvantages.

1.3.1 Horizontal Axis Wind Turbines

The Horizontal Axis Wind Turbine (HAWT) has the axis of rotation of the blade parallel to the wind stream and the ground. Most HAWTs today are single bladed, two-bladed or three-bladed. The horizontal axis wind turbine works when wind passes over both surfaces of the airfoil shaped blade. From the basic principles of aerodynamics, the air passing over the top surface of the airfoil will have a higher velocity than the wind at the lower portion leading to a pressure differential. The difference in the pressures of the top and bottom surfaces results in an aerodynamic lift. The blades of

the wind turbine are constrained to move in a plane with a hub at its centre. Thus, the lift acting on the blades will lead to the rotation of the blade around the hub [9].

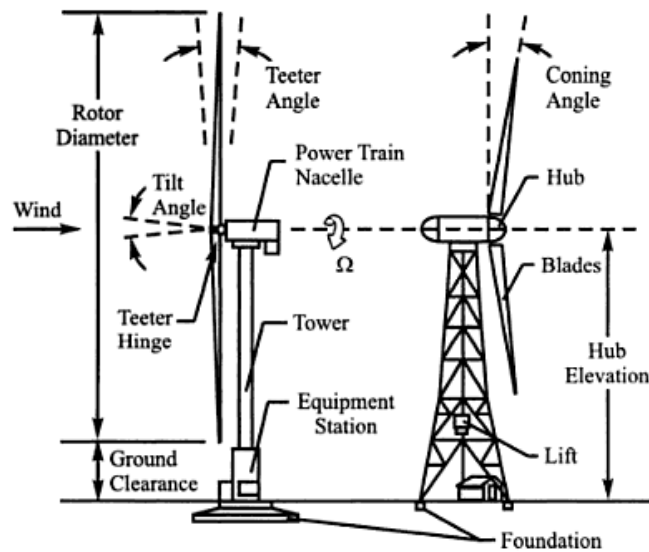


Fig. 1.7: Horizontal axis wind turbine [9]

Usually, HAWTs are preferred for wind projects because of the following advantages:

1. They have higher efficiency compared to VAWTs. Also, blades are to the side of the turbine's centre of gravity which makes it stable.
2. The turbine collects the maximum amount of wind energy as the angle of attack can be remotely adjusted using a wind sensor. This maximises efficiency.
3. They have the ability to pitch the rotor blades in a storm so that damage is minimized.
4. The tall tower of a HAWT allows the access to stronger wind in sites with wind shear. They can also be placed on uneven land or in offshore locations.

However, HAWTs have some disadvantages like

1. HAWTs are not self-starting and have difficulty operating near the ground.
2. The tall towers and long blades are hard to transport and construct and they need a special installation procedure.
3. They have high maintenance and operational costs.

1.3.2 Vertical Axis Wind Turbines

Vertical Axis Wind Turbine (VAWT) is an old technology, dating back to almost 4,000 years. Unlike the HAWT, the rotor of the VAWT rotates vertically around its axis. Though it is not as efficient as a HAWT, it does offer benefits in low wind situations where it is infeasible to use a HAWT. It tends to be easier and safer to build, can be mounted close to the ground and handles wind turbulence better than the HAWT.

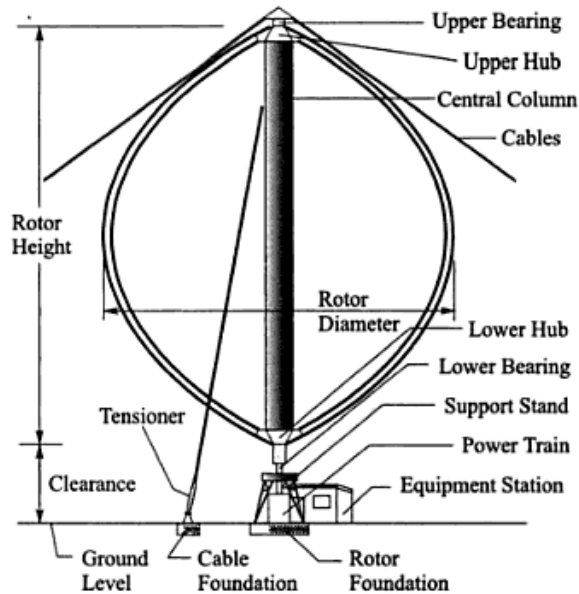


Fig. 1.8: Vertical axis wind turbine [9]

Figure 1.8 shows a typical VAWT. The different types of VAWTs are:

1. Darrieus turbine
2. Giromill turbine
3. Savonius turbine

The Darrieus turbine consists of a vertical rotor and several vertically oriented blades. This turbine is not self-starting and it requires a small starter motor. When it reaches sufficient speed, the wind passing through the airfoils generate torque and thus, the rotor is driven around by the wind. This turbine is powered by the lift forces produced by the airfoils. The turbine can achieve speeds which are higher than the actual speed of the wind. This makes the Darrieus turbine well-suited to electricity generation when there is a turbulent wind [9].

The Giromill Turbine is a special type of Darrieus wind turbine which uses the same lift principle to capture energy. However, it uses straight blades individually attached to the vertical axis instead of curved blades. Sometimes, helical blades are attached around the vertical axis to minimize the pulsating torque. These turbines work well in turbulent wind conditions and are an affordable option where a standard horizontal axis windmill type turbine is not suitable for installation.

The Savonius wind turbine is one of the simplest vertical axis turbines. It is a drag type device that consists of two to three scoops. The curvature causes drag to act on the blades and the drag is more when it is moving with the wind than when it is moving against the wind. This differential drag causes the Savonius turbine to spin. The Savonius turbine being a drag-type device, it extracts much less power than the other vertical axis turbines [9].

The advantages of VAWTs are

1. Maintenance is simpler as the turbines are placed close to the ground
2. Production, installation and transportation costs are low
3. The turbines will work even when the wind is not unidirectional
4. They can be easily installed in hilltops, ridgelines and passes
5. It does not harm the birds, unlike HAWTs which spin at high speeds, in the event of a collision

Some disadvantages of VAWTs are

1. Less efficient than HAWTs because of the drag forces acting on the blades
2. Although they work under turbulent conditions as well, the turbulence can cause secondary effects like vibration of the base
3. They need guy wires to hold them up as there is the issue of imbalance

1.4 Savonius wind turbines

Savonius wind turbines are a type of VAWT, used for converting the force of the wind into torque on a rotating shaft. The turbine consists of a number of blades vertically mounted on a rotating shaft or framework, either ground stationed or tethered in airborne systems. The Savonius turbine is one of the simplest turbines.

Aerodynamically, it is a drag-type device, consisting of two or three scoops. Looking down on the rotor from above, a two-scoop machine would look like an "S" shape in cross section. Much of the swept area of a Savonius rotor may be near the ground making the overall energy extraction less effective due to the lower wind speeds found at lower heights.

Some of the advantages of Savonius turbines are

1. It is self-starting. The turbine only requires a low amount of torque to extract power from it. Thus, its cut-in speed is low.
2. Easy manufacturability and cost effective. The turbine can be easily manufactured because of simple parts.

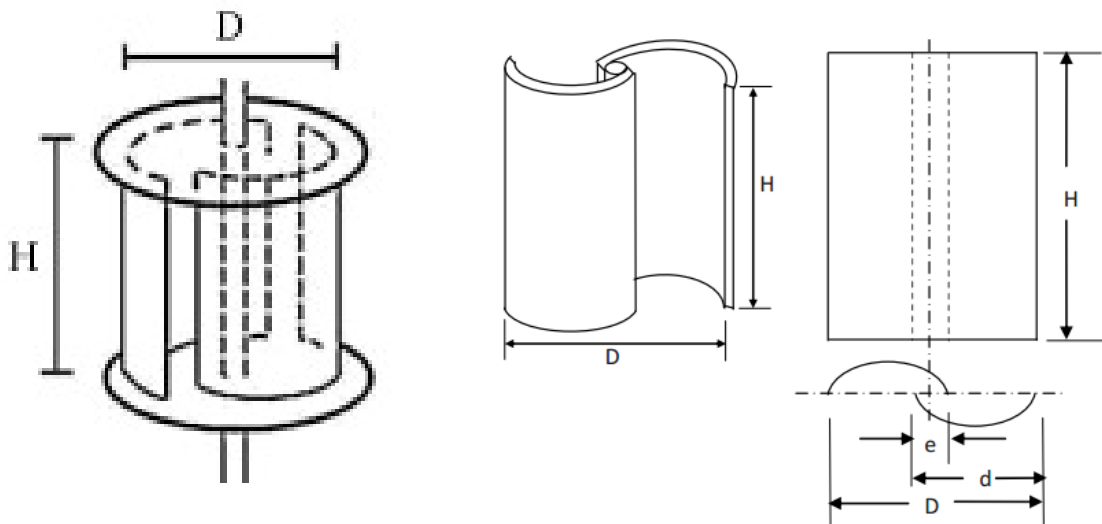


Fig 1.9: CAD models of a Savonius turbine [10]

In Figure 1.9 'e' is the overlap of the two blades on each other. The overlap ratio is defined as ' e/d ' and has an effect on the performance of the turbine. The aspect ratio is a derivative of the frontal area of the turbine and is given by ' H/D '

1.5 Societal relevance of the project

The present day scenario of energy in the Karnataka state is that more than 50% of the rural population does not have access to continuous electricity. The prime reason behind many villages not having electricity is not just shortage of power, but also the distance from a power grid. Putting into use, the present day technology of vertical axis wind turbines to produce electricity at such remote places is a novel idea. This will not only

create energy independent villages but also mitigates climate change, develops rural areas and will be the best way to move towards sustainable development.

Wind energy offers an attractive alternative to the conventional fuel sources. Karnataka has an estimated wind energy potential of 13983 MW while only 2595 MW has been harnessed [4]. If awareness about wind energy is increased and more wind projects are sanctioned, Karnataka has the potential to become self-sufficient with its energy requirements. The state also has a favourable wind power density averaging to 150 W m^{-2} , corresponding to a wind velocity of 6.25 ms^{-1} . Northern districts of Karnataka like Belgaum, Dharwad, Bagalkot, Gadag, Bidar, Haveri, Koppal, Raichur are located in this favourable wind zone [7]. The villages in these districts are the major areas facing energy shortage. Lack of infrastructure has resulted in non-fulfilment of localized demand even though there is an excess supply of wind energy in the region. The twin turbine system will fulfil this demand by local production of electricity and thereby minimizing the grid dependence of rural masses.

1.6 Literature review

Detailed literature survey of wind power generation systems has been carried out to acquire knowledge of similar projects around the world. It is also vital to assess the computational fluid dynamics techniques used in such projects to extend the same to the current research. Design of experiments is an important tool used to simulate many experiments and optimise the system for the best output.

1.6.1 Review on vertical axis wind turbine performance

In a review paper by Walker [11], the dominant methodology for estimation of power output for small-scale turbines using the power curve of the turbine and a wind speed frequency distribution is obtained using the equation

$$P(\text{turbine}) = \int_{U_{ci}}^{U_{co}} P(\text{output})(u) \times f(u) du \quad (1.1)$$

Where $P(\text{output})(u)$ is the instantaneous power output at wind speed u (usually taken from the power curve), $f(u)$ is the frequency of wind speed u (from Weibull or Rayleigh distribution wind speed distribution measurement for a specified period of time) and $P(\text{turbine})$ is the estimated average output for the wind turbine over the same specified time period (normally one year or one month). It has also been found that for urban areas, the terrain roughness is high, and that adjacent buildings can cause

wind shadow. Toja-Silva et.al, [12] analysed the characteristics of urban wind and perspectives and proposals to exploit it have been researched and analysed in the literature. The results show that urban winds have a strong multidirectional component and requires analysing the wind turbine behaviour. To explain the influence of the multidirectional wind on the turbine, a simulation of the airflow around a building section was performed, the sections of various wind turbines were superimposed on the velocity fields, and their aerodynamic behaviour was qualitatively studied.

VAWTs, based on the lift or drag, can be differently configured. The review work of Bhutta et.al, [10] compares the different configurations of the VAWTs and lists out the individual merits and demerits. The paper considered six different configurations of VAWTs, viz. Darrieus rotor, Savonius rotor, combined Darrieus – Savonius rotor, two leaf semi rotary VAWT, Sistan type wind mill and Zephyr turbine, and concluded that combined Darrieus – Savonius rotor was the most efficient with an efficiency reaching 0.35, for different overlaps. However, it was also noted that all the considered configurations were unsuitable to be mounted in urban landscapes as they posed stringent structural requirements. It also suggested the application of Crossflex wind turbine, a variant of Darrieus rotor, for local electricity production.

Even though Savonius rotor suffers from low efficiency (typically around 0.22) and low torque, it has been widely researched owing to its self-starting capability and low maintenance requirement. Many attempts have been made to increase the power coefficient of the same. Altan et.al, [13] have conducted numerical analysis as well as experimental investigation on the effect of a curtain placed in front of the returning blade. It was concluded that the increase in efficiency was directly proportional to the length of the curtain. Works of Mohamed et.al, [14] have determined the optimum location and angle of the curtain to obtain the highest efficiency, by using Evolutionary Algorithms, and has reported an increase in efficiency of about 27 %.

The effect of overlap ratio, which is the ratio of overlap between the blade of the turbines and the turbine diameter, and the aspect ratio, which is ratio of the height of the turbine to the diameter of the turbine, has been studied by Menet [15] and Newman [16], and values ranging from 0.15 to 0.3 for overlap ratio and 1.5 to 3 for aspect ratio was reported to be the best.

Since the blades of a straight bladed Savonius rotor come in contact with the impinging air intermittently, the torque generated also fluctuates with time. This has adverse impact on the generated electricity which keeps fluctuating. To minimize the fluctuations, Damak et.al, [17] and Saha et.al, [18] have come up with blades, twisted along the length of the rotor. It is reported that the twisted blades are superior to conventional straight blades in terms of efficiency, smooth running as well as self-starting capability.

Yao et.al, [19] placed tower cowling over the conventional Savonius rotors and obtained an increase in efficiency by 100%. Saha et.al, [20] investigated the effect of number of blades and number of vertical stages experimentally and concluded that two staged, two bladed, twisted Savonius rotor had a higher efficiency when compared with the conventional single staged rotor.

Ahmed [21], combined the horizontal and vertical axis turbines, thereby creating a hybrid, whose performance was better than a conventional Savonius rotor. Many efforts are underway to install the VAWTs in urban high rise buildings to delocalise the generation of electricity. Works of Ahmed [21], Chong et.al, [22] and Letcher [23] are a step towards the same.

1.6.2 Review on computational fluid dynamics and simulation studies on VAWTs

Bhutta et.al, [10] have summarised the various configurations of the wind turbine and have listed out the differences between the various configurations. They have stated the various design considerations such as efficiency, energy analysis, CFD analysis, aerodynamic analysis and blade element method. They have also experimentally stated 23 different methods that are used such as particle image velocimetry, modal analysis, and vibration and fatigue analysis. This paper has been used as a benchmark to refer for various configurations and the methods of analysis for them.

Lee et.al, [24] have developed various techniques to analyse the aerodynamics of a counter rotating wind turbine. Using a numerical method based on the vortex lattice method, they have analysed the counter-rotating wind turbine and determined its feasibility. Jaohindy et.al, [25] have studied the variation of transient forces of a vertical axis Savonius wind turbine using computational fluid dynamics. Using an unsteady, Reynolds averaged Navier Stokes CFD has been simulated for two different rotors. The

first rotor had an aspect ratio of 1.1 and simulations were conducted by incorporating the dynamic equations of the rigid-rotor motion using a one degree-of-freedom (1-DOF) module to evaluate the rotor's free motion. The second rotor had an aspect ratio of 0.7 and simulations were conducted by specifying a fixed rotational velocity. They observed that at TSR above 0.6, the effect of the longitudinal drag force on the rotor operation increased and the lateral lift force contribution decreased. The resultant force angle was shown to become more acute due to the increase in the longitudinal force with increasing TSR.

Zhou et.al, [26] have explored the nonlinear two dimensional unsteady flow over a Savonius wind turbine and performed simulations using STAR CCM+. The motion of the blades is solved by using a moving mesh. Comparative studies of the two types of rotors were carried out, and numerical simulation results were compared with experimental data. A discussion of the causes of these differences is presented, that is based on a detailed study of the respective flow field characteristics, including the behaviour of moment coefficients, velocity vectors and pressure distribution.

Trivellato et.al, [27] have conducted numerical studies on the stability restrictions in rotating grids and have found that a stringent CFL criterion of < 0.15 is needed to ensure accurate prediction of power coefficient. It is also noted that even a small time step corresponding to 1° rotation does not necessarily warrant an accurate prediction of power coefficient at lower Tip Speed Ratios and finer meshes.

Many works such as [28-30] have numerically analysed the dynamic performance of Savonius rotor for various operating conditions using commercial softwares such as STAR CCM+ and ANSYS Fluent. The reported values for peak power coefficient range between 0.2 and 0.25. Nasef et.al, [31] conducted numerical studies on the influence of different turbulence models on the accuracy of predicted power coefficient and found that SST $k-\omega$ was more accurate compared to the other models.

Sargolzaei et.al, [32] have used Artificial Neural Networks to predict the output of Savonius turbines. Experimental data obtained from seven different Savonius prototypes was used for the training set. The results have shown acceptable accuracy between the predicted and measured power coefficients and may prove to be a viable alternative to computationally costly simulations.

1.6.3 Review on vertical axis wind turbine arrays

Interest has now moved from optimising an isolated VAWT for peak performance to optimising an array of closely spaced VAWTs for collective efficiency. A paper by Whittlesey et.al, [33] has investigated the behaviour of a school of fish and applied the same concept theoretically to an array of Darrieus turbines. Dabiri [34] and Kinzel et.al, [35] have set up an array of Darrieus turbines in California and have measured an increase in power density by an order of one. Kumar et.al, [36] have performed 2D numerical and experimental analysis on contra rotating Darrieus turbine and have verified the increase in power output due to the positive aerodynamic interference between the individual turbines.

Shigetomi et.al, [37] using Particle Image Velocimetry have identified potential relative locations of the Savonius turbines which would enhance the efficiency of power extraction. Golecha et.al, [38] experimentally studied the influence of distance of separation between the turbines on the power coefficient of hydrokinetic Savonius turbines. They concluded that a separation distance greater than 8 times the turbine diameter, effectively decouples the turbines and no interaction takes place. Kim et.al, [39] placed a deflector in front of a straight bladed Darrieus turbine array and concluded that the deflector increases the power output of the lift driven system and the increase is dependent on the size of the deflector. Sun et.al, [40] have studied the coupling effects between the Savonius turbines for different separation distances, angle of separation and blade phase angles and have reported an increase in power coefficient to 0.30. However, the parameters were not varied systematically and the SST $k-\omega$ was not used even though it was reported to be the most accurate by Nasef et.al, [31].

1.6.4 Review on Design of experiments and optimisation techniques

A system becomes more robust when the response is insensitive to noise. In the case of wind turbines, robustness as well as maximum response can be achieved by utilising design of experiments principles and orthogonal array testing methods. Kacker [41] has explored the offline quality control techniques, to ensure that quality can be built into a product during the process design stage and not after the product has been manufactured. The orthogonal array testing methods minimise the number of experiments to be performed to ensure optimum output.

There have been several instances where the orthogonal array testing has been successfully implemented in the industry. Relevant to wind energy, Hu et.al, [42] have done studies on robust design of horizontal axis wind turbines. They have considered variables like twist angle, blade chord length, number of blades among other variables and have used the L_{27} orthogonal array to minimise the number of experiments. An energy output improvement of 31.6% was reported by them which is an appreciable improvement.

1.6.5 Literature gap

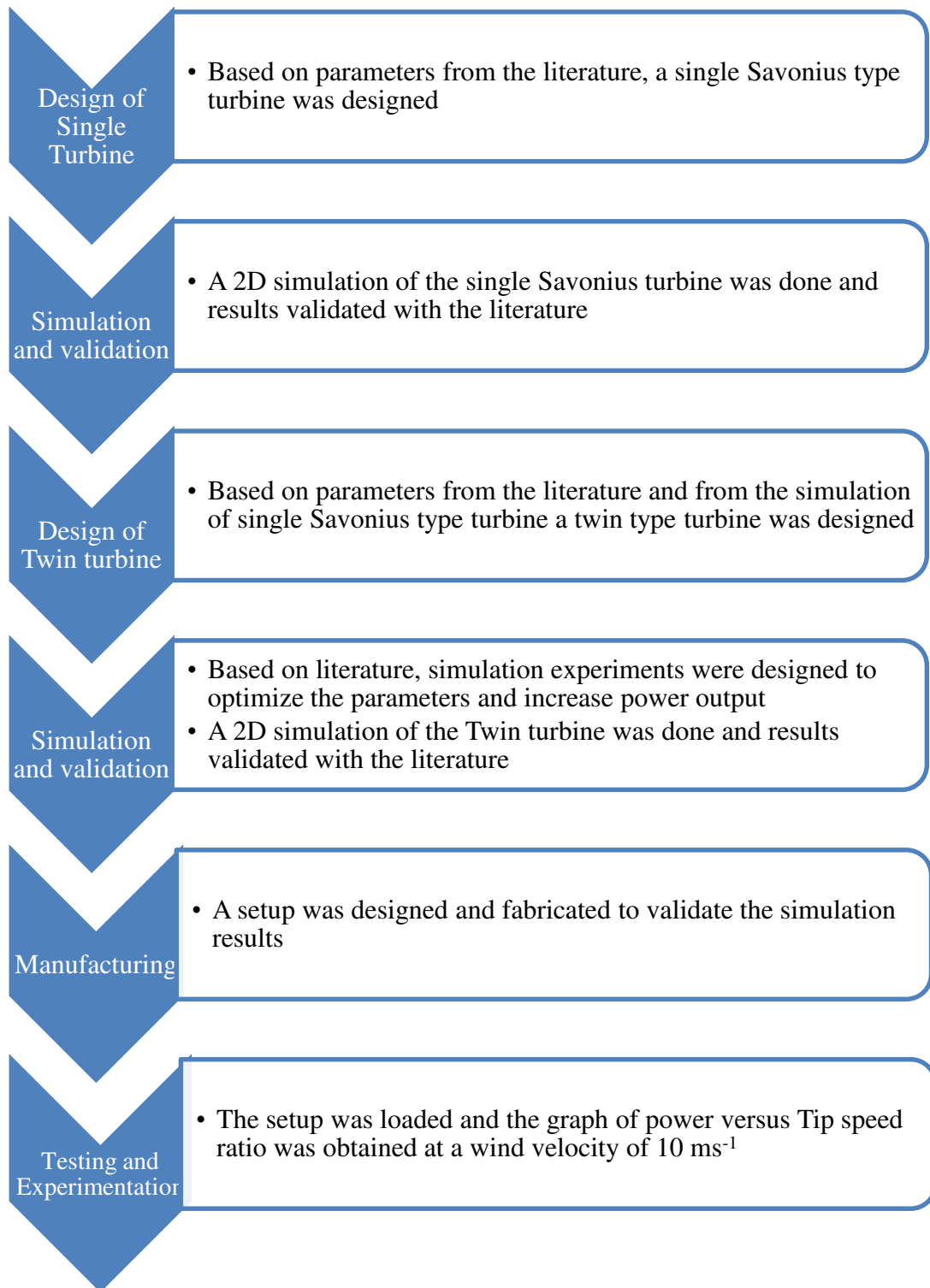
Based on the above detailed literature survey [10-42], it was concluded that there is limited information on the aerodynamic coupling between two Savonius rotor operating in close proximity. Also, no empirical relation, between the various parameters and the power coefficient exists, to the best of our knowledge.

1.7 Objectives of the project

1. To model a Savonius type vertical axis wind turbine based on the available literature and to perform simulations to compare performance of various configurations.
2. To model and simulate Savonius type Twin-Vertical Axis Wind Turbines (T-VAWT) and determine the configuration that results in maximum power output using orthogonal array technique.
3. To fabricate and test the T-VAWT

1.8 Methodology of the project

The methodology adopted to accomplish the objectives of the project has been outlined as shown below. The project aimed to design, fabricate and test Twin-Vertical Axis Wind Turbine (T-VAWT)



1.9 Organisation of the report

The project report is presented as SEVEN chapters:

Chapter 1 INTRODUCTION presents an overview of the current energy scenario in India, introduction to wind energy and wind turbines and the societal relevance the current project. This is followed by a literature review of topics pertaining to the current

project. The chapter concludes by describing the objectives that will be achieved by the project and the methodology adopted.

Chapter 2 WIND ENERGY AND SAVONIUS WIND TURBINES gives a description of the theory and concepts pertaining to wind energy and harnessing it. Further description regarding computational fluid dynamics and design of experiments have been presented.

Chapter 3 MODELING AND SIMULATION OF SAVONIUS WIND TURBINES describes the various models and the simulations performed on vertical axis wind turbines. The significance of the chosen models are also explained. Orthogonal array testing is employed with five different variables and is explained in detail.

Chapter 4 DESIGN AND FABRICATION OF THE TWIN VERTICAL AXIS WIND TURBINE SETUP highlights the setup used in the experiment, materials, manufacturing processes and the test rig used. Cost analysis of the project is also presented here.

Chapter 5 RESULTS AND DISCUSSIONS presents the results obtained from the experiments and useful inferences. The simulations are performed on the models and the best configurations are determined. The results include simulation results as well as the results from testing the T-VAWT setup.

Chapter 6 CONCLUSION AND SCOPE FOR FUTURE WORK presents the key outcomes of the project and concepts for future work which can be carried out.

1.10 Summary

In this chapter, a basic introduction to wind turbines and the literature review conducted was elaborated. Critical gaps in literature were identified, the project objectives were formulated and the methodology to achieve the set objectives was outlined.

WIND ENERGY AND SAVONIUS WIND TURBINES

The theory and concepts pertaining to harnessing wind energy has been elaborated in this chapter. The working of Savonius wind turbine and the factors which affect the power output from it has been elucidated. CFD simulations which are used to determine the power output from Savonius turbines and the experiments that need to be designed for the same has been introduced.

2.1 Harnessing wind energy

Figure 2.1 shows the airflow through a pipe having cross sectional area 'A'. The wind speed is 'u' and the density is 'ρ'. The power, P_{wind} , the wind transfers to this cross sectional area [9] is given by.

$$P_{wind} = \frac{1}{2} \rho A V^3 \quad (2.1)$$

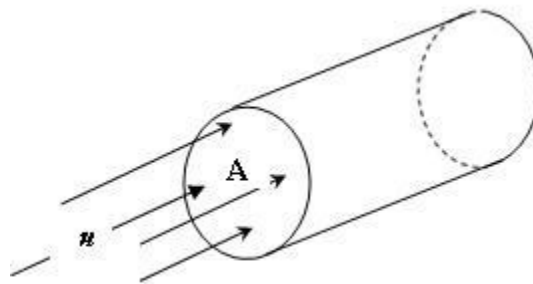


Fig. 2.1: Power delivered by wind flow through a cylinder [43]

This concept can be extended to harnessing wind energy through a turbine. In this case, the swept area by the rotor is 'A'. The power generated by the turbine is given by

$$P = C_p \frac{1}{2} \rho A V^3 \quad (2.2)$$

C_p is the power coefficient of the turbine which is a merit of the conversion efficiency of the turbine. This can be extended to vertical axis wind turbines as well.

2.2 Betz limit

By extracting power, the turbine itself has an effect on the wind. Downwind of the turbine, the air moves more slowly than the upwind portion. The wind starts to slow

down even before it reaches the blades, reducing the wind speed through the ‘disc’ and hence reducing the available power [9].

Some of the wind that was heading for the disc diverts around the slower-moving air and misses the blades entirely. This means that no power can be extracted. Thus, for a given disc diameter, only a portion of the maximum available wind energy can be harnessed. Maximum energy can be harnessed when the wind speed reduces to about two thirds the original value as it passes the turbine, though even then the wind just before the turbine will have lost about a third of its speed. This allows a theoretical maximum of 59.3% of the wind’s power, called the Betz’s limit, to be harnessed. In practice only 45-50% is achieved by current designs [42].

2.3 Principle of working of Savonius turbine

The Savonius wind turbine, being a drag type turbine derives its torque from the differential pressure distribution on both sides of the turbine blades as well as from the shear stress distribution. The total force on the turbine [43] can be calculated as follows:

$$\vec{F}_a = \vec{a} \cdot \vec{P} + \vec{a} \cdot \vec{F}_v \quad (2.3)$$

Where \vec{a} is the specified force vector

\vec{P} is the pressure force vector.

F_v is the viscous force vector

The torque on the turbine can be calculated by multiplying the force vectors with the moment arm [43].

$$\vec{T} = \vec{r}_{ab} \times \vec{P} + \vec{r}_{ab} \times \vec{F}_v \quad (2.4)$$

Where \vec{r}_{ab} is the specified moment arm vector.

\vec{P} is the pressure force vector.

F_v is the viscous force vector.

The power can then be calculated by multiplying the moment with the angular speed of the turbine.

$$P = T \omega \quad (2.5)$$

Where ω is the angular velocity of the turbine in radians/s

T is the torque of the turbine in N- m.

2.4 Factors affecting power generation

The power output from a Savonius turbine depends on many parameters like solidity, tip speed ratio, wind speed, overlap ratio and aspect ratio [44]. Their effect on the power output is explained below.

2.4.1 Solidity

It is defined as the percentage of the circumference of the rotor, which contains material rather than air. High solidity is not preferred because of lower peak C_p and steep performance curve. Very low solidity is equally undesirable because of very high operating speeds and low peak C_p .

2.4.2 Tip Speed Ratio

Tip Speed Ratio (TSR) is defined as the ratio of the speed of tip of the blade to the wind speed. It is one of the important factors that is used to evaluate the performance of the turbine. The graph of C_p vs. TSR is shown in Figure 2.2. The TSR is given by

$$\text{TSR} = \frac{\omega r}{V} \quad (2.6)$$

Where ' ω ' is the angular velocity, ' r ' is the radius of the turbine and ' V ' is the velocity of the wind impinging on the blade.

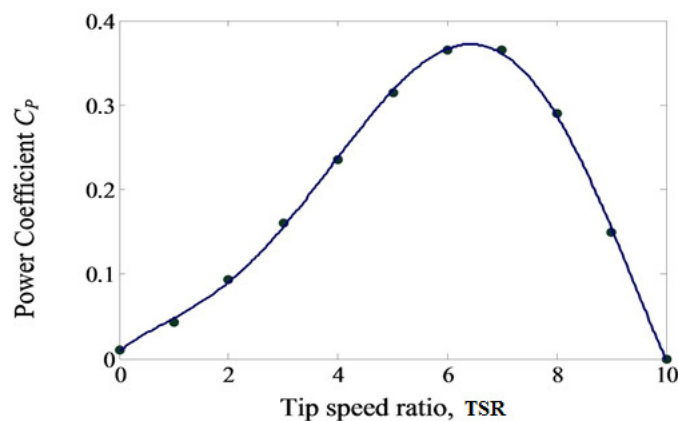


Fig. 2.2: Relationship between C_p and Tip Speed Ratio for HAWT [9]

2.4.3 Wind Speed

Coefficient of power increases by 19% as Reynolds number, an effect of the wind speed, increases from 80,000 to 150,000 [45]. For conventional Savonius rotor (at a given rotor diameter) the delayed separation around the blades at higher wind velocities may be responsible for the increase in the maximum coefficient of power with the increase in the Reynolds number.

2.4.4 Overlap ratio

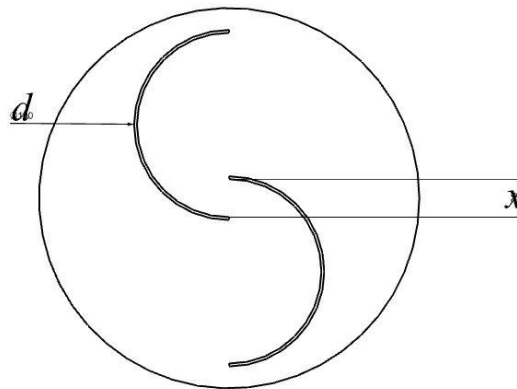


Fig. 2.3: Overlap ratio of a Savonius rotor

Primary overlap that Savonius considered was $0.25 (x/D)$, as shown in Figure 2.3. However, different studies show that the shape of the blades induce different values.

The increase in the static torque with the increase of overlap ratio is mainly triggered by the increased pressure on the concave side of the returning blade because of the flow through the overlap. However, it is realized that as the overlap ratio increases beyond an optimum value, the effective pressure on the concave side of the advancing blade reduces. Thus, at an optimum overlap ratio of 0.20, the peak static torque characteristic of the turbine is observed [46].

From the literature, it is also seen that with the increase of wind free stream velocity, the mean static torque coefficients also increases. In addition, it is observed that the average static torque coefficient increases with the increase of overlap ratio up to 0.20. However, it decreases beyond an overlap ratio of 0.20. The major drawback of large variation in torque coefficient is also reduced with the increase of overlap. Besides, a positive static torque value is achieved for all angular positions with the higher overlap

ratios. Rotor with a zero overlap ratio have higher coefficient of power at high wind speeds and Reynolds numbers of 120,000 and 150,000 [45].

Increasing the overlap ratio (from 0.0 to 0.1 and 0.16) for modified Savonius rotor (blade arc angle of 124°), increases the losses due to vorticities. This increase in the vorticity losses decreases the aerodynamic performance. However, for a conventional Savonius rotor (blade arc angle of 180°) the vorticity loss increases above overlap ratio of 0.15. Thus, conventional Savonius rotors show better performance at overlap ratios of 0.15, whereas modified Savonius rotors show better performance at overlap ratio of zero [46].

Moreover, low overlap condition in the rotor stabilizes the Coanda flow through the overlap. This increases the power coefficient of the rotor at that overlap condition. However, as the overlap increases further, these aerodynamic advantages would be circumvented by the effect of circulation across the overlap. This again is responsible for the drop in power coefficient [46].

2.4.5 Aspect ratio

The aspect ratio (H/D) plays an important role in the aerodynamic performances of Savonius rotor. Globally high values of aspect ratio should greatly improve this efficiency. Literature suggests that the ideal aspect ratio is two [15]. Aspect ratio also plays a major role in power generation of the turbine. The power output is directly proportional to the frontal area of the turbine, and this area depends on the aspect ratio.

2.5 Computational Fluid Dynamics

Many of the physical process occurring in nature are accurately described by differential equations, either Ordinary Differential Equations (ODEs) or Partial Differential Equations (PDEs) [47]. Single phase fluid flow is no exception to this and is described by a set of governing PDEs called as Navier Stokes equations [48], given below:

$$\frac{\partial \rho}{\partial t} + \nabla \cdot (\rho \mathbf{V}) = 0 \quad (2.7)$$

$$\rho \frac{D\mathbf{V}}{Dt} = \rho \mathbf{g} - \nabla p + \mu(\nabla^2 \mathbf{V}) \quad (2.8)$$

Equation 2.7 is the continuity equation, which mathematically states that fluid can neither be created nor be destroyed in the region of fluid flow, unless there is a sink or

a source. Equation 2.8, a vector equation with three components in the direction of coordinate axes, is the momentum balance equation and relates the total acceleration of the fluid with the viscous forces, pressure forces and gravitational force acting on the fluid. For a general three dimensional, compressible, viscous flow, the unknowns to be determined are the three components of velocity, u , v , w , pressure, p and the density ρ . This necessitates another equation and conservation of energy equation is used as the same [48].

$$\rho \frac{D}{Dt} \left(e + \frac{V^2}{2} \right) = \rho \dot{q} + k \nabla \cdot (\nabla T) - p(\nabla \cdot \mathbf{V}) + \rho \mathbf{g} \cdot \mathbf{V} + \text{Viscous dissipation} \quad (2.9)$$

However, the energy equation introduces another variable, T , the temperature. Closure is provided by using equation of state, dependent on the fluid under study, which takes the form

$$\rho = \rho(p, T) \quad (2.10)$$

The solution is obtained by determining u , v , w , p , T , ρ , throughout the domain of interest, satisfying both the governing equations as well as the boundary conditions imposed by the physical nature of the problem. The methods implemented to obtain the solutions are theoretical, experimental and computational.

Theoretical approach involves making various assumptions about the nature of the flow such as inviscidness, incompressibility, reduced geometry etc. which significantly simplify the governing equations making them amenable to analytical solutions. Since the governing equations are highly coupled and nonlinear, it is highly difficult to obtain analytical solution to complex geometries and flows, which introduce intricate boundary conditions. It is interesting to note that no closed form analytical solution exists for the complete set of Navier Stokes equation. Hence theoretical approach is rarely used to obtain information regarding real engineering flows [47].

Experimental approach comprises of creating a scaled model of the object under study, subjecting it to the fluid flow and measuring the required flow properties (u , v , w , p , T) at discrete locations. Suitable interpolations are carried out to obtain the properties at desired locations. Tracer particles might be added to obtain visual information about the flow. Even though this approach is costlier than the other two, owing to the

expenditure of creation of model, wind tunnel maintenance etc., it is widely used as it provides hands on, measurable solution of the equations [47].

Computational approach uses high speed computers to implement numerical methods and algorithms to solve the governing equations with their associated boundary conditions. Since it has not been possible to obtain an analytical solution for the NS equations for the complex flow physics and boundary conditions, numerical algorithms convert the set of PDEs to a set of algebraic equations. Considering the coupling between the equations, simultaneous solution of the generated algebraic equations leads to the determination of velocity field as well as pressure field [47].

Computational Fluid Dynamics (CFD) is a branch of fluid mechanics that uses numerical methods, algorithms to solve problems that involve fluid flows. Computers are used to perform the calculations required to simulate the interaction of liquids and gases with surfaces defined by boundary conditions.

The general methodology adopted [47] to solve a flow problem in CFD is:

1. The geometry (physical bounds) of the problem is defined.
2. The fluid volume is divided into discrete cells (the mesh).
3. Physics of the problem is defined – for example, the motion + radiation + species conservation + heat source
4. Fluid behaviour and properties at the boundaries of the problem are provided, constituting the boundary conditions. Initial conditions are also provided for unsteady flows
5. Resulting algebraic equations are iteratively solved to obtain the solution
6. Post processing is carried out to visually represent the solution

Many methods have surfaced over the years to discretise the NS equation. Based on the discretization adopted, they are distinguished as

1. Finite Volume Methods
2. Finite Difference Methods
3. Finite Element Methods

ANSYS Fluent is a commercially available CFD software by ANSYS Inc. which is suitable for the simulation of low subsonic, laminar or turbulent, viscous or in viscid, non-reacting flows. The latest release is version 16. The simulations were conducted on

version 14.5. Fluent is a finite volume based solver, since the method is more stable and easy to implement for unstructured meshes.

2.6 Design of Experiments

When the response of a system is being analysed, it is necessary to take into account the various factors and variables which dictate the response. The presence of multiple variables and levels will necessitate proper design of experiments where the effect of individual variables and interactions are vital. Full factorial design of experiments will consider all possible combination of variables and measure the response [49]. Although this is a robust method to measure the effects, it becomes time consuming and expensive. Thus, most systems utilise fractional factorial designs where only a subset of the full factorial design is considered. Orthogonal array testing is a method of designing experiments where each level of a single variable interacts with all the levels of another variable at least once [50].

2.6.1 Orthogonal arrays

Orthogonal arrays were invented in early 1987 by a French mathematician, Jacques Hadamard. These arrays are depicted as $L_a(b^c)$ where 'a' is the number of rows, 'b' is the number of levels and 'c' is the number of columns. The commonly used orthogonal arrays are L_4 , L_8 , L_9 , L_{16} , L_{27} etc [50]. The digit refers to the number of experiments that needs to be carried out for the particular array i.e. number of rows of the matrix [50]. The speciality of the orthogonal arrays is that each level of a particular variable is tested at least once with all levels of another variable. Consider an experiment with three variables each having two levels. L_4 orthogonal array testing can be utilised for the experiments to predict the response and is as shown in Table 2.1.

Table 2.1: L_4 orthogonal array

Experiment	Factor 1	Factor 2	Factor 3
1	1	1	1
2	1	2	2
3	2	1	2
4	2	2	1

In the first experiment, all the factors are kept at the first level and the response is measured. In the second experiment, factor 1 is at level 1 and factors 2 and 3 are at level

2 and the experiment is performed. The uniqueness of the orthogonal array is that if factor 1 is considered, both its levels are tested for all levels of the other two variables. This method of experimentation reduces the number of experiments that needs to be carried out when compared to a full factorial design which requires eight experiments.

2.6.2 Regression analysis

Regression analysis is a statistical tool for the investigation of relationships between variables [51]. It is used to obtain functional relationship among multiple variables, out of which, one is dependent. In the elementary sense, regression analysis corresponds to curve fitting, in which the error between the actual value and the predicted value of dependent variable is minimized by the method of least squares. However, the analysis doesn't predict any kind of causal relationship between the variables.

General mathematical model is given by

$$y = f(\gamma, X) \quad (2.11)$$

Where y is the dependent variable, X is the vector of independent variables and γ is the vector of parameters to be predicted by the analysis. The form of f is required to perform regression analysis. Usually, depending on the process being analysed, the nature of f is obtained. If the functional form is not available, a suitable polynomial function is used, since any function can be converted to polynomial function using Taylor series. Regression analysis can performed if the number of components in X exceeds the number of components in γ , ensuring that the components of γ can be exactly determined. Based on the number of independent variables and the form of f , regression analysis can be classified into:

- Linear Regression Analysis (LRA) is applied for a single independent variable and a linear function. It fits the measured data to a straight line.
- Multivariate Linear Regression Analysis (MLRA) is applied in cases where the dependent variable is a linear function of multiple independent variables. It fits the measured data to a hyper plane
- Non Linear Regression Analysis (NLRA) is exercised when the process to be modelled is nonlinear in nature.

2.7 Summary

In this chapter, theory and concepts pertaining to harnessing energy from wind have been explained. Various factors which affect the power output from a Savonius wind turbine have been identified. Computational methods to find the turbine response along with the concerned equations have been derived. Finally, orthogonal array testing method which can optimise the system having multiple variables has been introduced along with regression analysis.

MODELING AND SIMULATION OF SAVONIUS WIND TURBINES

In this chapter, modeling of a single rotor Savonius type wind turbine has been considered. The blade profile and the number of blades were compared to determine their effect on the performance. The purpose of this study was to perform detailed simulations and identify the ideal turbine parameters to be chosen for subsequent simulations on a twin vertical axis wind turbine setup. For the twin vertical axis wind turbine setup, detailed simulations were performed further as per orthogonal array testing for a set of parameters to obtain the maximum power output

3.1 Modeling of Savonius VAWT

Turbines having different number of blades have been simulated to find the better configuration. Also, the blade profile is an important parameter that dictates the power output. It is vital to understand how these parameters influence the power. This necessitates modeling and subsequent simulations to be performed.

3.1.1 Blade profile

An important aspect which influences the power output is the blade profile. The different blade profiles considered were triangular, bach type and semicircular. These configurations are depicted in Figures 3.1 (a), 3.1 (b) and 3.1 (c) respectively. The triangular and semicircular profiles are based upon the top view of the turbine whereas the bach turbine blades are a continuous unit.

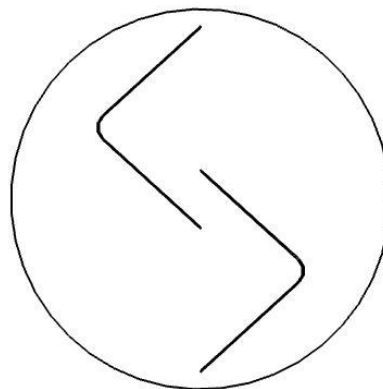


Fig. 3.1 (a): Triangular profile

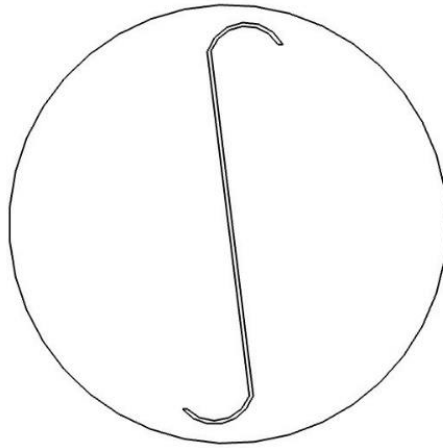


Fig. 3.1 (b): Bach profile

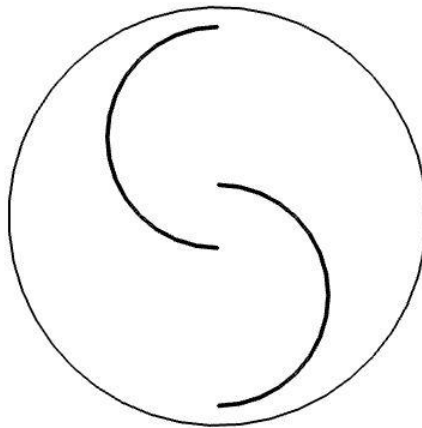


Fig. 3.1 (c): Semicircular profile

4.1.2 Number of blades

Figure 3.2 (a) and Figure 3.2 (b) depicts the representative top views of the two bladed configuration and the three bladed configuration respectively.

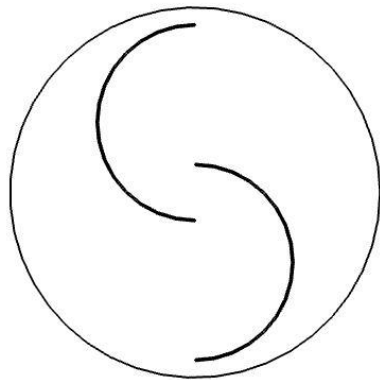


Fig. 3.2 (a): Two bladed configuration

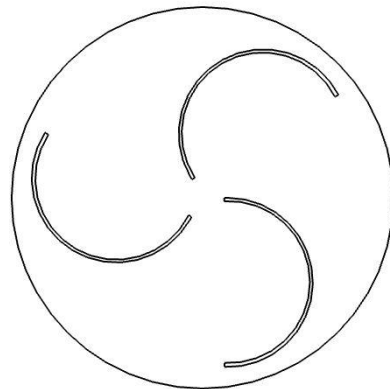


Fig. 3.2 (b): Three bladed configuration

3.1.3 Number of turbines

Since the objective of the project is to design an array of vertical axis wind turbines, it was necessary to determine the number of turbines to be present in the array. Thus, modeling of a two array system as well as a three array system were done. The representative drawings are depicted in Figures 3.3 (a) and 3.3 (b) respectively.

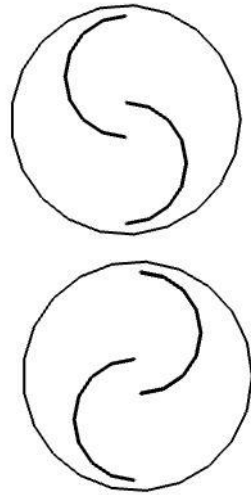


Fig. 3.3 (a): Two turbine array

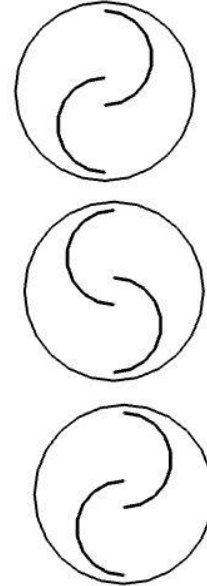


Fig. 3.3 (b): Three turbine array

3.2 Simulation studies on single Savonius turbine

A detailed explanation of the simulations conducted on the Savonius wind turbine to determine its power output is provided. Even though the end application of the designed wind turbine stipulates the use of wind velocity of 6 ms^{-1} , a wind velocity of 10 ms^{-1} is simulated, considerations being given to the practical limitation of the turbine size during testing.

The power generated by the turbine, P , is given as,

$$P = \frac{1}{2} C_p \rho V^3 A = C_p P_{wind} \quad (3.1)$$

Or, equivalently,

$$C_p = \frac{P}{P_{wind}} \quad (3.2)$$

Hence, it can be observed that C_p , called as Coefficient of Performance, is an efficiency factor, which shows the maximum power absorbed by the turbine from the free flowing

wind. C_p is a function of many variables, notable being, wind velocity, shape of the turbine blades, RPM of the turbine and turbulence in the air.

A plot of C_p vs. Tip Speed Ratio (TSR), which is the non-dimensional speed, defined below, is called the characteristic of the turbine and is used to predict the power generated by the turbine at various RPMs. The aim of the simulations is to obtain the value of C_p at various TSRs.

$$TSR = \frac{\omega r}{v} \quad (3.3)$$

From the simulations conducted, a non-dimensional torque coefficient, C_t , is obtained. The torque generated by the turbine, T , is then given as,

$$T = \frac{1}{2} C_t \rho V^2 A r \quad (3.4)$$

Torque is then multiplied with the RPM at which the turbine is rotating to obtain the power generated.

$$P = T \omega \quad (3.5)$$

Using the equation for coefficient of power, the coefficient of performance of the turbine, at that particular RPM is obtained. Characteristic of the turbine is obtained by varying the RPM of the turbine, resulting in TSR variation.

Different blade profiles were investigated for their efficiency in generating torque, based on torque coefficients. Based on this data, optimum blade configuration was selected. The number of blades were decided by comparing the characteristic curve of two bladed and three bladed turbines. Simulations were not conducted to determine the length of the turbine, owing to the high computational costs. Detailed simulations were carried out on all the configurations explained above in order to find the best parameters for the turbine array. These simulations are as explained below.

3.2.1 Computational domain and boundary conditions

Standard three dimensional simulation of a wind turbine requires upwards of two million elements in the mesh, resulting in an unreasonable computational time on a standard computer. Hence a two dimensional simulation of the turbine was carried out. The domain of flow is a rectangular region even though the flow of wind over a wind turbine is an open flow situation. Fluid domain is shown in Figure 3.4.

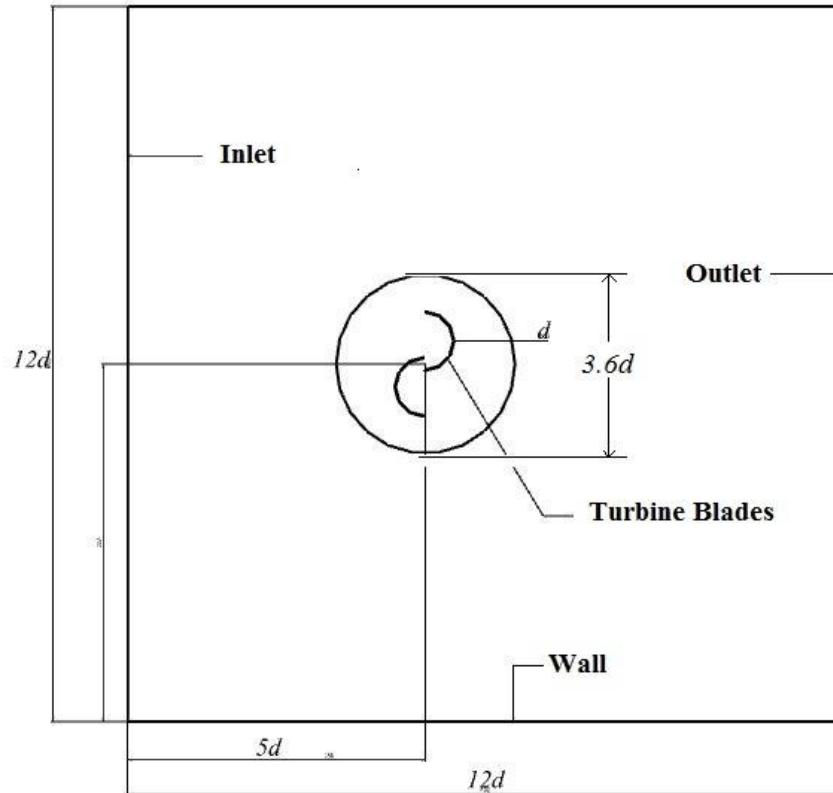


Fig. 3.4: Computational fluid domain

To mitigate the effect of the bounding walls on the turbine, the separation distance between them was decided to be $12d$, d being the diameter of the turbine blade. The inlet to the turbine was placed at a distance of $5d$ from the centre of the turbine, whereas the outlet was placed at a distance of $7d$ from the centre of the turbine, to prevent the effect of reversed flow (if generated) on the turbine. The boundary conditions are as shown in Table 3.1.

Table 3.1: Boundary conditions adopted for the simulations

Parameter	Boundary	Magnitude
Velocity Inlet	Inlet	10 ms^{-1}
Pressure Outlet	Outlet	0 Pa (Gauge)
No Slip Wall	Turbine Blades, Bounding walls	-

3.2.2 Meshing

Meshing refers to the process of dividing the fluid domain into a large number of small cells. Meshing was carried out using ANSYS Meshing toolbox. To accomplish the rotational motion of the turbine in the flow domain, either sliding mesh technique or adaptive mesh refinement technique can be used. In sliding mesh technique, a sub

domain of the mesh rotates about its centre point in the global mesh. In adaptive mesh refinement technique, after each time step, since the blade rotates, the mesh changes to conform to the new geometry. Due to the ease in application and the accuracy provided, it was decided to use sliding mesh technique in the simulation. To obtain a sliding mesh, a circle of diameter $3.6d$ was placed around the turbine, with its centre coinciding with the turbine centre. A mesh interface was created at the circle edge and rotational frame motion was given to the region bounded by the circle to imitate turbine rotation. The angular velocity of rotation was varied to obtain different TSRs of the turbine.

Free meshing was done using triangular elements. The density of meshing was increased inside the rotating domain since gradients in the flow variable is very high due to the presence of the blades in this region. The generation of torque on the blade is due to both the pressure distribution on either side of the blade as well as the viscous shear stress distribution on the blade surface. To obtain the correct shear stress, resolution of boundary layer is of paramount importance. In this regard, 15 inflation layers of growth rate 1.2 has been used.

The number of elements in the domain varies with the geometry under investigation, but in all cases, it exceeded 50000. Minimum orthogonal quality, which is a merit of angle between the edges in an element, was kept above 0.4. Maximum aspect ratio, which is the ratio of longest edge to the shortest edge in an element, was maintained below 10. Figure 3.5 shows the meshing on a two bladed turbine.

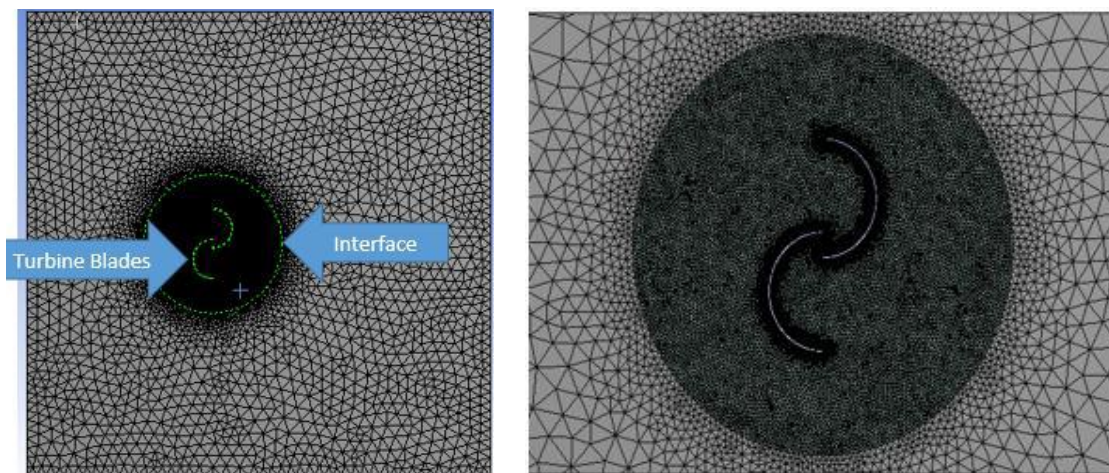


Fig. 3.5: Meshing on a two bladed turbine

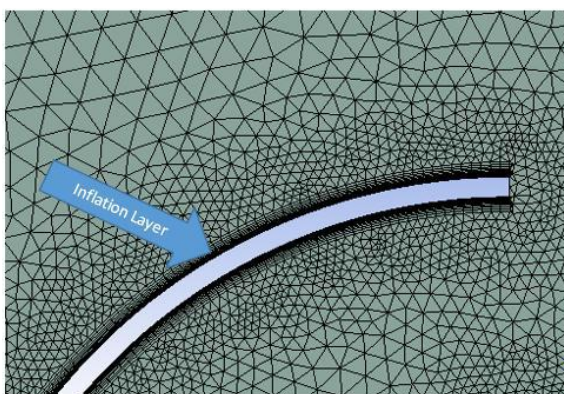


Fig. 3.6: Inflation layer

3.2.3 Setup

Density based solvers are suitable for flows where compressibility effects dominate. The flow being low subsonic, compressibility effects are negligible and hence pressure based solver was used. The motion of the turbine creates an unsteady flow necessitating the usage of transient conditions. Due to the high Reynolds number and unsteady flow, the flow around the turbine is essentially turbulent and hence Reynolds Averaged Navier Stokes (RANS) equations have to be solved instead of NS equations. Various turbulence models like $k-\epsilon$ model, $k-\omega$ models, Transition Shear Stress Transport (SST) etc., exist and the works of Dobrev et al. [30] give $k-\omega$ model as the best model to describe the turbulent flow around a VAWT, and hence it has been used. In $k-\omega$ model, k relates to the turbulent kinetic energy and ω gives the specific dissipation rate of the kinetic energy in turbulence. Turbine motion is set up as stated in the previous section.

Semi Implicit Method for Pressure Linked Equations (SIMPLE), a pressure based solver, was chosen since it has a good convergence rate and required accuracy. Second order upwind method has been used in discretising the RANS equations, as well as the $k-\omega$ equations, to obtain the desired accuracy. For time stepping, to obtain the transient behaviour, first order implicit method is used. Advantage of implicit method is that it does not place any restrictions on the time step (Δt) for stability and hence larger time steps, corresponding to 1° rotation of the turbine can be used. This results in overall faster computation time, even though implicit methods are more computation intensive than explicit methods.

A residual of 10^{-5} was given for continuity, velocity, k and ω equations. For convergence, as the number of iterations increase, the residuals must tend to zero. The

iterations stop when the residuals in all the cells for all the field variables achieve the set value. The simulation setup described is comparable to the work of Dobrev et.al,[30]

It was observed that the torque fluctuated in a periodic manner after two rotations of the turbine and hence the simulation was conducted for 1800 time steps, corresponding to five rotations of the turbine. The torque coefficient value generated by Fluent was imported into MATLAB, and the average torque was calculated.



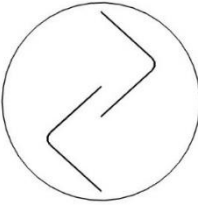
3.3 Comparison of power output

As per the simulation conditions explained above, simulations were carried out in ANSYS Fluent 14.5 and the key outcomes from the experiments have been presented in this section.

3.3.1 Blade profile

Different blade profiles were simulated for TSR 0.7, since 0.7 TSR corresponds to peak power for VAWTs and Table 3.2 summarises the results. For blade profile No.2, overlap was selected to be $0.2d$, since overlap between $0.15d$ and $0.25d$ gives the highest torque.

Table 3.2: Coefficient of torque for different blade profiles

Sl. No.	Blade Profile	C_t
1		0.1734
2		0.1904
3		0.0557

It is seen that semi-circular blades generate the most torque resulting in higher power and hence further studies were conducted only on this profile. The explanation for the same is given below.

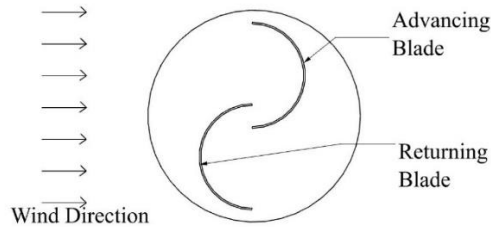


Fig. 3.7: Savonius turbine in a flow field

In the Figure 3.7, the blade moving with the wind is called the advancing blade and the blade moving against the wind is called the returning blade. During the rotation of the turbine, fluid from the advancing blade, flows through the gap between the turbine and impinges on the returning blade. The dynamic pressure of the impinging fluid, due to its velocity, is converted into static pressure. Thus the pressure differential across the returning blade decreases, leading to lower drag on that blade. The lower drag on the returning blade results in higher torque being generated and hence higher coefficient of torque. Since the Bach turbine is a continuous turbine, there is no provision for the flow to traverse from advancing to the returning blade directly and hence there is no pressure conversion, resulting in higher pressure differential across the blade and lower torque. In the third case, because of the geometry of the blades, even though the flow impinges on the returning blade, it does so not in the tangential direction to the circle of rotation, but rather in the radial direction. Hence, there is no improvement in torque coefficient. The velocity vectors showing the same phenomenon is shown in Figure 3.8.

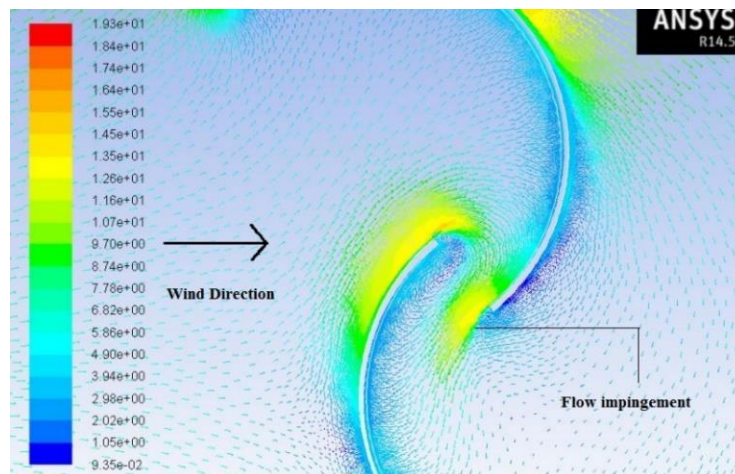


Fig. 3.8: Flow impingement in a Savonius turbine

3.3.2 Number of blades

Torque generated by the VAWT varies during the rotation of the turbine, as opposed to constant torque generated by conventional HAWTs, since blades come in contact with the air intermittently. This time varying torque places extra requirements on the electrical circuits connected to the generator to produce constant current. Intuitively, it can be noted that more the number of blades, lesser the magnitude of fluctuation in torque, since it can be expected that the probability of positive torque producing blade, in contact with the incoming wind, at any point in time, during the rotation, is higher with higher number of blades. The torque generated by the turbine can be generalised as

$$T = A_n(n, TSR) \sin(n\alpha) + T_m \quad (3.6)$$

Where, A_n is the amplitude of torque variation, n is the number of blades, α is the azimuthal angle (angle made by the blade with the incoming wind) and T_m is the mean torque about which fluctuation takes place. A_n can be expected to be low, and hence advantageous, for a higher bladed turbine. But it can be observed that higher the number of blades, higher the frequency of variation and also higher number of blades might result in aerodynamic interference between the blades resulting in lower T_m . To validate this hypothesis, a comparative study was conducted between a two bladed and a three bladed turbine. The geometric models and the domains of two bladed and three bladed configuration are shown in Figure 3.9 and 3.10 respectively

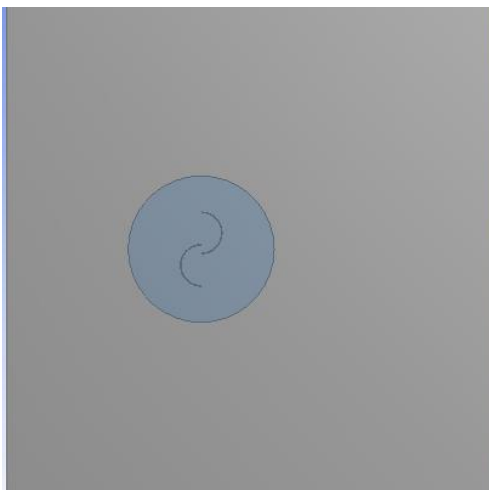


Fig. 3.9: Two bladed configuration

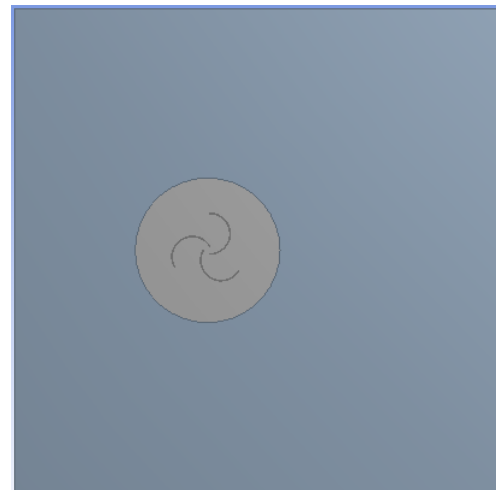


Fig. 3.10: Three bladed configuration

Sliding mesh technique was used to generate the rotating motion of the turbines. Coefficient of torque v/s azimuthal angle was plotted for TSR of 0.7 in Figure 3.11 for

both the configurations. It was seen that torque variation reduces with increased number of blades.

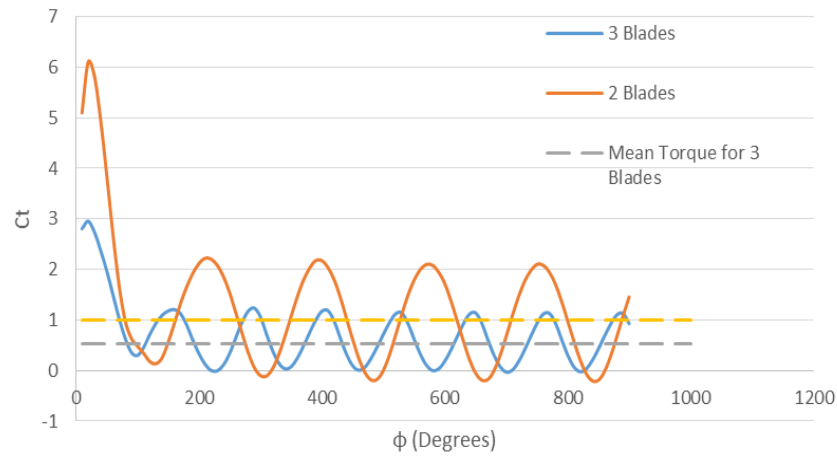


Fig. 3.11: Comparison of coefficient of torque between three bladed and two bladed configuration of vertical axis wind turbine

The power coefficients were calculated at various tip speed ratios and have been tabulated in Table 3.3.

Table 3.3: Power coefficients at various TSR for two and three bladed turbine

TSR	C _p		% Change
	Two Blades	Three Blades	
0.1	0.057	0.038	33.86
0.2	0.113	0.088	21.75
0.3	0.163	0.120	26.16
0.4	0.211	0.149	29.51
0.5	0.238	0.157	34.08
0.6	0.251	0.156	37.78
0.7	0.231	0.140	46.48
0.8	0.245	0.111	54.66
0.9	0.223	0.0675	69.68
1.0	0.187	0.011	94.01
1.1	0.134	0	-
1.2	0.065	0	-
1.3	0	0	-

The power coefficient is plotted for various tip speed ratios as shown in Figure 3.12.

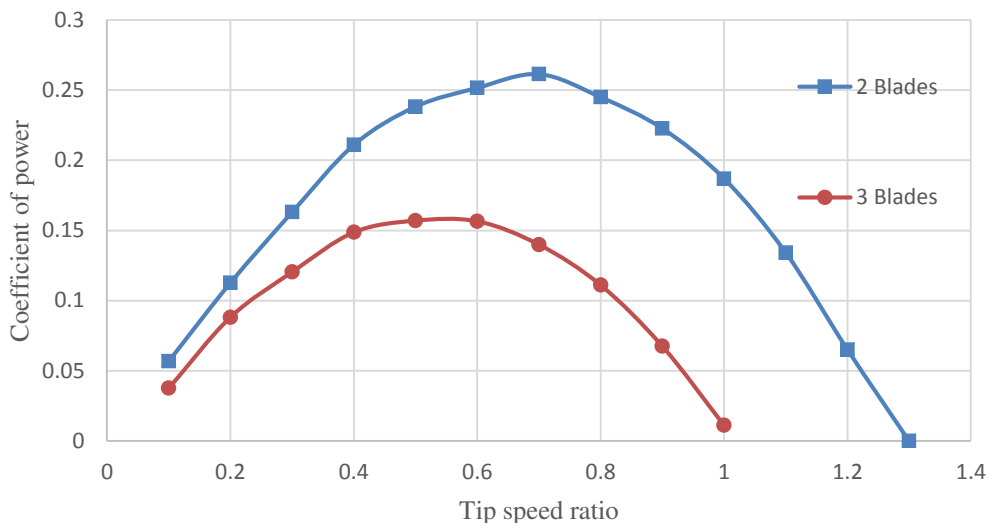


Fig. 3.12: Comparison of coefficient of power of three bladed and two bladed turbine at different tip speed ratios

3.3.3 Turbine arrays

Due to aerodynamic interactions in an array of wind turbines, the power output from a single turbine will be higher. Thus, to simulate the arrays and find the optimum number of turbines to be present in the array, a semi-circular profile was chosen for the blades and a two bladed turbine was selected over its three bladed counterpart.

In the design of turbine array, overlap will also be varied from $0.15d$ to $0.25d$. Aspect ratio, the ratio of length of the turbine to its diameter, will be maintained close to 2.

It is known that the wake of a HAWT adversely affects the efficiency of downstream turbines. Golecha et.al, [38] have shown that there is a positive influence on the C_p of each turbine, when two Savonius water turbines are placed in close proximity. Recent experimental work by Dabiri [34] has shown that Darrieus wind turbine also shows similar effect. A preliminary investigation was carried out to determine the influence of one Savonius turbine on the other. It is to be noted that the two turbines can rotate either in the same direction or in the opposite direction. When the turbines rotate in the same direction, the returning blade of one turbine destructively interacts with the advancing blade of the other, leading to reduced power generation. Hence, counter

rotating turbines were considered for simulation. Two sets of simulations were conducted. In the first case, the advancing blades were on the inside of the turbine system, hereafter referred to as *Advancing Inside*. In the latter case, returning blades were on the inside of the turbine system, hereafter referred to as *Advancing Outside*.

The computational domain was expanded to accommodate the second turbine. Domain width at the inlet was increased to $40d$ and domain length was increased to $30d$. Figure 3.13 shows the domain including the turbines.

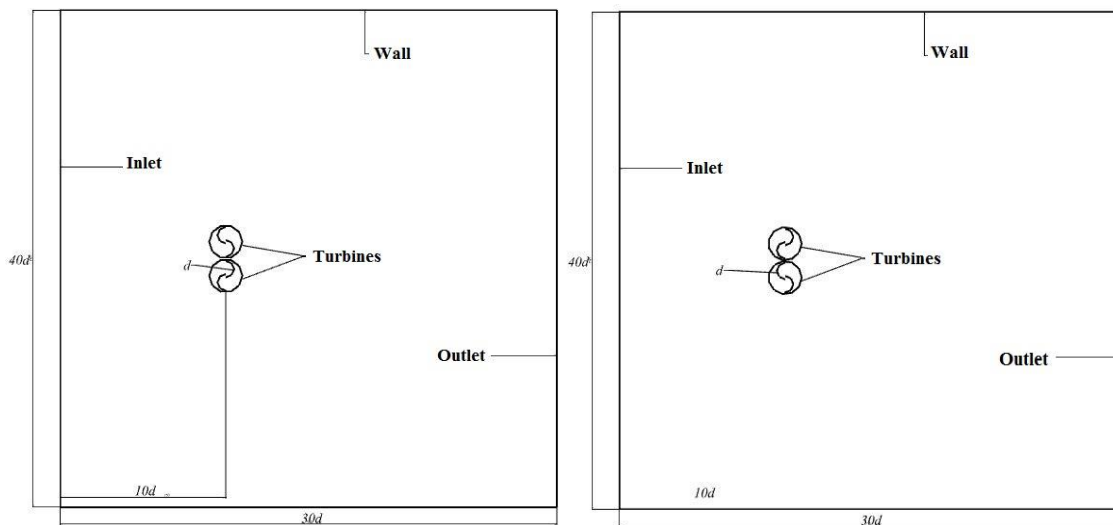


Fig. 3.13: Fluid flow domain

Meshing was carried out in a similar way as done for the isolated turbine. However, a higher number of cells were placed between the turbines, as this was the region of aerodynamic interaction between the two turbines. The resulting mesh had cells around 105,000 in number. The separation distance was maintained at $0.25d$, for the preliminary analysis. Simulation parameters were kept the same as described before with the sole change being that the two turbines were given opposite rotation relative to each other.

Simulation was carried out for TSRs ranging from 0.1 to 1.3, where the power generated reaches 0, in steps of 0.1 and the results are tabulated in Table 3.4. Percentage change was calculated by considering the C_p of an isolated turbine rotating at the same TSR.

Table 3.4: Comparison of coefficient of power for advancing inside and advancing outside turbines

Advancing Inside			Advancing Outside		
TSR	C_p	% Change	TSR	C_p	% Change
0.1	0.079	39.76	0.1	0.067	18.60
0.2	0.149	32.27	0.2	0.130	14.89
0.3	0.217	33.37	0.3	0.191	16.89
0.4	0.271	28.45	0.4	0.246	16.56
0.5	0.307	29.02	0.5	0.279	17.04
0.6	0.315	25.23	0.6	0.294	16.96
0.7	0.308	18.00	0.7	0.297	13.49
0.8	0.303	23.95	0.8	0.279	13.89
0.9	0.275	23.76	0.9	0.251	12.90
1.0	0.246	31.73	1.0	0.207	10.78
1.1	0.200	49.08	1.1	0.149	11.01
1.2	0.140	114.43	1.2	0.066	1.03
1.3	0	0	1.3	0	0

It is to be noted that the simulation was conducted for a coarse mesh and the results obtained are only indicative in nature. Further analysis was carried out to determine the exact increase in C_p . However, it is clear that turbines in close proximity, do in fact increase the efficiency of each other, which is evident from $C_p / C_t - \text{TSR}$ curves of Figure 3.14 and Figure 3.15.

It is also to be noted that the turbines in which the advancing blades were placed on the inside, produced higher power when placed otherwise. The reason behind this synergy phenomenon can be explained by considering Figure 3.16 and Figure 3.17 which shows the velocity field in the region between the turbines.

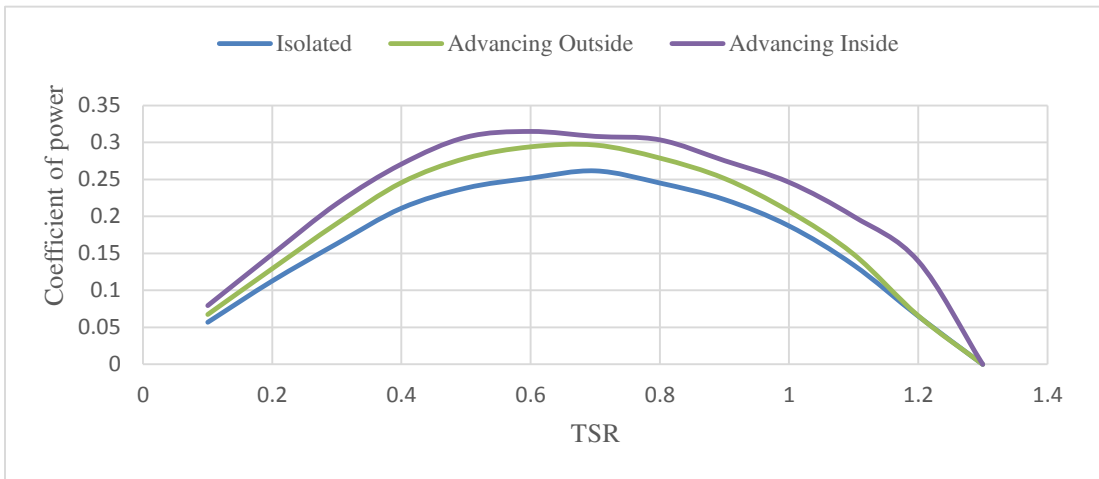


Fig. 3.14: Coefficient of power vs. Tip Speed Ratio for different configurations

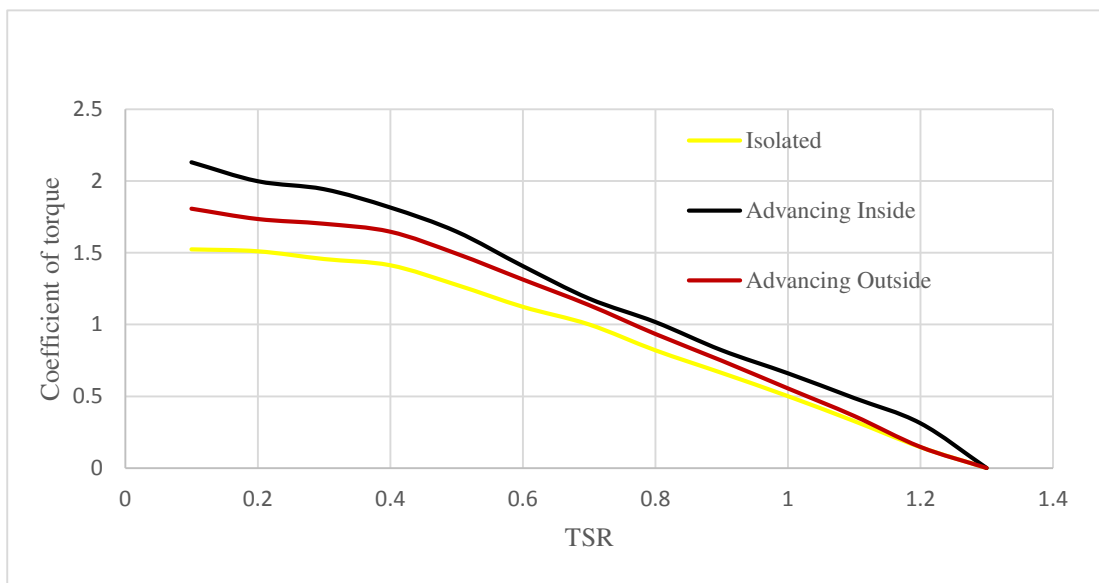


Fig. 3.15: Coefficient of torque vs. Tip Speed Ratio for different configurations

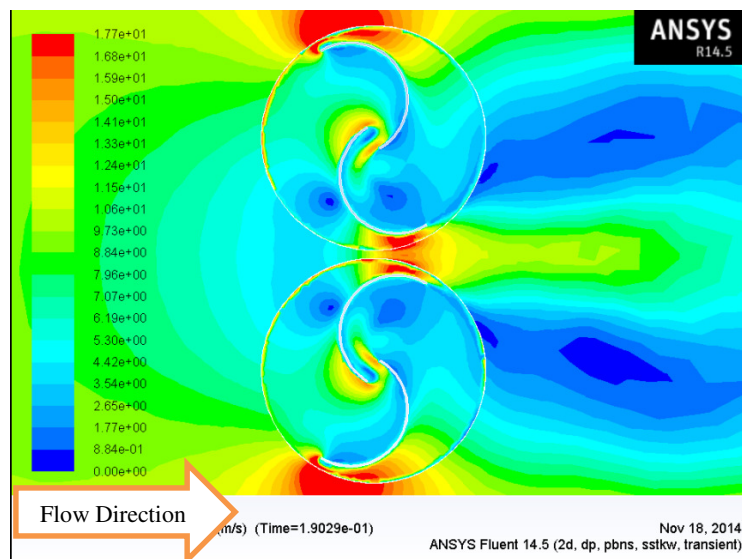


Fig. 3.16: Advancing outside velocity contours

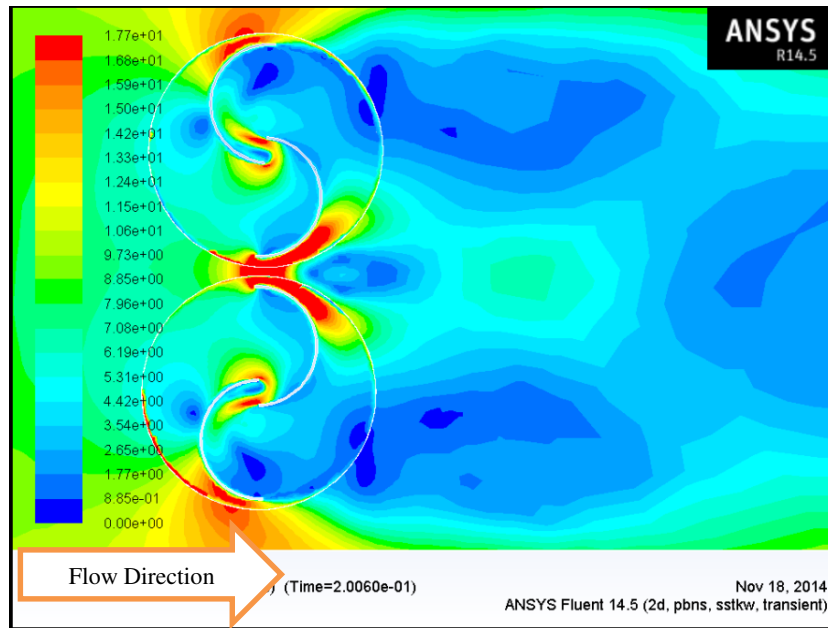


Fig. 3.17: Advancing inside velocity contours

As the blades of the two turbine come in close proximity, during their rotation, they constrict the flow region between them. To maintain a constant mass flow rate, the flow accelerates, resulting in velocities in excess of 17 ms^{-1} . The high velocity air impinges on the blades, imparting a higher force to the turbine blades, resulting in power generation in excess of that of an isolated turbine. When the advancing blade is on the inside of the array, the direction of the accelerated flow and the direction of rotation of turbine is the same and hence higher power is generated when compared to turbines with advancing blade on the outside of the turbine.

For a three turbine collinear array, simulations were carried out for TSR ranging from 0.5 to 0.8, since peak C_p occurs around 0.7 TSR. Separation distance between the turbines was maintained at $0.25d$. The flow domain was the same as that used for the two turbine array. Figure 3.18 shows the geometry of the array and Table 3.5 shows the C_p values obtained from simulations.

In the three turbine array, the turbine pair 2-3, forms an *Advancing Outside* configuration and the turbine pair 1-2, forms an *Advancing Inside* configuration. This means that their direction of rotation is mutually opposite to each other.

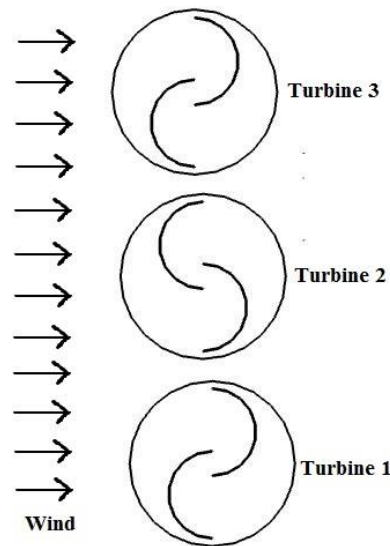


Fig. 3.18: Three turbine array

Table 3.5: Coefficient of power for the three turbine array

TSR	Turbine 1		Turbine 2		Turbine 3	
	C_p	% Change	C_p	% Change	C_p	% Change
0.5	0.288	20.92	0.212	-11.05	0.309	29.85
0.6	0.281	11.88	0.218	-13.48	0.347	38.05
0.7	0.268	2.55	0.181	-30.73	0.358	36.88
0.8	0.234	-2.56	0.163	-33.4	0.356	45.34

The results are plotted in Figure 3.19 and compared with the characteristic curve of an isolated turbine in the same range of TSRs. It is seen that the centre turbine's efficiency is sacrificed to increase the efficiency of the outer turbines. It is also to be noted that the turbine pair 2-3, forming an *Advancing Outside* configuration is more efficient than the turbine pair 1-2, forming an *Advancing Inside* configuration, which is inverse of the case of two turbines.

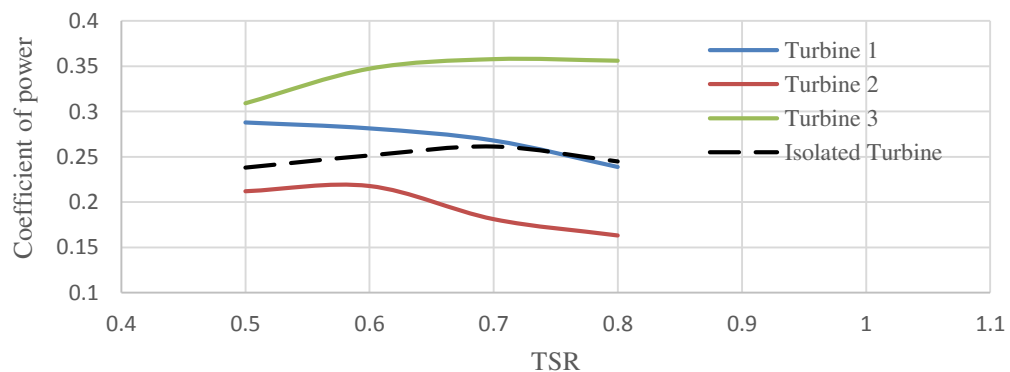


Fig. 3.19: Coefficient of power vs. Tip Speed Ratio for three turbines array

To decide on the number of turbines in the array, average C_p of both the twin turbine system and three turbine system is plotted for the required TSRs in Figure 3.20. It is evident that twin turbine system has a higher average C_p , of 12%, when compared to three turbine system, and hence is chosen for further studies.

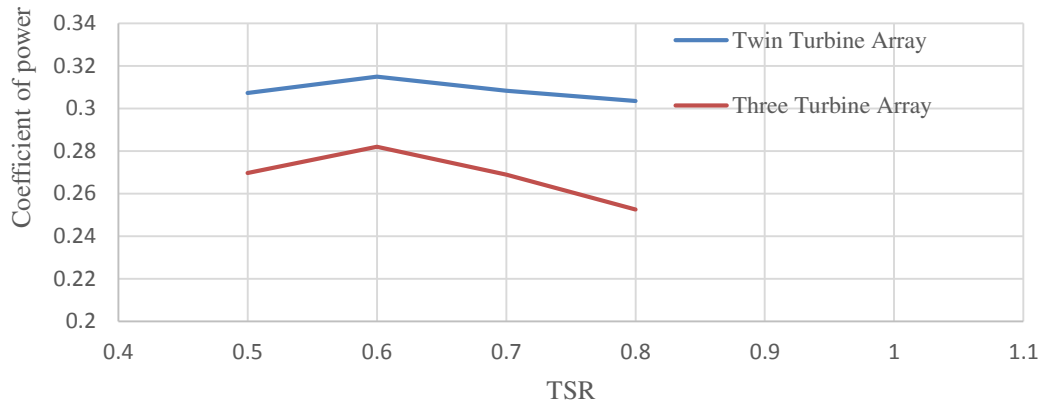


Fig. 3.20: Coefficient of power vs. Tip Speed Ratio for two and three turbine arrays

Based on the inferences drawn from the above simulation studies, the parameters of the twin vertical axis wind turbines were finalised as shown in Table 3.6.

Table 3.6: Optimal settings for harnessing power from Savonius turbine

Parameter	Optimal setting
Number of blades	Two
Blade profile	Semicircular
Number of turbines in the array	Two

3.4 Modeling of twin-vertical axis wind turbines

Twin-vertical axis wind turbines have many design parameters like rotor angle offset, angle between the turbines and the distance between turbines. Also the overlap ratio of each turbine in the array and their tip speed ratios can be considered as design parameters. These variables affect the power output from the system. A particular set of variables can be chosen among the five variables for which the power output can be determined.

It is vital to understand the changes in power output from the system with respect to these variables. Thus, detailed modeling of the system by varying all these parameters has been considered to find their effects on the power output. Some salient parameters are defined in the next section.

3.4.1 Rotor angle offset

It is the angle made by the blades of one turbine with the blades of the other, which is shown in Figure 3.21. It is expected that the flow from the advancing blade of one turbine interacts with the advancing blade of the other turbine, contributing constructively or destructively to the power generation of the second turbine. To study this effect, the Rotor Angle Offset was varied from -60° to 90° . θ is positive in the counter clockwise direction.

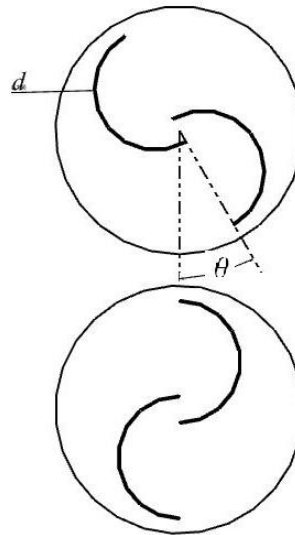


Fig. 3.21: Rotor angle offset

3.4.2 Angle between turbines

It is the angle between the line joining the centres of the turbine and a line perpendicular to the free stream velocity. It is shown in the Figure 3.22. As the angle between the turbines, α , varies from 0° to 90° , the second turbine begins to come in the wake of the first and hence its power output gets effected. When the angle equals 90° , the second turbine is completely in the wake of the first and hence its power output reduces drastically. Hence this parameter is only simulated from 0° to 60° .

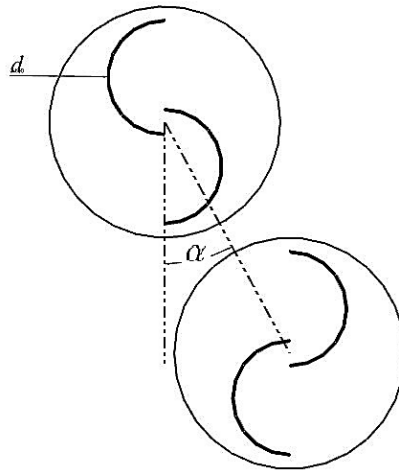


Fig. 3.22: Angle between turbines

3.4.3 Distance between turbines

Separation distance between the turbines is the distance between the tip of the blade of one turbine with the tip of the other, when the Rotor Angle Offset is 0° . It is shown in the Figure 3.23. Separation distance plays the same role for the twin turbine system as overlap plays for the single turbine. Larger distance between the turbines reduces the flow acceleration, decoupling the two turbines. Smaller distance between the turbines, creates a blockage effect during the rotation of the turbines, again contributing to lower C_p . Again, an optimum value of separation distance is needed and hence this parameter is varied from $0.1d$ to $0.3d$.

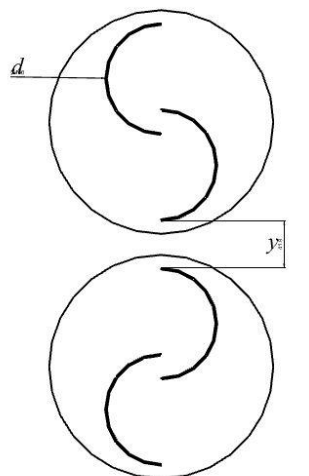


Fig. 3.23: Distance between turbines

3.4.4 Tip Speed Ratio (TSR)

It is the ratio of the speed of the tip of the blade to the speed of the wind at the periphery. C_p varies with TSR and hence this parameter has been chosen. Since peak C_p during the

initial analyses occurred between 0.6 and 0.7, this parameter is varied in the range of 0.5 – 0.7

3.4.5 Overlap Ratio

Lower overlap between the blades, results in lower mass of air impinging on the returning blade, and hence lower reduction in drag and lower C_p . Higher overlap between the blades, results in lower acceleration of the fluid and hence lower velocity of impingement resulting in lower C_p . Hence an optimum amount of overlap is to be provided. An overlap between 0.15 – 0.25 is optimum for an isolated turbine. Hence, overlap has been varied in this range in the current study.

3.5 Orthogonal array testing

Based upon the initial simulation results of a single rotor Savonius turbine, a twin turbine system has been devised. The modeling of this setup is considered in this section. Modeling of the twin turbines were done to observe the changes in power output with varying distance and other parameters of the two turbines. The parameters that were varied and their levels are shown in Table 3.7.

Based upon the theory of orthogonal arrays, L_{18} orthogonal array was chosen for the testing purpose. All the design variables listed in Table 3.7 were incorporated into the array. The experiments have been performed for a turbine of diameter 100 mm and have been shown in Table 3.8.

Table 3.7: Parameter variables and their levels

Variable	Level 1	Level 2	Level 3	Level 4	Level 5	Level 6
Rotor angle offset	-60°	-30°	0°	30°	60°	90°
Tip speed ratio	0.5	0.6	0.7	-	-	-
Overlap (mm)	15	20	25	-	-	-
Angle between turbines	0°	30°	60°	-	-	-
Distance between turbines (mm)	10	20	30	-	-	-

Table 3.8: L₁₈ orthogonal array experiments

Simulation no.	Rotor Angle Offset (°)	Tip Speed Ratio	Overlap (mm)	Angle between turbines (°)	Distance between turbines (mm)
1	-60	0.5	20	0	20
2	-60	0.6	20	30	20
3	-60	0.7	25	60	30
4	-30	0.5	15	30	20
5	-30	0.6	20	60	30
6	-30	0.7	25	0	10
7	0	0.5	20	0	30
8	0	0.6	25	30	10
9	0	0.7	15	60	20
10	30	0.5	25	60	20
11	30	0.6	15	0	30
12	30	0.7	20	30	10
13	60	0.5	20	60	10
14	60	0.6	25	0	20
15	60	0.7	15	30	30
16	90	0.5	25	30	30
17	90	0.6	15	60	10
18	90	0.7	20	0	20

The number of elements in the mesh were around 2,05,000 which is higher than that used for the simulations of the single turbine. This was done to obtain a more accurate result. The simulation setup and boundary conditions were the same as that of the single turbine and the results of the orthogonal array testing experiments are presented in the Table 3.9. The table shows change in C_p from a single turbine for all the 18 experiments.

Table 3.9: Results from the orthogonal array experiments

Simulation No	C_t	C_p	% Change from single turbine	Simulation No	C_t	C_p	% Change from single turbine
1	0.579	0.175	-32.78	10	0.453	0.153	-41.10
2	0.683	0.262	0.54	11	0.600	0.217	-16.49
3	0.503	0.238	-8.46	12	0.468	0.209	-19.69
4	0.735	0.222	-14.73	13	0.648	0.206	-20.57
5	0.409	0.156	-39.78	14	0.499	0.202	-22.20
6	0.466	0.220	-15.22	15	0.598	0.253	-2.85
7	0.665	0.212	-18.42	16	0.587	0.198	-23.80
8	0.448	0.181	-30.22	17	0.451	0.163	-37.26
9	0.331	0.139	-46.29	18	0.634	0.283	8.83

Percentage change in C_p was calculated with respect to the C_p of an isolated turbine at TSR 0.7, which is 0.261. It is noted that most of the combination of different parameters produce reduction in power coefficient. Only the 18th configuration shows significant increase in power coefficient and hence experimental validation was carried out for the 18th configuration.

3.6 Summary

The chapter on modeling and simulation of Savonius turbines considered the various configurations of a single rotor Savonius turbine and aimed to find the best parameters among them. Detailed simulations of twin Savonius rotors were also presented and orthogonal array testing experiments were devised.

**DESIGN AND FABRICATION OF THE TWIN
VERTICAL AXIS WIND TURBINE SETUP**

A twin vertical axis wind turbine was designed using the simulation results obtained in section 3.5 and fabricated. In this chapter, the fabrication process of each of the components has been explained. The reason for using the particular material and the manufacturing process has been presented. The electrical loading circuit was devised and the technical details have been presented. Finally, the cost incurred for procuring materials and manufacturing of the setup has been tabulated.

4.1 Turbine dimensioning

The following assumptions are made to obtain the turbine dimensions:

A wind velocity, ' V ', of 10 ms^{-1} , air density, ' ρ ', of 1.225 kg m^{-3} and a coefficient of performance of the turbine, ' C_p ', of 0.20.

In order to get the rated power output of 50 W from the generator, each turbine in the twin turbine system should produce at least 25 W. Further, it is necessary to run the generator at a speed of 600 RPM which is its rated speed.

From the simulations, the peak power is observed at 0.7 TSR which corresponds to 495 RPM if the turbine blade has a diameter of 0.153 m. To match the peak power RPMs, a gear ratio of 1.2 is selected.

From equation 3.1, the turbine area of 0.2 m^2 is necessary to generate the required power. Turbine diameter of 0.28 m (based on available pipe diameter) and length of 0.72 m is selected, resulting in an aspect ratio of 2.5, close to the ideal value of two [15].

4.2 Assembly

Based on the dimensions obtained, the twin turbine setup was designed in Solidworks and the salient dimensions and isometric view of the same is shown in Figure 4.1 (a) and Figure 4.1 (b) respectively. The final fabricated setup is shown in Figure 4.2. The manufactured components were assembled as per the drawing attached in the appendix.

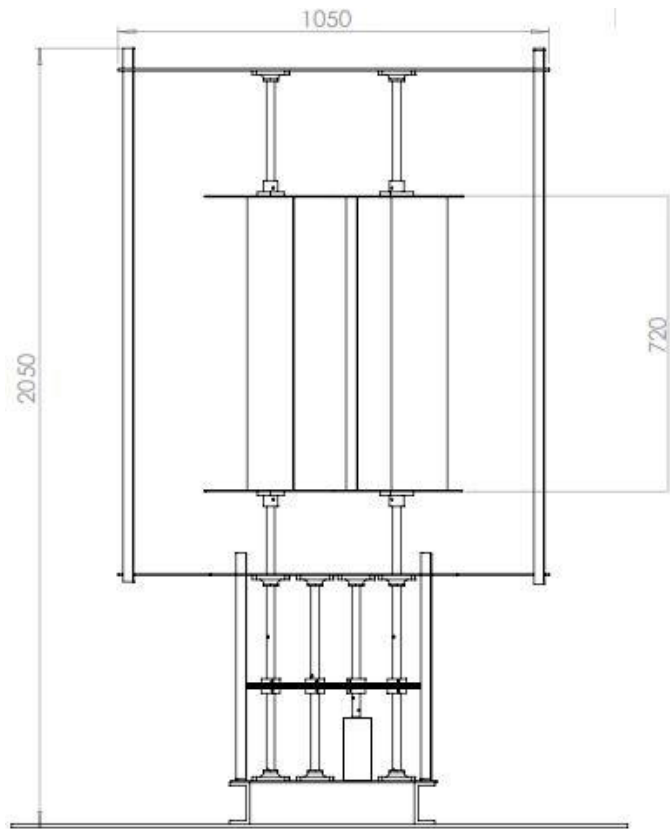


Fig. 4.1 (a): Front view of the T-VAWT setup

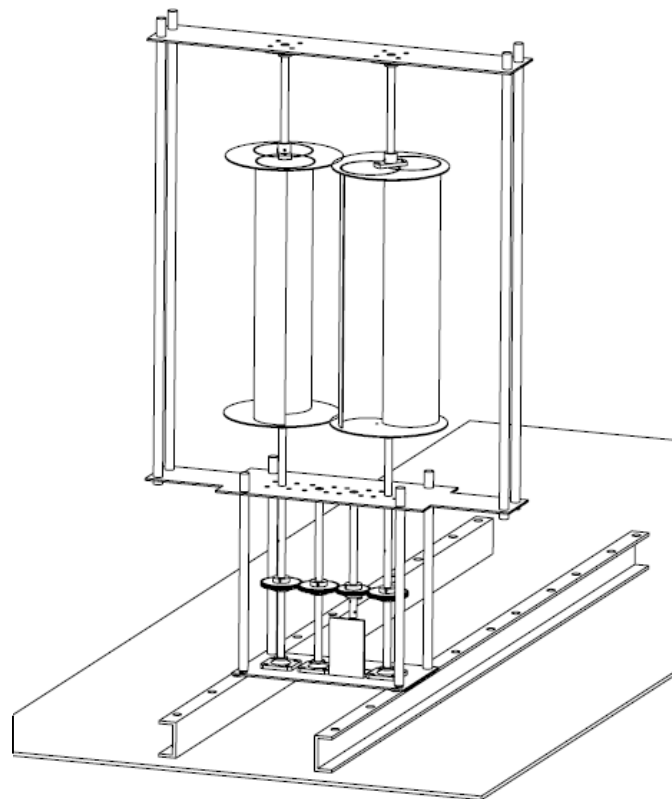


Fig. 4.1 (b): Isometric view of the T-VAWT

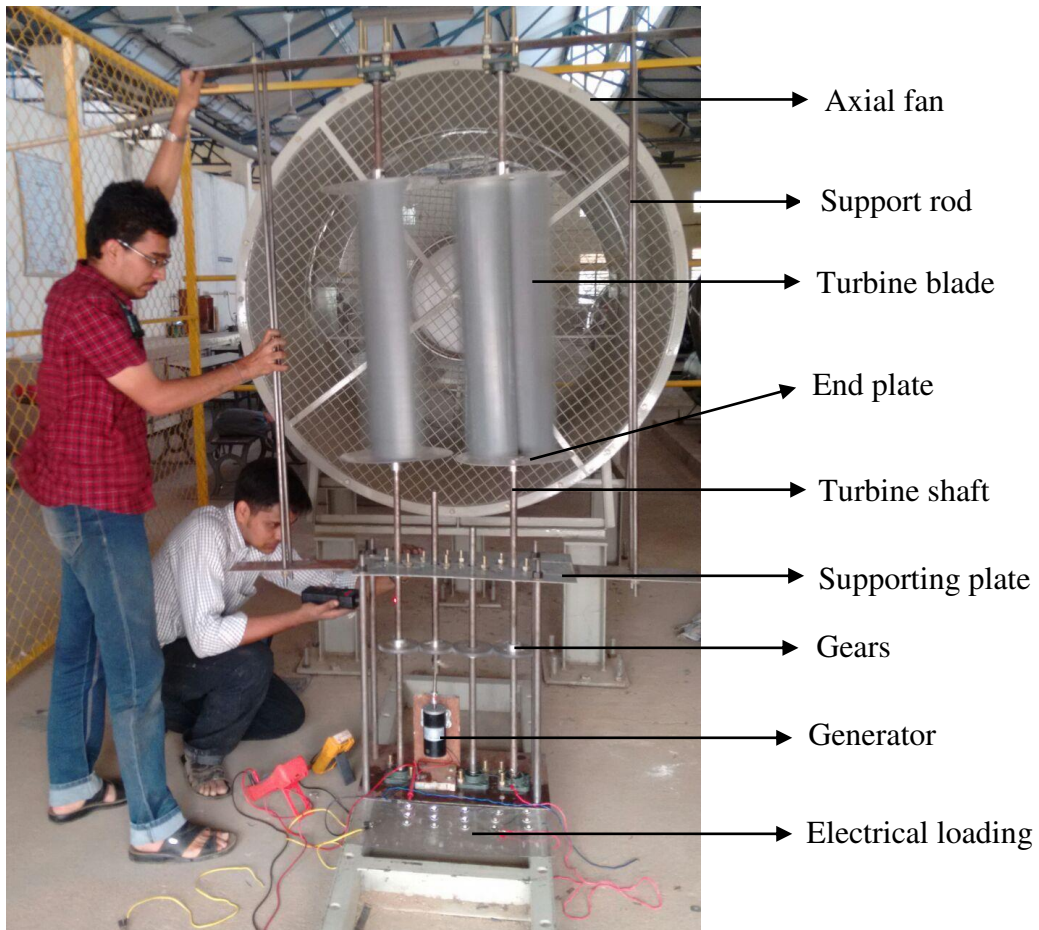


Fig. 4.2: Twin Vertical Axis Wind Turbine (T-VAWT) assembly

The detailed engineering drawings and the dimensions of each part are provided in the appendix. The manufacturing process and key attributes of each part have been elucidated below.

4.2.1 Turbine blades

The wind turbine blade fabricated is as shown in Figure 4.3. The blade material is PVC and the diameter and length of the blade is 156 mm and 720 mm respectively. The surface area and the curvature of the blade provides a surface to harness the wind energy. The blade is fabricated by cutting a 156 mm diameter PVC commercial pipe along the length and inserting it into the grooves of the end plate. Two such blades are fabricated for the twin turbine system. The engineering drawing of the part is attached in the appendix.

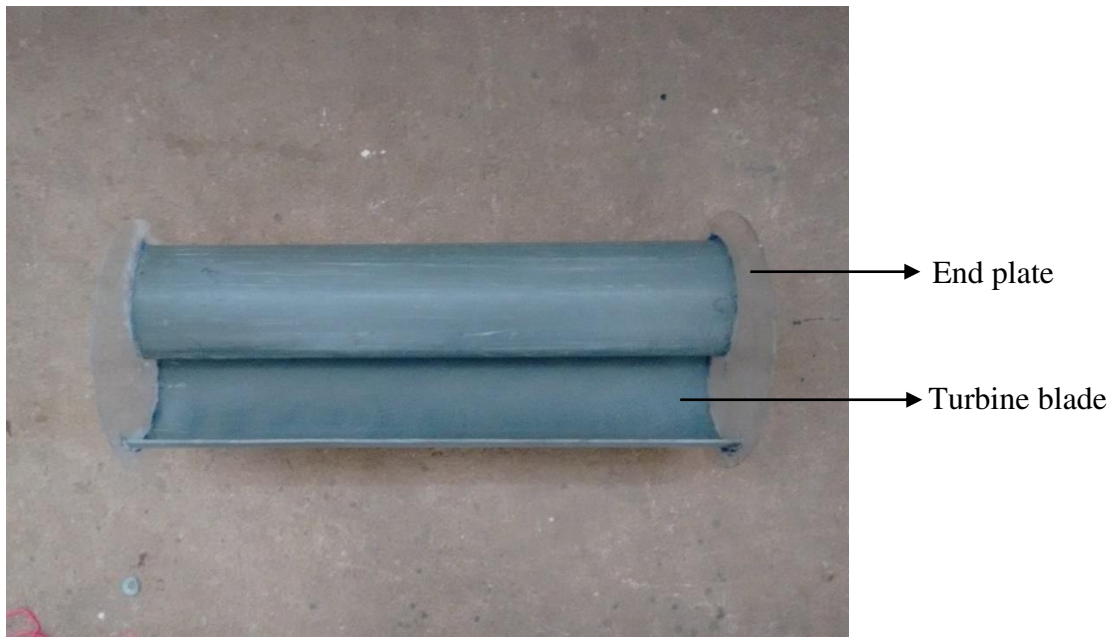


Fig. 4.3: Blade profile and end plates

4.2.2 End plates

The end plate, which holds the turbine blades in position, is shown in Figure 4.3. The material used in the form of a circular disc is acrylic. The circular disc has a diameter of 300 mm. The purpose of using the end plate is to prevent axial flow of wind into the turbine as well as provide support to the turbine blades by virtue of grooves etched as per the blade profile. It also has holes drilled near the centre to attach the flanges. Four such end plates are fabricated for the twin turbine system. The engineering drawing of the part is attached in the appendix.

4.2.3 Flanges



Fig. 4.4: Flanges

The flanges used to connect the shaft with the turbine blades are as shown in Figure 4.4. It is made of Aluminium 2 series material which is turned and milled to the required dimension. Four such flanges are used to support the twin turbine system. The engineering drawing of the part is attached in the appendix.

4.2.4 Shafts

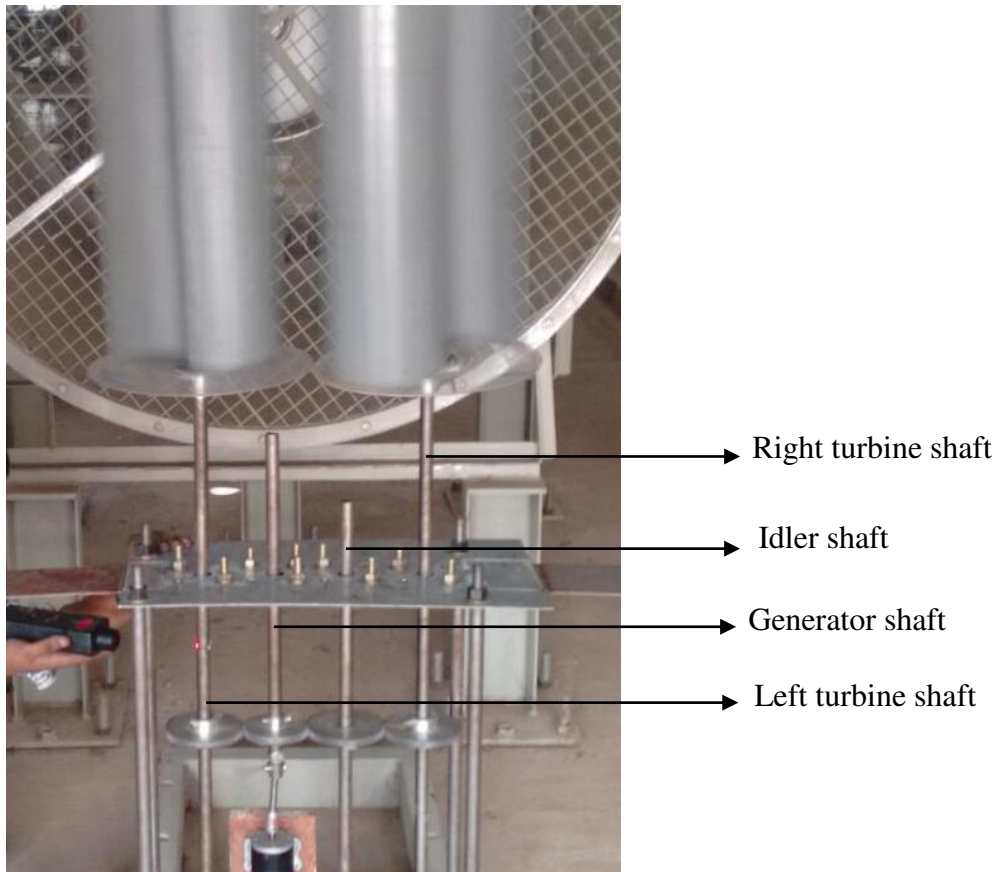


Fig. 4.5: Shafts used in the assembly

Shafts are the elements used for power transmission from the turbine system. All the shafts used in the system have a diameter of 20 mm and are shown in Figure 4.5. The idler shaft has a length of 700 mm and is used to obtain a contra rotating system of turbines by the virtue of gears. The generator shaft, having a length of 350 mm, is coupled with the generator to produce power. The main shafts from the turbines, having a length of 850 mm, are designated as the turbine shafts. These shafts are linked through an elaborate gearing system. The engineering drawing of the part is attached in the appendix.

4.2.5 Gears

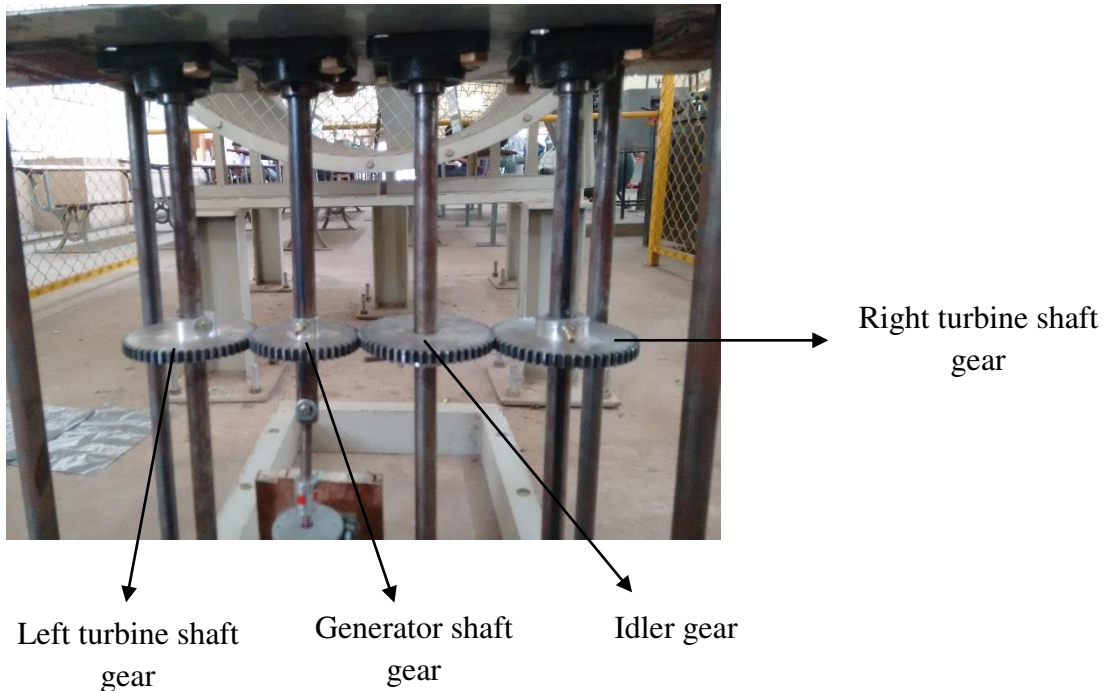


Fig. 4.6: The gearing arrangement of the assembly

A gearing system is used in the setup as a part of the power transmission unit. The turbine generates its rated power at 495 RPM whereas the generator is rated at 600 RPM. Hence, a gear ratio of 1.2 has been used. These gears link the turbine shaft with the generator shaft. An idler gear is also used to obtain a contra rotating system. The idler gear and the gears on the turbine shaft have 54 teeth and a pitch circle diameter of 108 mm. The generator gear has 45 teeth and a pitch circle diameter of 90 mm. The gear material used is Aluminium 2 series and the fabricated gearing system is as shown in Figure 4.6. The engineering drawing of the part is attached in the appendix.

4.2.6 Supporting plates

The supporting plates are used to provide support to the shafts and house the bearings. Mild steel plates are used for this purpose. Holes are drilled as per the required dimensions. The bottom plate and the middle plate has dimensions of 500 mm \times 250 mm \times 3 mm. There are supporting extensions welded into the middle plate for extra support and they have dimensions of 480 mm \times 100 mm \times 3 mm. Finally, the top plate has dimensions of 1300 mm \times 100 mm \times 3 mm. The engineering drawing of the part is attached in the appendix.

4.2.7 Supporting rods

The twin turbine setup requires supporting rods to hold the supporting plates in position. These rods are made of mild steel. Support rods from the bottom plate to the middle plate have a diameter of 20 mm and a length of 700 mm. Support rods from the middle plate to the top plate have a diameter of 14 mm and a length of 1300 mm. The engineering drawing of the part is attached in the appendix.

4.3 Assembly for preliminary testing



Fig. 4.7: Preliminary testing

The single turbine shown in Figure 4.7 was fabricated to test the stability of the turbine during operation.

4.4 Description of the test rig

The test rig comprises of the axial fan with 20 hp motor, T-VAWT setup, base rails and the control unit.

4.4.1 Axial fan

The axial fan used to simulate the air is shown in Figure 4.8. They move the airstream along the axis or shaft of the fan. The air is pressurized by the aerodynamic lift generated by the fan blades, much like a propeller, or an airplane wing.



Fig. 4.8: Axial fan

The specifications of the axial fan is shown in Table 4.1.

Table 4.1: Axial fan specifications

Full load current	21.9 A
Motor type	Three phase induction motor
Motor speed	3500 RPM
Rotor diameter	1.5 m
Rotation	Counter clockwise from front
Fan blade material	Aluminum
Housing material	Iron

4.4.2 Loading conditions

The objective of the electrical loading circuit is to absorb the power generated by the wind turbine and measure the same. The components that have been used and their specifications are as shown in Table 4.2.

Table 4.2: Electrical loading components

Components	Specifications
Coupling	Input: 10mm shaft, Output: 8mm shaft
Dynaflux PMDC Motor (Used as Generator)	16V DC, 3.9A, 50W
Voltage Regulator	15V DC regulated

Light Emitting Diodes	3W, 2V
Heat Sinks	For LED's
Resistors	150 Ω, 0.5W
	4.7 Ω, 2W
Button Switches	10A maximum capacity

The electrical loading circuit consists six rows of 3 W LEDs connected in parallel, each row containing three LEDs in series as shown in Figure 5.9. Button switches are provided for each loop to be loaded individually. The net circuit consumes a power of 50 W at an input voltage of 12 V.

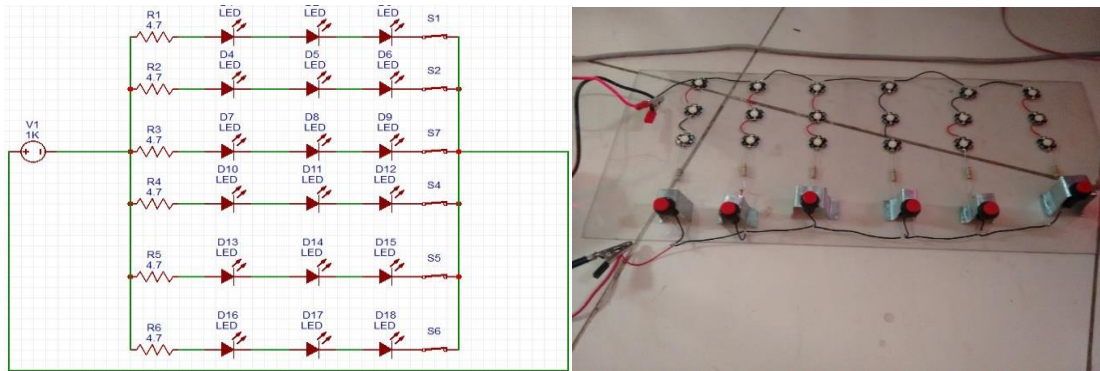


Fig. 4.9: Schematic and the fabricated loading circuit

4.4.3 Generator specifications

The generator used to harness power from the wind turbines is actually a Dynaflux make PMDC (permanent magnet DC) motor. The specifications are listed in Table 4.3.

Table 4.3: Generator specifications

Model name	SM02A
Power rating (W)	50
DC Voltage current (V)	16
DC Current rating (A)	5.2
Speed (RPM)	600
Torque (Kg-cm)	3.2
Length (mm)	130
Weight (Kg)	1.2
Mounting type	Face

4.5 Cost analysis

The cost analysis of the project is presented in Table 4.4.

Table 4.4: Cost analysis

Sl. no.	Specification	Cost (INR)
1	Generator	2,863.00
2	Electrical components	610.00
3	Bearings	1,688.00
4	Aluminum material	3,600.00
5	Shafts	1,541.00
6	End plates	700.00
7	Base plates	815.00
8	Blades	400.00
9	Nuts, bolts, washers	780.00
10	Machining cost	4,645.00
11	Miscellaneous	760.00
Total		18402.00

4.6 Summary

In this chapter, the twin vertical axis wind turbine assembly was presented along with a detailed description of the constituent parts. The parts were manufactured based upon the drawings attached in the appendix and were assembled. The electrical loading circuit which was used to load the wind turbine was also explained and finally, the cost analysis of the project was also presented.

RESULTS AND DISCUSSIONS

The simulation results on single and twin Savonius turbines have been examined in this chapter. The fabricated turbine was tested at a wind velocity of 10 ms^{-1} and the results are discussed. An empirical relation between the coefficient of performance and the geometrical parameters of the array has been developed using non-linear regression technique and validated with the simulations.

5.1 Simulation studies on single Savonius turbine

Figure 5.1 shows the power coefficients of two bladed and three bladed configuration from the simulation results from section 4.3. It can be seen that the two bladed configuration is much more efficient than the three bladed counterpart.

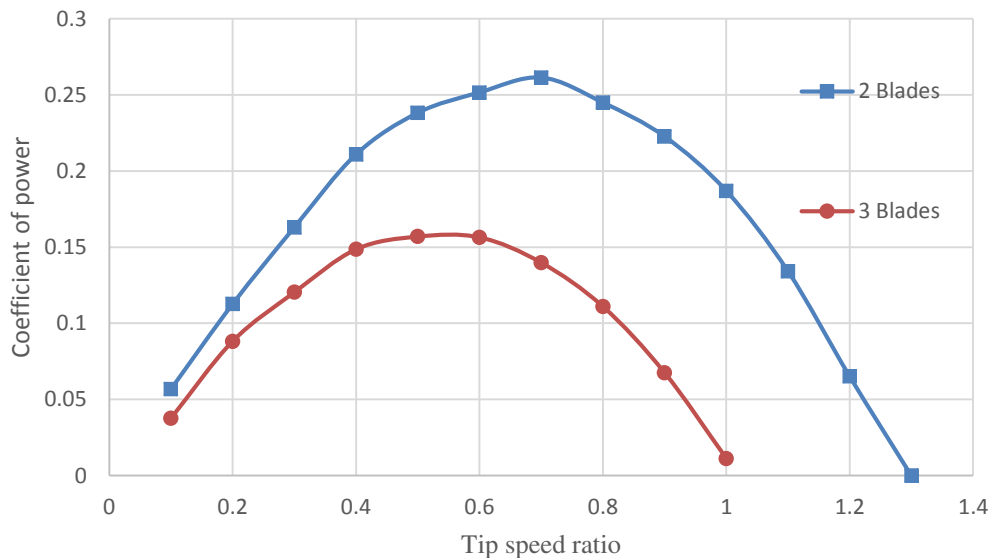


Fig. 5.1: Comparison of coefficient of power of three bladed and two bladed turbine at different tip speed ratios

The reason for the drastic reduction in power of the three blade turbine can be explained using Figure 5.2 and 5.3, which depict the velocity vectors near the overlap of the blades.

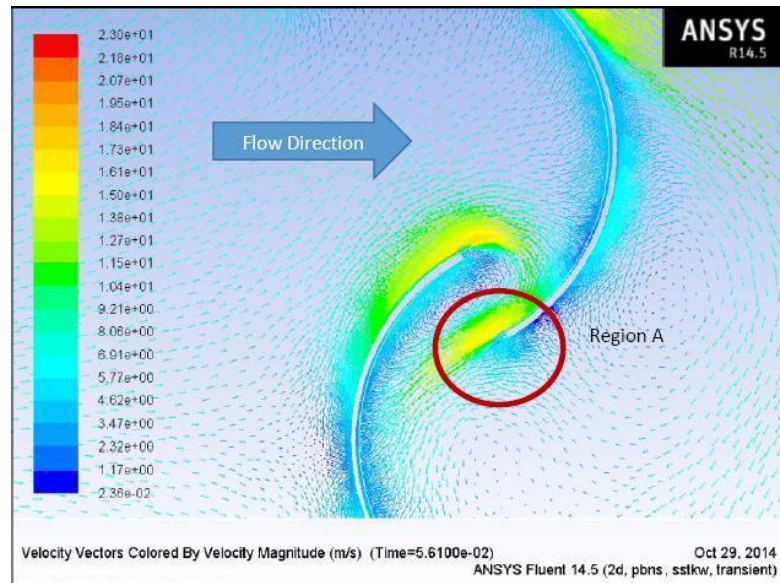


Fig. 5.2: Velocity vectors near the overlap of the two blades

With reference to Figure 5.2, the blade moving along the flow is the advancing blade and the other, the returning blade. At the shown configuration, the flow from the concave side of the advancing blade impinges on the concave side of the returning side, converting its dynamic pressure to static (Region A). This phenomenon reduces the pressure differential across the convex and concave surfaces of the returning blade, resulting in reduced drag on the returning blade. This increases the torque generated and hence the power.

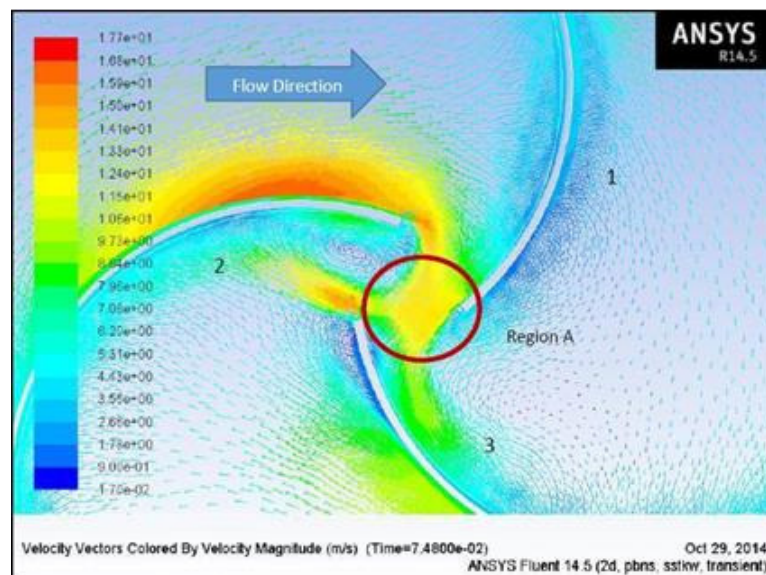


Fig. 5.3: Velocity vectors near the overlap of three blades

With reference to Figure 5.3, blade 1 is the advancing blade. As seen, the flow “slips” over blade two, and impinges on blade one. Major part of the flow from blade one (Region A) impinges on blade three and flows through, without effecting the blade two at all. The remaining flow impinges on blade two, resulting in pressure conversion from dynamic to static. In two bladed turbines, most of the flow is used in reducing pressure differential across the returning blade. Here, only a part of the flow reduces the pressure differential and hence three bladed turbine experiences more drag resulting in overall lower torque and power generated.

5.2 Simulation studies on Twin Vertical Axis Wind Turbines

The orthogonal array testing conditions described in section 3.5 were subject to simulations and C_p obtained for the same has been tabulated in Table 5.1. Figures 5.4 and 5.5 shows sample meshed geometries for simulation numbers 3 and 14 respectively.

Table 5.1: Results from the orthogonal array experiments

Simulation No	C_t	C_p	% Change from single turbine	Simulation No	C_t	C_p	% Change from single turbine
1	0.579	0.175	-32.78	10	0.453	0.153	-41.10
2	0.683	0.262	0.54	11	0.600	0.217	-16.49
3	0.503	0.238	-8.46	12	0.468	0.209	-19.69
4	0.735	0.222	-14.73	13	0.648	0.206	-20.57
5	0.409	0.156	-39.78	14	0.499	0.202	-22.20
6	0.466	0.220	-15.22	15	0.598	0.253	-2.85
7	0.665	0.212	-18.42	16	0.587	0.198	-23.80
8	0.448	0.181	-30.22	17	0.451	0.163	-37.26
9	0.331	0.139	-46.29	18	0.634	0.283	8.83

From the Table 5.1, it is seen that most of the configurations showed a decrease in efficiency due to destructive interference between the turbine blades. However, experiment 18 resulted in an increase in power coefficient which may be due to the acceleration of the local velocity field between the two turbines.

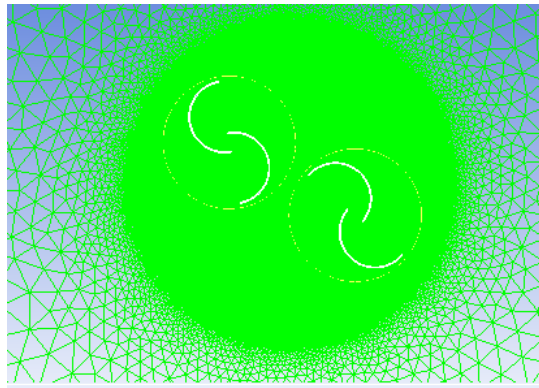


Fig. 5.4: Geometry number 3

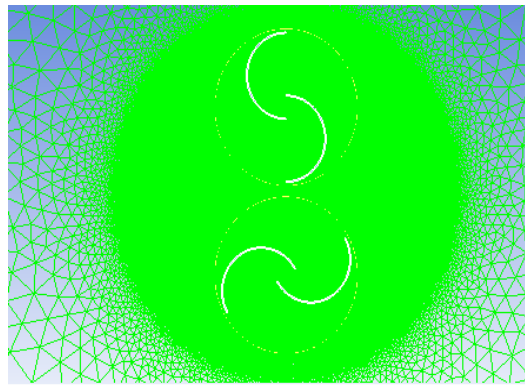


Fig. 5.5: Geometry number 14

5.3 Nonlinear regression analysis

From the 18 simulations conducted above, it is possible to obtain a functional relationship of the form

$$C_p = f \left\{ \begin{array}{l} \text{Rotor Angle Offset, TSR, Overlap,} \\ \text{Angle between turbines, Separation distance} \end{array} \right\}$$

Since the orthogonal array obtains the C_p at uniformly distributed points in the 5 dimensional space of the parameters, the functional relationship so obtained, is expected to be accurate in the range of values for which the simulations were conducted. In this regard nonlinear regression analysis was employed.

Since the aerodynamic interaction between the blades is nonlinear in nature, nonlinear regression analysis was applied to obtain the functional relationship between the variables. Cubic as well as quadratic functional forms were used and comparison between them is shown in Table 5.2. Minitab was used to determine the set of parameters in the regression model.

Table 5.2: Error comparison of quadratic and cubic regression models

Simulation No.	C_p	C_p (From quadratic regression model)	% Error	C_p (From cubic regression model)	% Error
1	0.175	0.177	1.379	0.173	-2.122
2	0.261	0.263	0.725	0.266	0.908
3	0.238	0.239	0.441	0.235	-1.713
4	0.222	0.221	-0.058	0.219	-1.345
5	0.156	0.156	-0.491	0.160	2.573
6	0.220	0.221	0.086	0.220	-0.314
7	0.212	0.212	0.067	0.211	-0.626
8	0.181	0.181	-0.055	0.181	-0.187
9	0.139	0.139	-0.548	0.140	0.915
10	0.153	0.152	-0.528	0.151	-0.742
11	0.217	0.216	-0.375	0.218	0.749
12	0.209	0.208	-0.344	0.209	0.461
13	0.206	0.202	-2.100	0.207	2.162
14	0.202	0.197	-2.313	0.205	3.696
15	0.253	0.248	-1.773	0.251	1.258
16	0.198	0.184	-6.977	0.198	7.094
17	0.163	0.149	-8.364	0.163	8.443
18	0.283	0.268	-5.154	0.282	4.768

It is seen that the quadratic model fits the data with minimal error when compared to the cubic model. The quadratic model obtained from the regression analysis is,

$$\begin{aligned}
 C_p = & 0.8427 + 0.000987a - 3.074b + 0.01841c + 0.007549d - 0.007234e \\
 & + 0.000005a^2 + 2.533b^2 - 0.000437c^2 - 0.000047d^2 \\
 & - 0.00007e^2 - 0.001259ab + 0.000003ad - 0.000039ae \\
 & - 0.008012bd + 0.02402be - 0.000068de
 \end{aligned}$$

Where, ‘ a ’ is the Rotor angle offset, ‘ b ’ is the Tip speed ratio, ‘ c ’ is the Overlap, ‘ d ’ is the angle between turbines and ‘ e ’ is the separation distance

5.3.1 Validation of the regression equation

The regression equation obtained from the orthogonal array experiments was validated for different sets of design variables. The two sets of variables are as shown in Table 5.3.

Table 5.3: Variables for regression equation validation

Set 1		Set 2	
Variable	Level	Variable	Level
Rotor angle offset	0°	Rotor angle offset	30°
Tip speed ratio	0.6	Tip speed ratio	0.5
Overlap	20 mm	Overlap	15 mm
Angle between turbines	30°	Angle between turbines	0°
Distance between turbines	30 mm	Distance between turbines	20 mm

The simulations were performed on the two sets of variables in ANSYS Fluent and the power coefficient was determined. The variables are also substituted in the regression equation to validate with the simulation. The results of these simulations are presented in Table 5.4.

Table 5.4: Regression equation validation

Variable set no.	C _p from simulations	C _p from regression equation	% error
1	0.207756	0.234674	-12.9565
2	0.203236	0.17612	13.3421

The regression equation is found to be quite accurate and agrees well with the simulation output. The error obtained can be rectified by conducting more orthogonal array experiments and fitting a better curve to the obtained power coefficient.

5.4 Wind mapping

The optimum positioning of the wind turbine is obtained by wind mapping studies on the axial fan. Considering a domain of 1.4 m diameter, at various points in this domain, wind speeds are measured. The points of measurement of wind speed measurement are as shown in Figure 5.6.

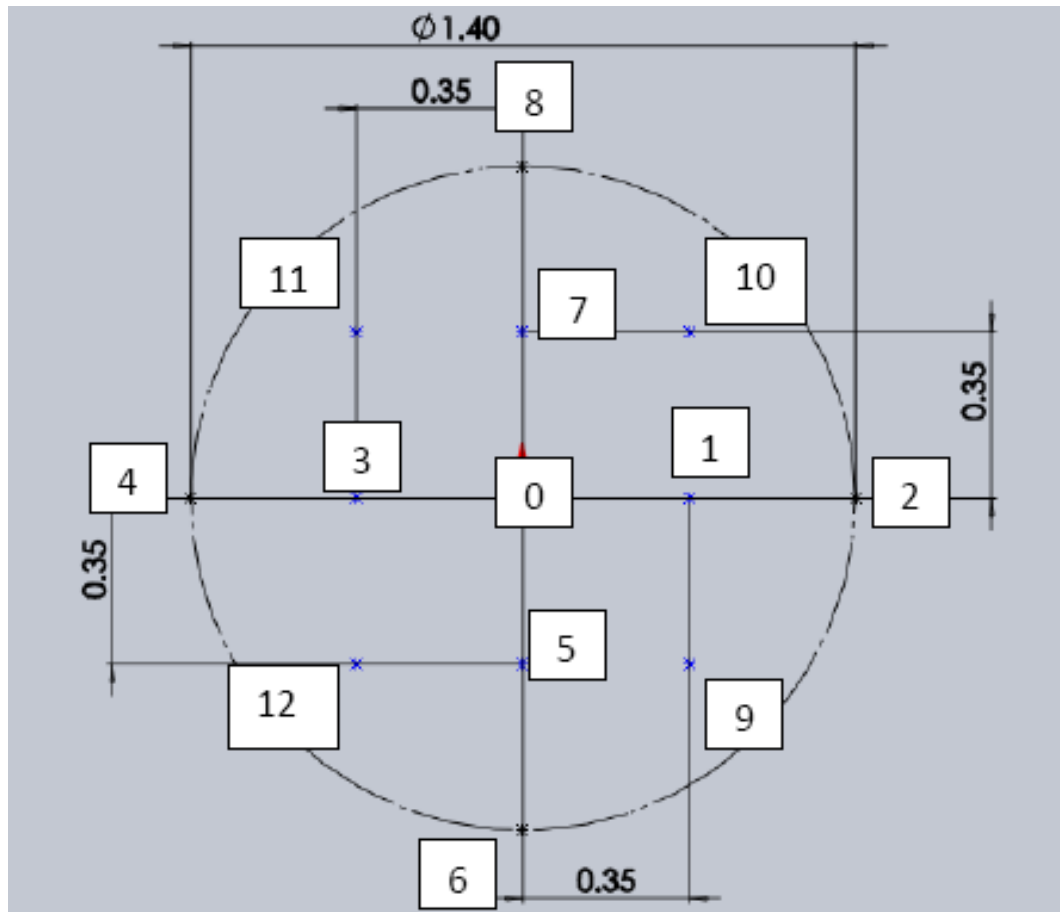


Fig. 5.6: Wind mapping domain

Anemometer was used to measure the wind speeds at the 12 locations of the axial fan at a fixed distance from it. The average values of the wind speeds measured are tabulated in Table 5.5.

Table 5.5: Wind mapping results

Wind speed (ms ⁻¹)	Position 0	Position 1	Position 2	Position 3	Position 4	Position 5
8	5.31	8.31	7.15	7.52	6.36	8.12
9	5.70	9.41	7.44	8.50	6.96	8.92
10	5.81	9.97	7.99	8.97	7.17	9.68
11	6.75	10.85	9.38	10.34	7.86	10.63
12	7.34	11.76	10.17	11.10	9.65	11.58

Wind speed (ms ⁻¹)	Position 6	Position 7	Position 8	Position 9	Position 10	Position 11	Position 12
8	5.49	5.91	7.41	7.36	8.07	6.33	7.17
9	6.46	6.02	8.24	8.85	8.72	7.62	8.31
10	7.75	7.60	9.16	10.66	10.02	8.17	8.94
11	8.23	8.38	9.73	10.61	11.46	8.72	9.68
12	7.94	8.67	10.68	11.20	11.71	10.14	9.80

The results from the wind mapping experiments showing the mean standard deviation for wind speeds at all the positions is tabulated in Table 5.6. It is observed that the mean standard deviation of wind speeds at positions 1, 3, 5, 7, 9, 10, 11 and 12 are the least. This indicates that the wind speed remains consistent and without much variation during the operation of the axial fan. The region subtended by positions 1, 3, 5, 7, 9, 10, 11 and 12 is used for the placement of the wind turbine rotors so that accurate analysis can be done. The rotors have been designed in such a manner that the aspect ratio for the frontal area is lesser than the area subtended by the region between the positions cited above.

Table 5.6: Mean standard deviation for various positions of the fluid flow domain

Position	Mean standard deviation
0	3.818
1	-0.060
2	1.574
3	0.714
4	2.400
5	0.214
6	2.826
7	2.684
8	0.956
9	0.264
10	0.004
11	1.804
12	1.220

5.5 Testing of the setup

The fabricated setup was tested at the Energy Conversion Laboratory in RVCE to measure the power output and validate with the simulation data.

5.5.1 Measurement of the power output

The results from the testing of the twin turbine system are tabulated in Table 5.7. Further, the setup is tested for power output from a single turbine as well by disengaging one of the turbine from the assembly to obtain the power curve for an isolated turbine. The C_p of each turbine in the array was found by using equation 3.2. The detailed results are presented in the Table 6.8 and 6.9. The C_p vs. TSR curves are also shown in Figure 5.7.

Table 5.7: Measurement of power output from twin turbine system

Loading	RPM	Voltage (V)	Current (A)	Power (W)	TSR	C_p
No Load	245.000	5.870	0.000	0.000	0.360	0.000
1	240.000	5.870	0.210	1.233	0.353	0.005
2	230.000	5.510	0.350	1.929	0.338	0.008
3	220.000	5.270	0.420	2.213	0.323	0.009
4	210.000	5.030	0.570	2.867	0.309	0.012
5	210.000	5.030	0.680	3.420	0.309	0.014

Table 5.8: Measurement of power output from single turbine (left)

Loading	RPM	Voltage (V)	Current (A)	Power (W)	TSR	C_p
No Load	230.000	5.500	0.000	0.000	0.338	0.000
1	225.000	5.500	0.060	0.330	0.331	0.001
2	220.000	5.270	0.120	0.632	0.323	0.003
3	220.000	5.270	0.200	1.054	0.323	0.004
4	200.000	4.800	0.270	1.296	0.294	0.005
5	200.000	4.800	0.330	1.584	0.294	0.006

Table 5.9: Measurement of power output from single turbine (Right)

Loading	RPM	Voltage (V)	Current (A)	Power (W)	TSR	C _p
No Load	210.000	5.030	0.000	0.000	0.309	0.000
1	210.000	5.030	0.060	0.302	0.309	0.001
2	200.000	4.800	0.100	0.480	0.294	0.002
3	200.000	4.800	0.180	0.864	0.294	0.003
4	195.000	4.660	0.280	1.305	0.287	0.005
5	195.000	4.660	0.320	1.491	0.287	0.006

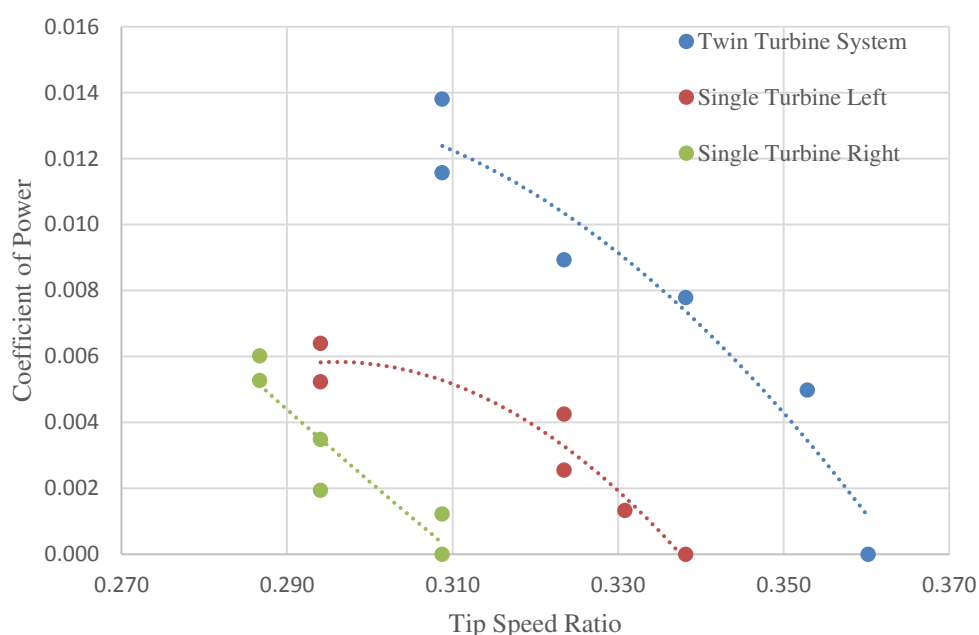


Fig. 5.7: Characteristic curve for the twin turbine assembly and the single turbines

In the Figure 5.7, the trendlines show that the speed of the turbine reduce with increasing load. It was also found that each turbine produced a higher power than if used in isolation.

5.6 Summary

The results obtained from the project were presented in this chapter. Simulations carried out on both the single rotor as well as the twin turbine system were explained in detail. A regression relation was found between the power output and the parameters of the turbine considered. The equation was validated with simulation results. The actual power output from the turbine was also measured and the power curve was drawn.

CONCLUSION AND SCOPE FOR FUTURE WORK

Vertical Axis Wind Turbines will continue to play a key role in the wind energy sector particularly in non-grid connected power generation systems. Even though they are less efficient than their horizontal axis counterparts, they have the advantage of simple construction and operation. In this work, an effort was made to understand the behavior of the Savonius type turbine in both isolated and in an array configuration using simulation and experimental methods.

6.1 Conclusions

The following important conclusions are drawn:

1. For a single Savonius rotor it was observed that the semi-circular blade profile gave the highest torque coefficient of 0.19.
2. The two bladed turbine of semi-circular profile had a higher power coefficient of 0.251 compared to that of the three bladed turbine.
3. The efficiency of a two turbine array configuration was found to be 12% higher than that a three turbine array configuration.
4. Simulations showed that each turbine in a twin turbine array produced 8% more power than an isolated turbine.
5. The fabricated setup was tested and it was shown that a turbine in an array produced more power than an isolated turbine.

6.2 Scope for future work

1. In the present work, two dimensional simulations were carried out. However, 3D simulations can be performed and aspect ratio, which would affect the performance of a turbine in the array, can be considered as another variable.
2. The wind turbine and its performance can be studied in a wind tunnel to accurately determine the efficiency of the system.
3. The concept of increase in power output due to the interaction between the two adjacently placed turbines can be extended to an hybrid Darrieus-Savonius type turbines.
4. Fabricate the turbine blades with glass and carbon fibre composites, which have higher strength to weight ratio, leading to further improvement in performance of the turbines.

REFERENCES

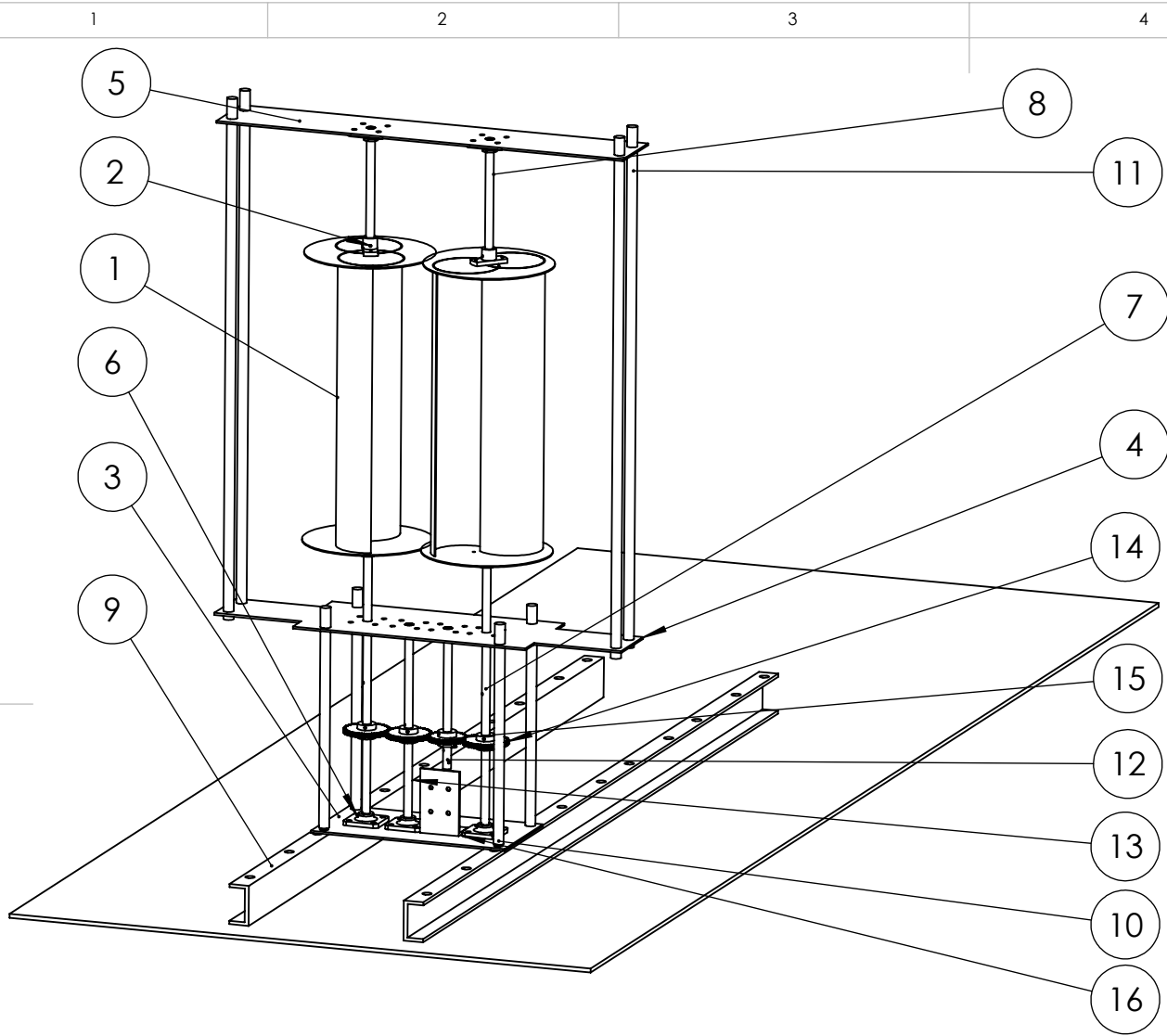
1. “Report on Indian Energy Consumption”, US Energy Information Administration, 2014
2. “Human Development Index – 2013”, United Nations Development Programme, 2013
3. “Installed Capacity of Power Utilities in India”, Ministry of Power, Government of India, 2015
4. “Annual Report - 2013-2014”, Ministry of New and Renewable Energy, Government of India, 2015
5. “Load Generation Balance Report - 2013-14”, Central Electricity Authority, Government of India, 2015
6. “Global Wind Report - 2013”, Global Wind Energy Council, 2014
7. “Annual Report – 2012-2013”, Centre for Wind Energy Technology, Government of India, 2014
8. “India’s Wind Power Potential”, National Institute of Wind Energy, Government of India, 2014
9. “Wind Energy : Renewable Energy and the Environment”, Nelson, V., CRC Press, 2013
10. Bhutta, M.M.A., Hayat, N., Farooq, A.U., Ali, Z., Jamil, S.E., Hussain, Z., “Vertical Axis Wind Turbine – A Review of Various Configurations and Design Techniques”, *Renewable and Sustainable Energy Reviews*, Vol. 16, 2012, pp. 1926–1939
11. Walker, S.L., “Building Mounted Wind Turbines and their Stability for the Urban Scale - A Review of Methods of Estimating Urban Wind Source”, *Energy and Buildings*, Vol. 43, 2011, pp. 1852–1862.
12. Silva, F.T., Santos, A.C., Gil, M.C., “Urban Wind Energy Exploitation System Behavior under Multidirectional Flow Conditions - Opportunities and Challenges”, *Renewable and Sustainable Energy Reviews*, Vol. 24, 2013, pp. 364–378
13. Altan, B.D., Atilgan, M., “An Experimental and Numerical Study on the Improvement of the Performance of Savonius Wind Rotor”, *Energy Conversion and Management*, Vol. 49, 2008, pp. 3425–3432
14. Mohamed, M.H., Janiga, G., Pap, E., Thevenin, D., “Optimization of Savonius Turbines using an Obstacle Shielding the Returning Blade”, *Renewable Energy*, Vol. 35, 2010, pp. 2618-2626

15. Menet, J.L., “A Double-Step Savonius Rotor for Local Production of Electricity: A Design Study”, *Renewable Energy*, Vol. 29, 2004, pp. 1843–1862
16. Newman, B.G., “Measurements on a Savonius Rotor with Variable Gap”, in *Proceedings of Univ. Sherbrooke, Conf. on Wind Energy, Sherbrooke, Canada, 1974.*
17. Damak, A., Driss, Z., Abid, M.S., “Experimental Investigation of Helical Savonius Rotor with a Twist of 180°”, *Renewable Energy*, Vol. 52, 2013, pp. 136-142
18. Saha, U.K., Rajkumar, M.J., “On the Performance Analysis of Savonius Rotor with Twisted Blades”, *Renewable Energy*, Vol. 31, 2006, pp. 1776–1788
19. Yao, Y.X., Tang, Z.P., Want, X.W., “Design Based on a Parametric Analysis of a Drag Driven VAWT with a Tower Cowling”, *Journal Wind Engineering and Industrial Aerodynamics*, Vol. 116, 2013, pp. 32–39
20. Saha, U.K., Thotla, S., Maity, D., “Optimum Design Configuration of Savonius Rotor Through Wind Tunnel Experiments”, *Journal of Wind Engineering and Industrial Aerodynamics*, Vol. 96, 2008, pp. 1359–1375
21. Ahmed, N.A., “A Novel Small Scale Efficient Wind Turbine for Power Generation”, *Renewable Energy*, Vol. 57, 2013, pp. 79-85
22. Chong, W.T., Pan, K.C., Poh, S.C., Fazlizan, A., Oon, C.S., Badarudin, A., Nik-Ghazali, N., “Performance Investigation of a Power Augmented Vertical Axis Wind Turbine for Urban High-Rise Application”, *Renewable Energy*, Vol. 51, 2013, pp. 388-397
23. Letcher, T., “Small Scale Wind Turbines Optimized for Low Wind Speeds”, *Journal of Wind Engineering and Industrial Aerodynamics*, Vol. 88, 2007, pp. 1014–1026
24. Lee, S., Kim, H., Lee, S., “Analysis of Aerodynamic Characteristics on a Counter-Rotating Wind Turbine”, *Current Applied Physics*, Vol. 10, 2010, pp. 339–342.
25. Jaohindy, P., McTavish, S., Garde, F., Bastide, A., “An Analysis of the Transient Forces Acting on Savonius Rotors with Different Aspect Ratios”, *Renewable Energy*, Vol. 55, 2013, pp. 286-295
26. Zhou, T., Rempfer, D., “Numerical Study of Detailed Flow Field and Performance of Savonius Wind Turbines”, *Renewable Energy*, Vol. 51, 2013, pp. 373-381.
27. Trivellato, F., Castelli, M.R., “On the Courant-Friedrichs-Lewy Criterion of Rotating Grids in 2D Vertical-Axis Wind Turbine Analysis”, *Renewable Energy*, Vol. 62, 2014, pp. 53-62
28. Dobrev, I., Massouh, F. “CFD and PIV Investigation of Unsteady Flow through Savonius Wind Turbine”, *Energy Procedia*, Vol. 6, 2011, pp. 711–720

29. McTavish, S., Feszty, D., Sankar, T., “Steady and Rotating Computational Fluid Dynamics Simulations of a Novel Vertical Axis Wind Turbine for Small-Scale Power Generation”, *Renewable Energy*, Vol. 41, 2012, pp. 171-179
30. Dobrev, I., Massouh, F., “Exploring the Flow around a Savonius Wind Turbine”, *Proceedings of 16th International Symposium on Applications of Laser Techniques to Fluid Mechanics, Lisbon, Portugal, 2012*
31. Nasef, M.H., El-Askary, W.A., Abdel-Hamid, A.A., Gad, H.E., “Evaluation of Savonius Rotor Performance : Static and Dynamic Studies”, *Journal of Wind Engineering and Industrial Aerodynamics*, Vol. 123, 2013, pp. 1–11
32. Sargolzaei, J., Kianifar, A., “Modeling and Simulation of Wind Turbine Savonius Rotors using Artificial Neural Networks for Estimation of the Power Ratio and Torque”, *Simulation Modeling Practice and Theory*, Vol. 17, 2009, pp. 1290–1298
33. Dabiri, J.O., Liska, S., Whittlesey, R.W., “Fish Schooling as a Basis for Vertical Axis Wind Turbine Farm Design”, *Bioinspiration and Biomimetics*, Vol. 5, 2010, pp. 35-41
34. Dabiri, J.O., “Potential Order-of-Magnitude Enhancement of Wind Farm Power Density via Counter-Rotating Vertical-Axis Wind Turbine Arrays”, *Journal of Renewable and Sustainable Energy*, Vol. 3, 2011, pp. 104-116
35. Dabiri, J.O., Kinzel, M., Mulligan, Q., “Energy Exchange in an Array of Vertical-Axis Wind Turbines”, *Journal of Turbulence*, Vol. 13, No. 38, 2012, pp. 1–13
36. Kumar, P.S., Abraham, A., Bensingh, R.J., Ilangovan, S., “Computational and Experimental Analysis of a Counter-Rotating Wind Turbine System”, *Journal of Scientific and Industrial Research*, Vol. 72, 2013, pp. 300-306
37. Shigetomi, A., Murai, Y., Tasaka, Y., Takeda, Y., “Interactive Flow Field around Two Savonius Turbines”, *Renewable Energy*, Vol. 36, 2011, pp. 536-545
38. Golecha, K., Eldho, T.I., Prabhu, S.V., “Study on the Interaction between Two Hydrokinetic Savonius Turbines”, *International Journal of Rotating Machinery*, Vol. 2012, Article ID 581658
39. Kim, D., Gharib, M., “Efficiency Improvement of Straight Bladed Vertical-Axis Wind Turbines with an Upstream Deflector”, *Journal of Wind Engineering and Industrial Aerodynamics*, Vol. 115, 2013, pp. 48–52
40. Sun, X., Luo, D., Huang, D., Wu, G., “Numerical Study on Coupling Effects among Multiple Savonius Turbines”, *Journal of Renewable and Sustainable Energy*, Vol. 4, 2012, pp. 053107 (1-16)

41. Kackar, R., “Off-Line Quality Control, Parameter Design, and the Taguchi Method,” *Journal of Quality Technology*, Vol. 17(4), 1985, pp. 176–188.
42. Hu, Y., Rao, S.S., “Robust Design of Horizontal Axis Wind Turbines using Taguchi Method”, *Journal of Mechanical Design*, Vol. 133, 2011, pp. 1-15.
43. ANSYS Help - Fluent, ANSYS 14.5, 2013
44. “Numerical Analysis of the Flow in a Two-Bucket Savonius Wind Turbine”, Kacprzak, K., Sobczak, K., Kiewicz, G.L., Lambert Academic Publishing, 2011
45. Kamoji, M.A., Kedare, S.B., Prabhu, S.V., “Experimental Investigations on Single Stage Modified Savonius rotor”, *Applied Energy*, Vol. 86, 2009, pp. 1064-1072
46. Roy, S., Saha, U.K., “Computational Study to Assess the Influence of Overlap Ratio on Static Torque Characteristics of a Vertical Axis Wind Turbine”, *Procedia Engineering*, Vol. 51, 2013, pp. 694-702
47. “Computational Fluid Dynamics – The Basics with Applications”, Anderson, J.D., Tata McGraw Hill Publications, 2012
48. “Computational Fluid Mechanics and Heat Transfer”, Pletcher, R.H., Tennehill, J.C., Anderson, D.C., Taylor and Francis, 1997
49. “Applied Design of Experiments and Taguchi Methods”, Krishnaiah, K., Shahabudeen, P., PHI Learning Private Limited, 2012
50. “Orthogonal Arrays - Theory and Applications”, Hedayat, A.S., Sloane, N.J.A., Stufken, J., Springer Publications, 1999
51. “Regression Analysis”, Freund, R.J., Wilson, W.J., Sa, P., Academic Press, 2006

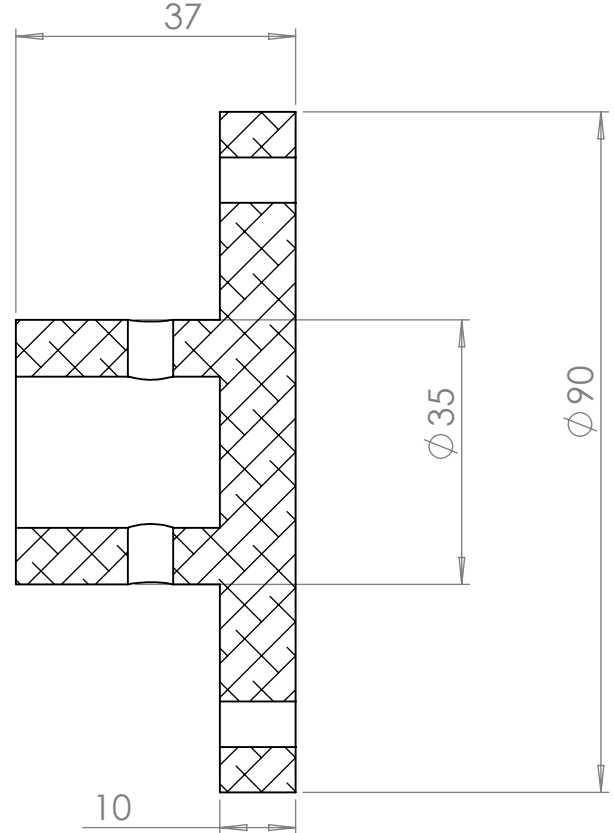
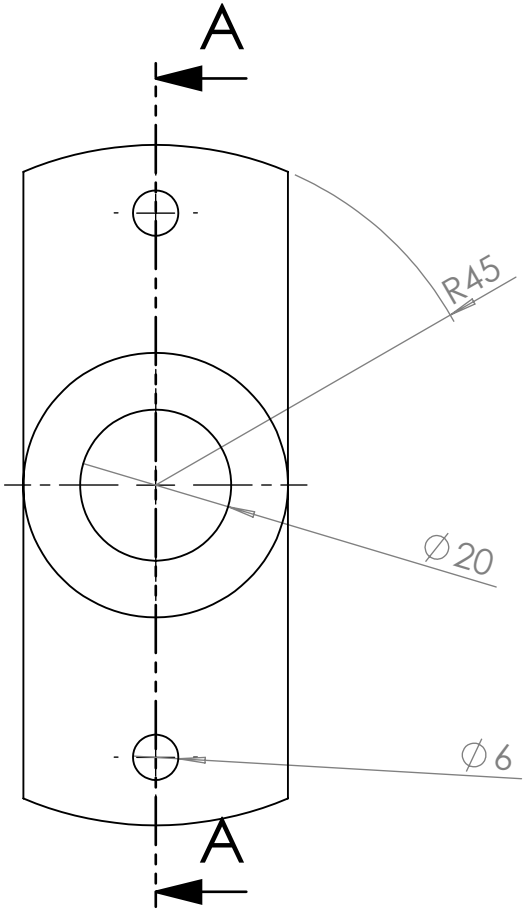
APPENDIX



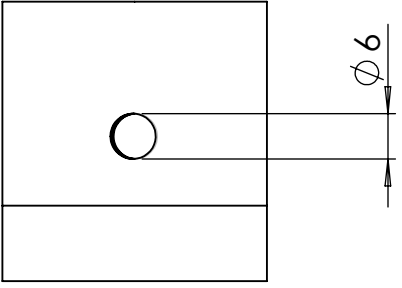
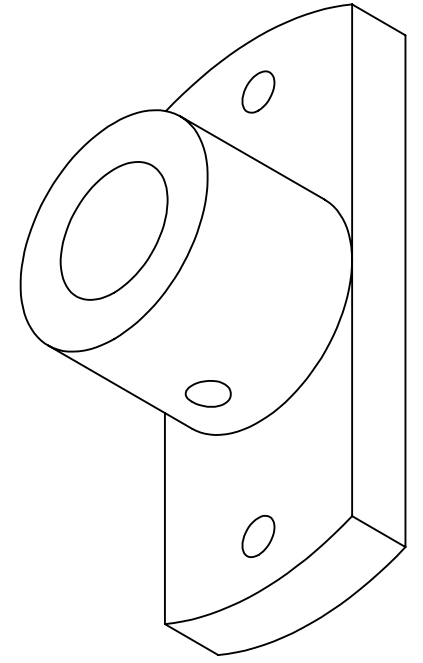
ITEM NO.	PART NAME	QTY.
1	TURBINE	2
2	FLANGE	4
3	BOTTOM BASE PLATE	1
4	MIDDLE BASE PLATE	1
5	TOP BASE PLATE	1
6	BEARING	9
7	TURBINE SHAFT	2
8	TOP SHAFT	2
9	C SECTION	2
10	SUPPORT ROD-SHORT	4
11	SUPPORT ROD-LONG	4
12	GENERATOR SHAFT	1
13	IDLER SHAFT	1
14	GEAR 1 - 54 TEETH	3
15	GEAR 2 - 45 TEETH	1
16	GENERATOR SUPPORT	1

	NAME	SIGNATURE	DATE	
DRAWN				
CHK'D				
APPV'D				
MFG				
Q.A				

TITLE:		<h1>Full Assembly</h1>
MATERIAL:		
DWG NO.		A4
WEIGHT:		
SCALE:1:100		SHEET 1 OF 1



SECTION A-A



UNLESS OTHERWISE SPECIFIED:

DIMENSIONS ARE IN mm
 TOLERANCES:
 FRACTIONAL \pm
 ANGULAR: MACH \pm BEND \pm
 TWO PLACE DECIMAL \pm
 THREE PLACE DECIMAL \pm

INTERPRET GEOMETRIC
 TOLERANCING PER:
 MATERIAL

DO NOT SCALE DRAWING

	NAME	DATE
DRAWN		
CHECKED		
ENG APPR.		
MFG APPR.		
Q.A.		
COMMENTS:		

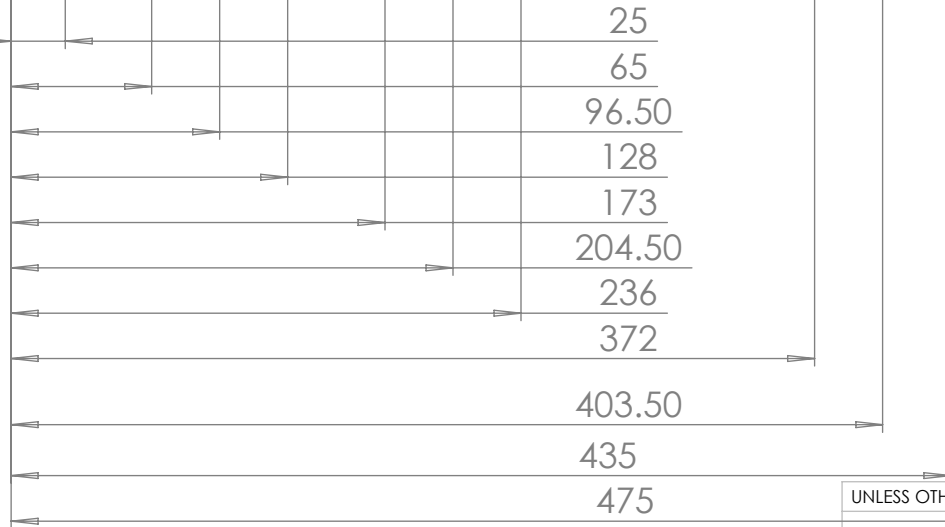
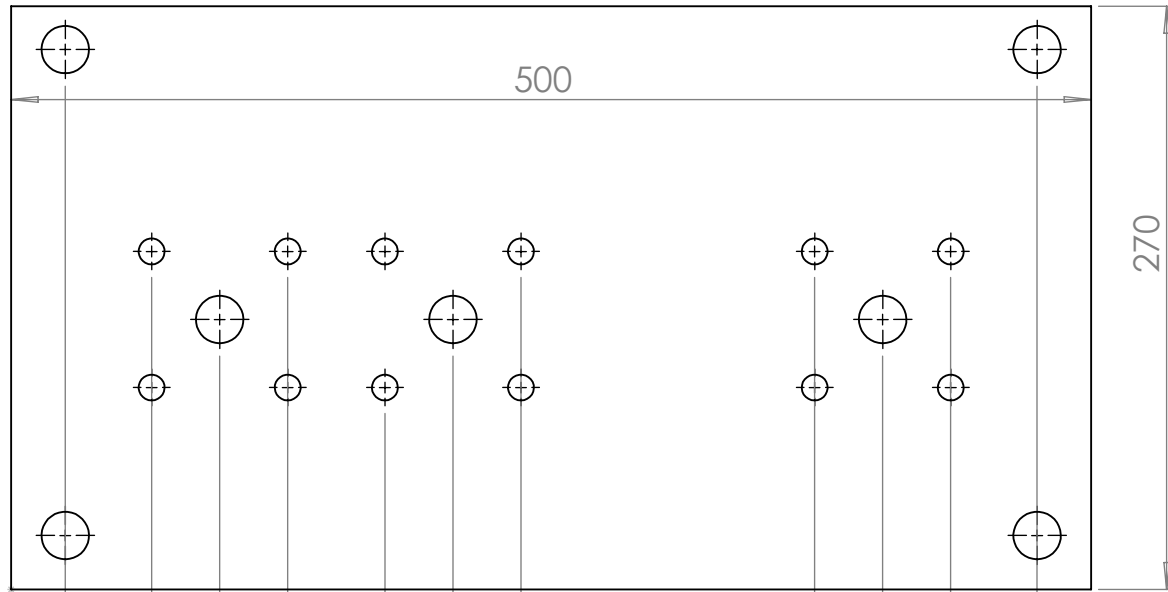
QUANTITY: 4

TITLE: FLANGE

MATERIAL:
 ALUMINIUM-2014

SIZE	DWG. NO.	REV
A	2	

SCALE: 1:2 WEIGHT: SHEET 1 OF 1



UNLESS OTHERWISE SPECIFIED:

DIMENSIONS ARE IN MM
 TOLERANCES:
 FRACTIONAL ±
 ANGULAR: MACH ± BEND ±
 TWO PLACE DECIMAL ±
 THREE PLACE DECIMAL ±

INTERPRET GEOMETRIC
 TOLERANCING PER:

MATERIAL

FINISH

DO NOT SCALE DRAWING

	NAME	DATE
DRAWN		
CHECKED		
ENG APPR.		
MFG APPR.		
Q.A.		

COMMENTS:

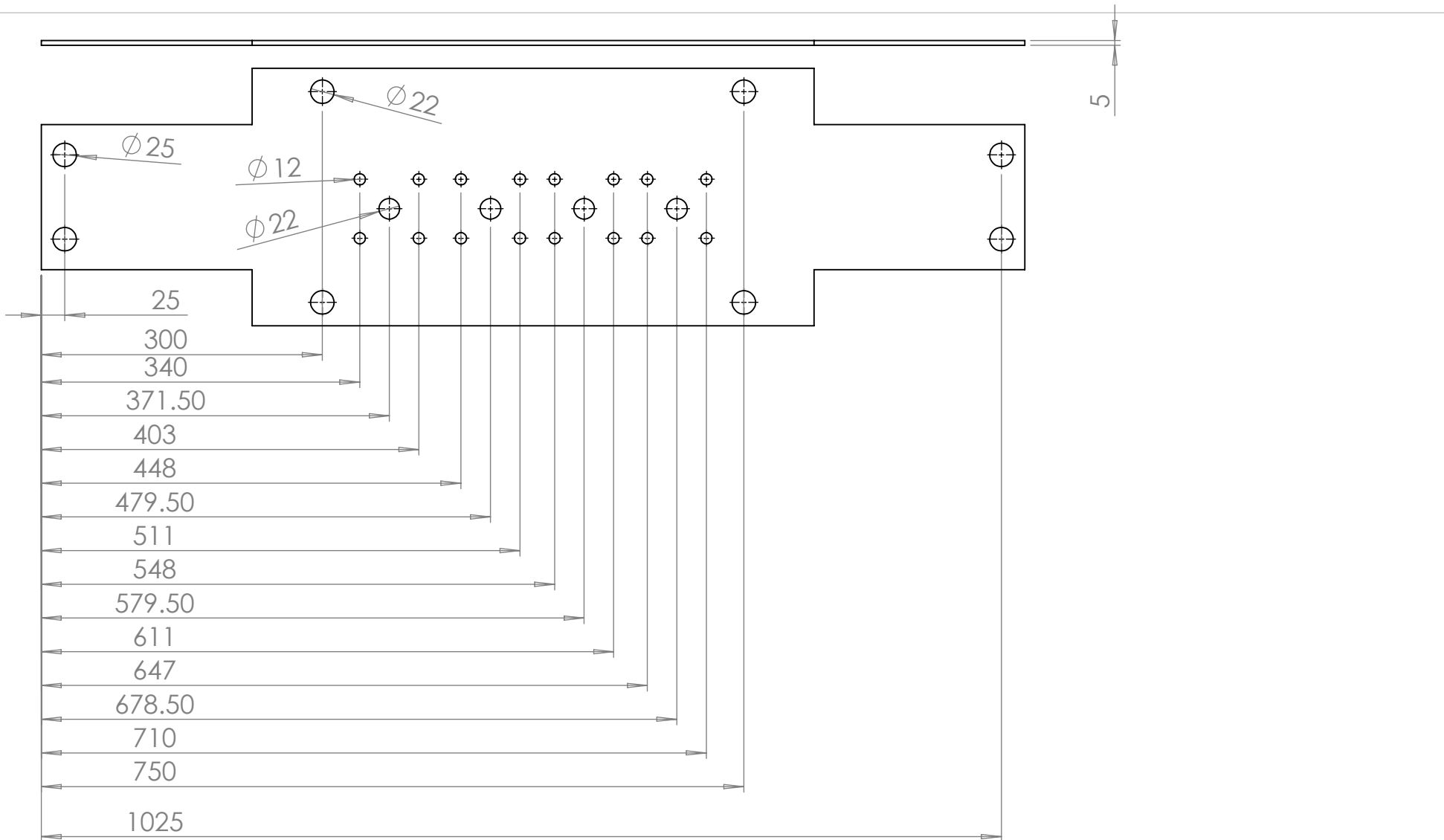
QUANTITY: 1

TITLE: **BOTTOM BASE PLATE**

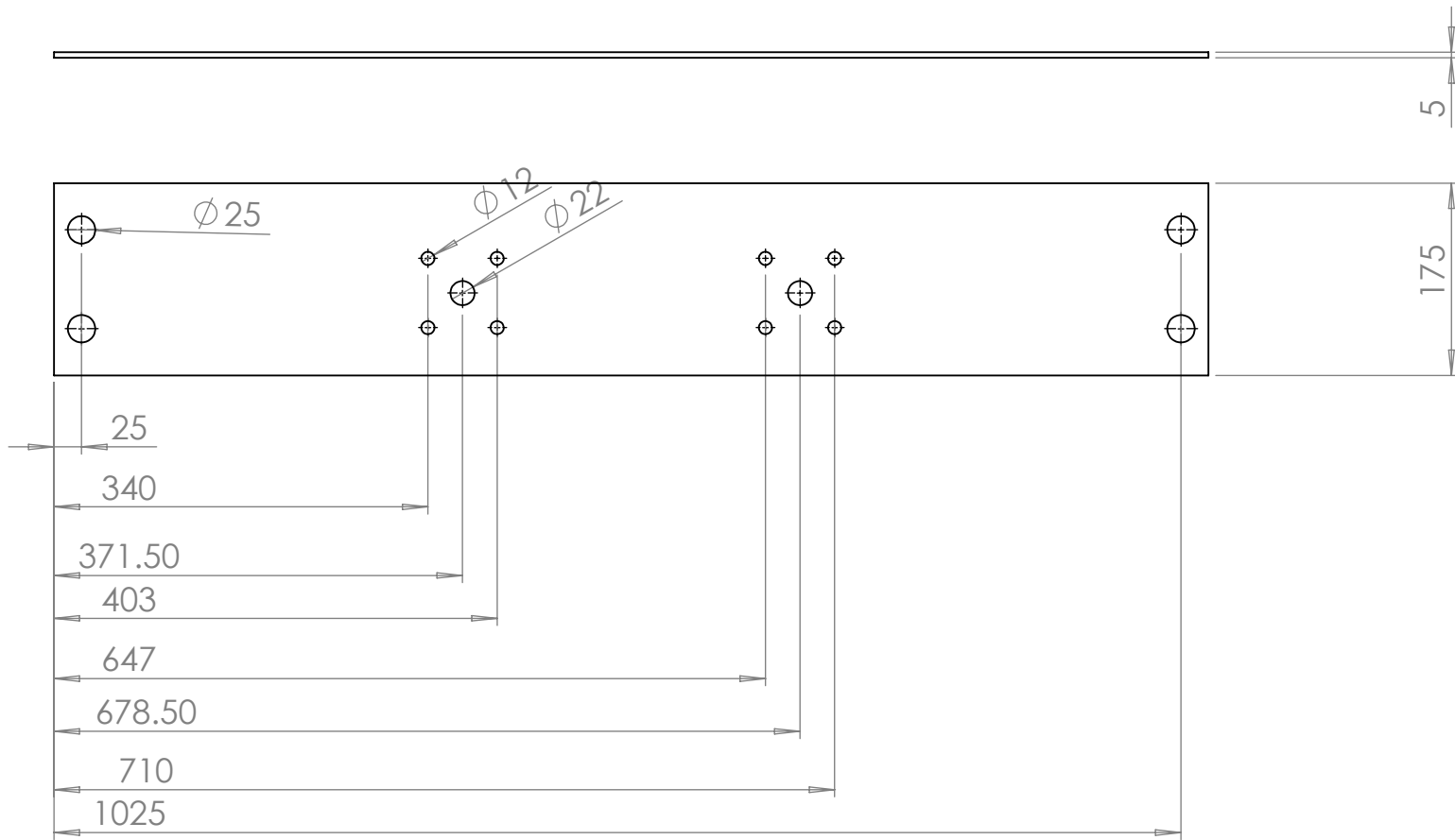
MATERIAL: **MILD STEEL**

SIZE	DWG. NO.	REV
A	3	

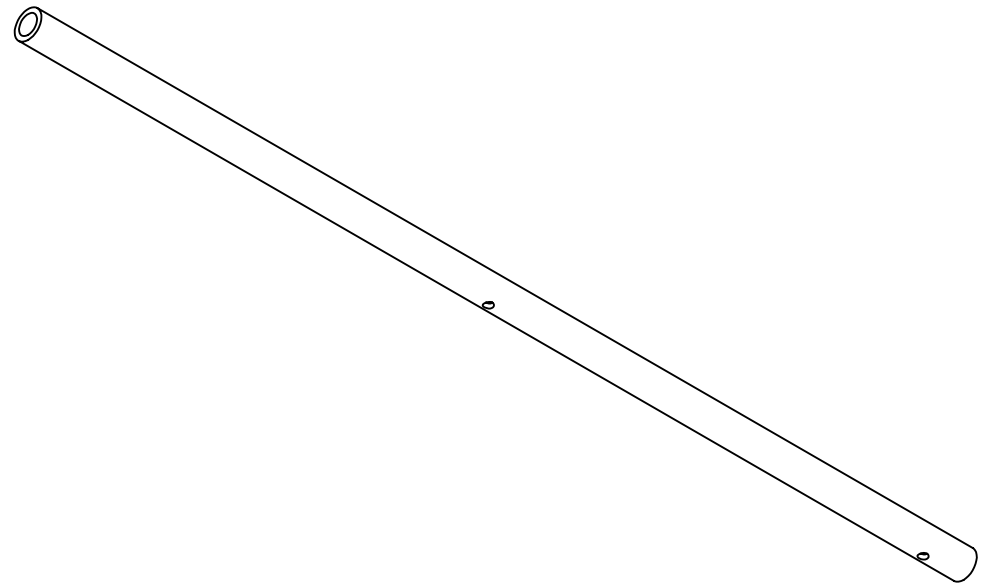
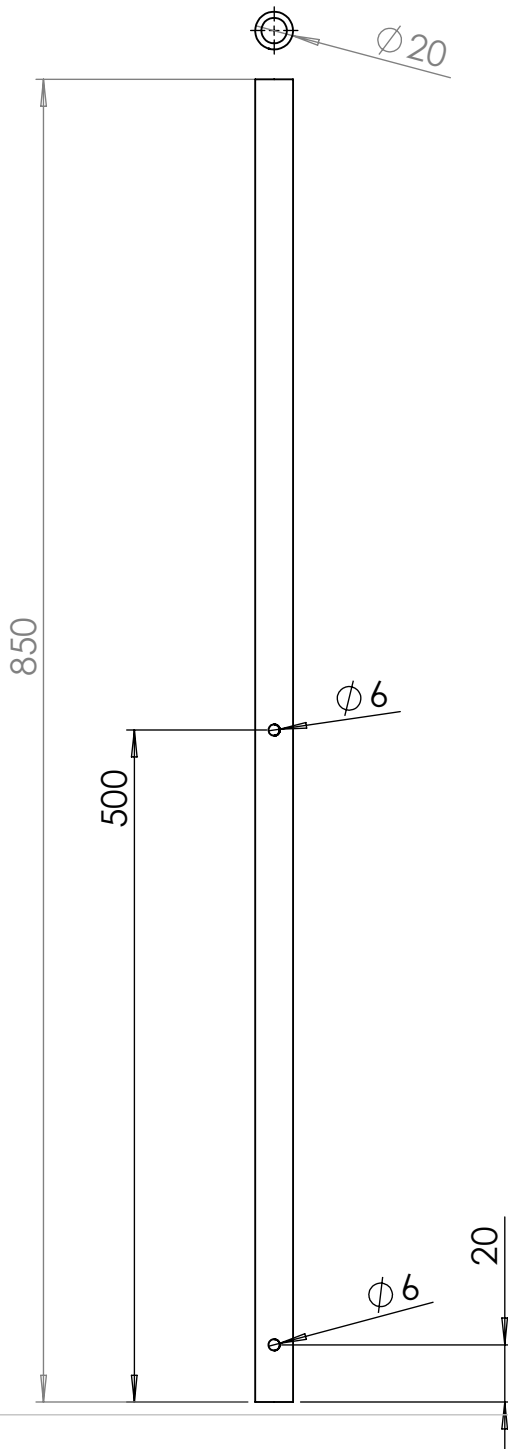
SCALE: 1:5 WEIGHT: SHEET 1 OF 1



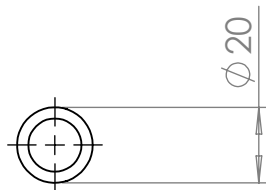
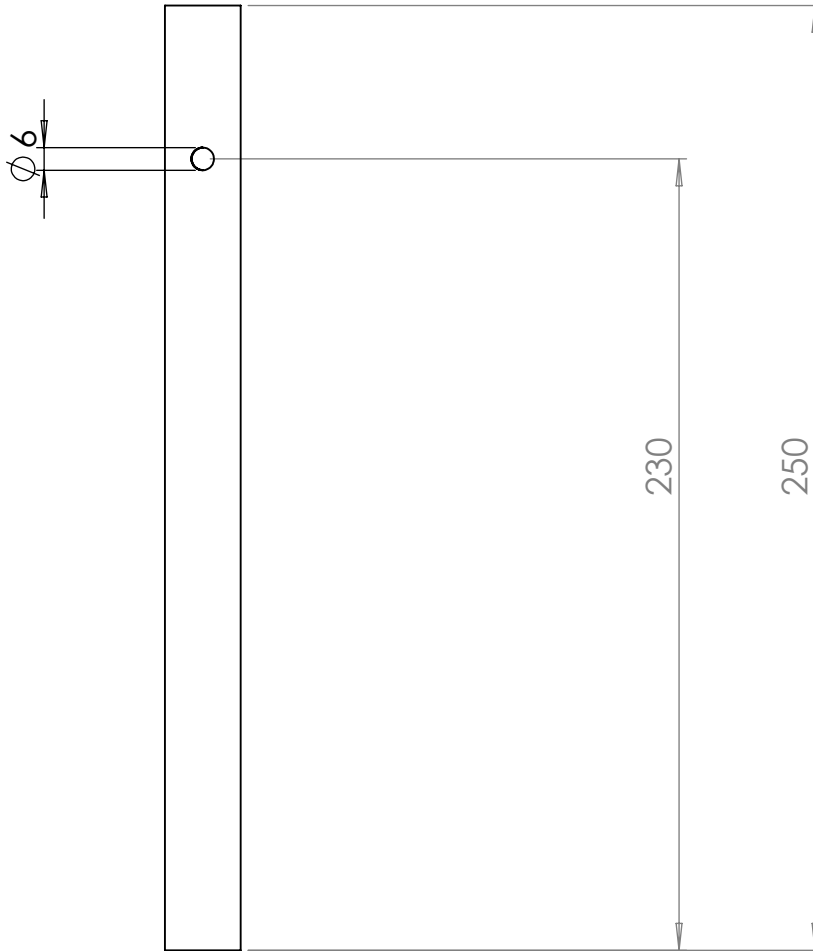
UNLESS OTHERWISE SPECIFIED: DIMENSIONS ARE IN INCHES TOLERANCES: FRACTIONAL \pm ANGULAR: MACH \pm BEND \pm TWO PLACE DECIMAL \pm THREE PLACE DECIMAL \pm INTERPRET GEOMETRIC TOLERANCING PER: MATERIAL FINISH DO NOT SCALE DRAWING	NAME	DATE	QUANTITY: 1		
	DRAWN		TITLE: MIDDLE BASE PLATE		
	CHECKED		MATERIAL: MILD STEEL		
	ENG APPR.		SIZE	DWG. NO.	REV
	MFG APPR.		A	4	
	Q.A.		SCALE: 1:10	WEIGHT:	SHEET 1 OF 1
	COMMENTS:				



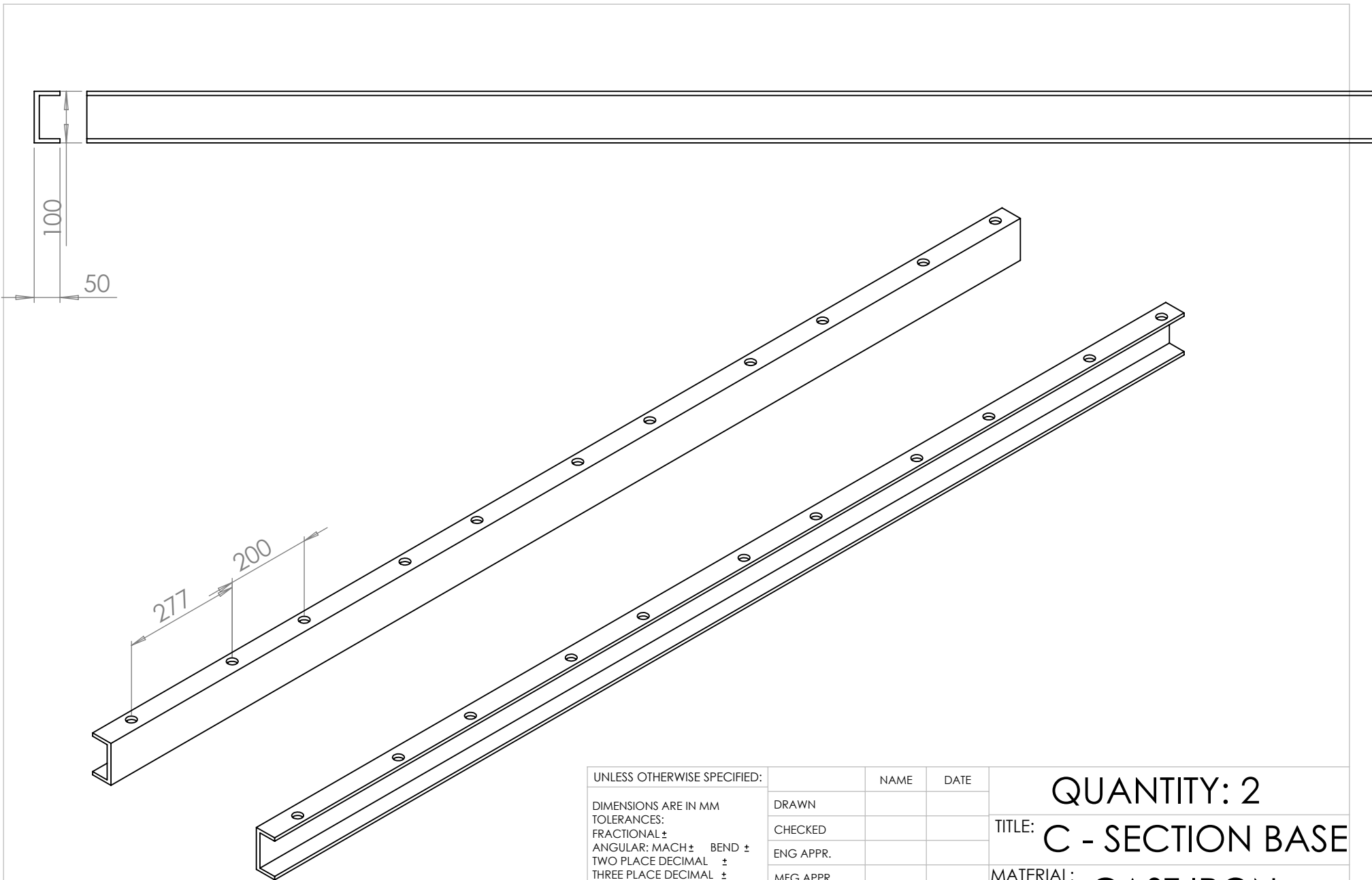
UNLESS OTHERWISE SPECIFIED:		NAME	DATE	QUANTITY: 1		
DIMENSIONS ARE IN MM TOLERANCES: FRACTIONAL \pm ANGULAR: MACH \pm BEND \pm TWO PLACE DECIMAL \pm THREE PLACE DECIMAL \pm	INTERPRET GEOMETRIC TOLERANCING PER:	DRAWN		TITLE: TOP BASE PLATE		
	MATERIAL	CHECKED				
	FINISH	ENG APPR.		MATERIAL: MILD STEEL		
	DO NOT SCALE DRAWING	MFG APPR.				
		Q.A.		SIZE	DWG. NO. 5	REV
		COMMENTS:		SCALE: 1:10	WEIGHT:	SHEET 1 OF 1



UNLESS OTHERWISE SPECIFIED:		NAME	DATE	QUANTITY: 2	
DIMENSIONS ARE IN MM		DRAWN		TITLE: TURBINE SHAFT	
TOLERANCES:		CHECKED			
FRACTIONAL ±		ENG APPR.			
ANGULAR: MACH ± BEND ±		MFG APPR.			
TWO PLACE DECIMAL ±		Q.A.		MATERIAL: MILD STEEL	
THREE PLACE DECIMAL ±		COMMENTS:		SIZE DWG. NO. REV	
INTERPRET GEOMETRIC TOLERANCING PER:				A 7 1	
MATERIAL				SCALE: 1:10 WEIGHT: SHEET 1 OF 1	
FINISH					
DO NOT SCALE DRAWING					

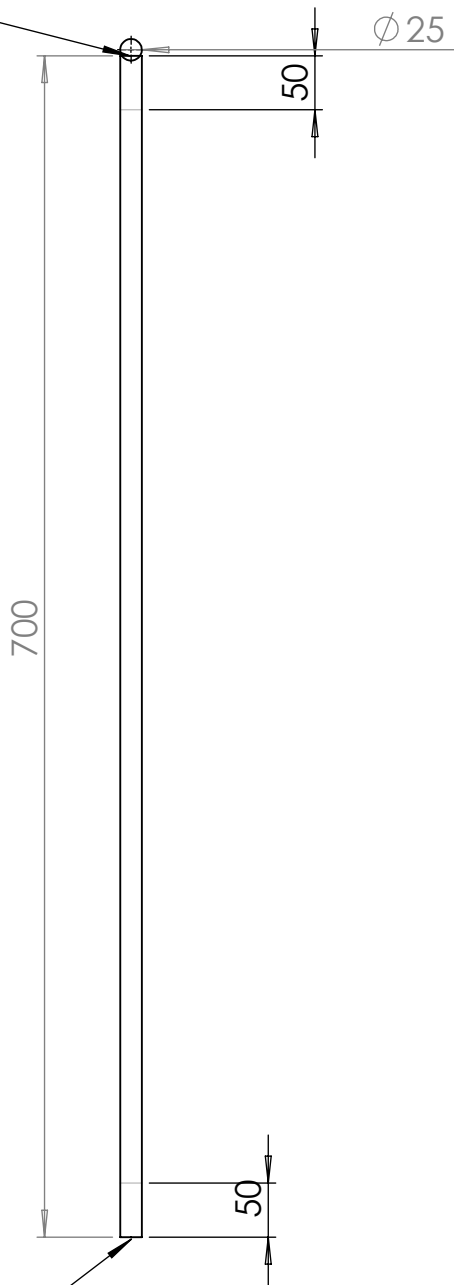


UNLESS OTHERWISE SPECIFIED:		NAME	DATE	QUANTITY: 2	
DIMENSIONS ARE IN MM		DRAWN		TITLE: TOP SHAFT	
TOLERANCES:		CHECKED			
FRACTIONAL ±		ENG APPR.			
ANGULAR: MACH ± BEND ±		MFG APPR.			
TWO PLACE DECIMAL ±		Q.A.		MATERIAL: MILD STEEL	
THREE PLACE DECIMAL ±		COMMENTS:		SIZE DWG. NO. REV	
INTERPRET GEOMETRIC TOLERANCING PER:				A 8	
MATERIAL				SCALE: 1:50 WEIGHT: SHEET 1 OF 1	
DO NOT SCALE DRAWING					



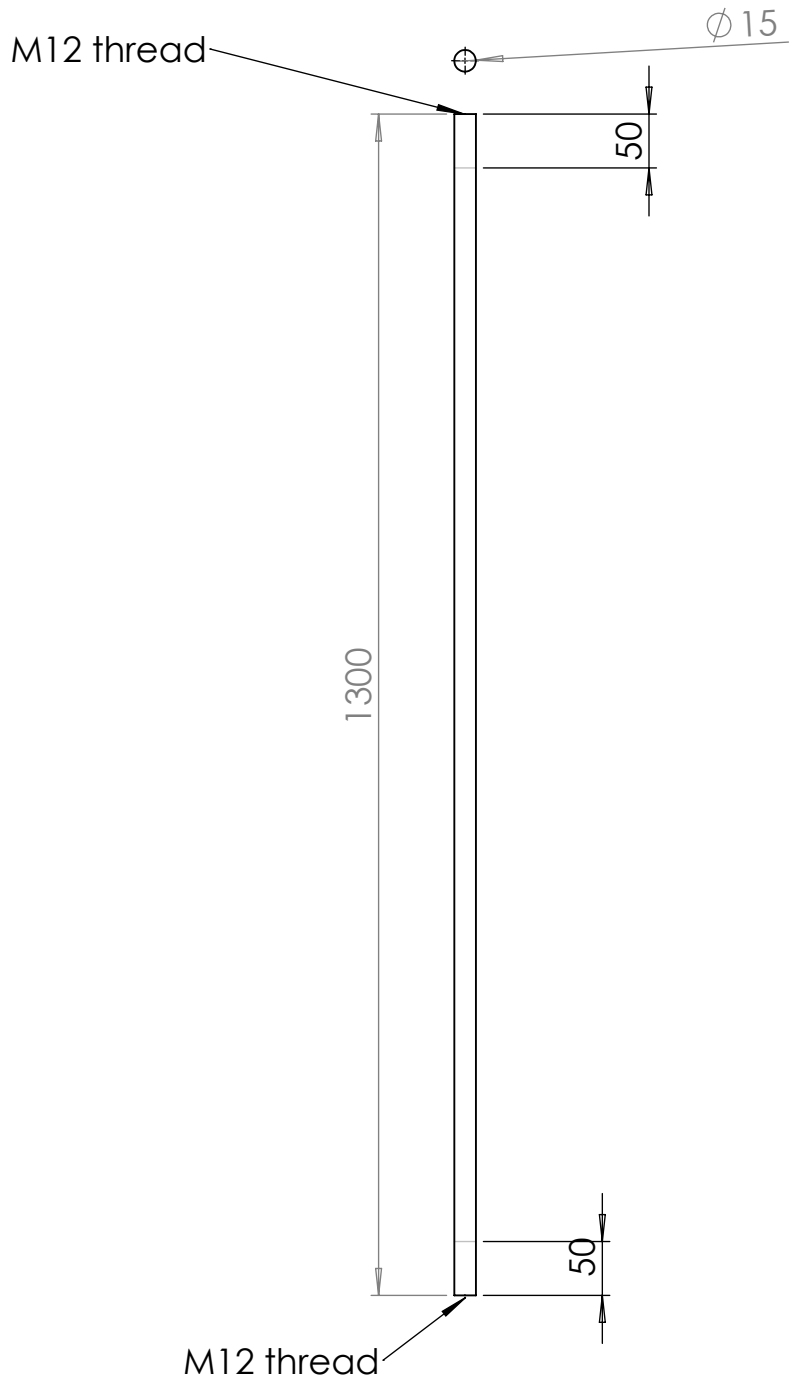
UNLESS OTHERWISE SPECIFIED:		NAME	DATE	QUANTITY: 2	
DIMENSIONS ARE IN MM		DRAWN		TITLE: C - SECTION BASE	
TOLERANCES:		CHECKED		MATERIAL: CAST IRON	
FRACTIONAL ±		ENG APPR.		SIZE	DWG. NO.
ANGULAR: MACH ± BEND ±		MFG APPR.		A	9
TWO PLACE DECIMAL ±		Q.A.		REV	
THREE PLACE DECIMAL ±		COMMENTS:		SCALE: 1:50	WEIGHT:
INTERPRET GEOMETRIC TOLERANCING PER:				SHEET 1 OF 1	
DO NOT SCALE DRAWING					

thread

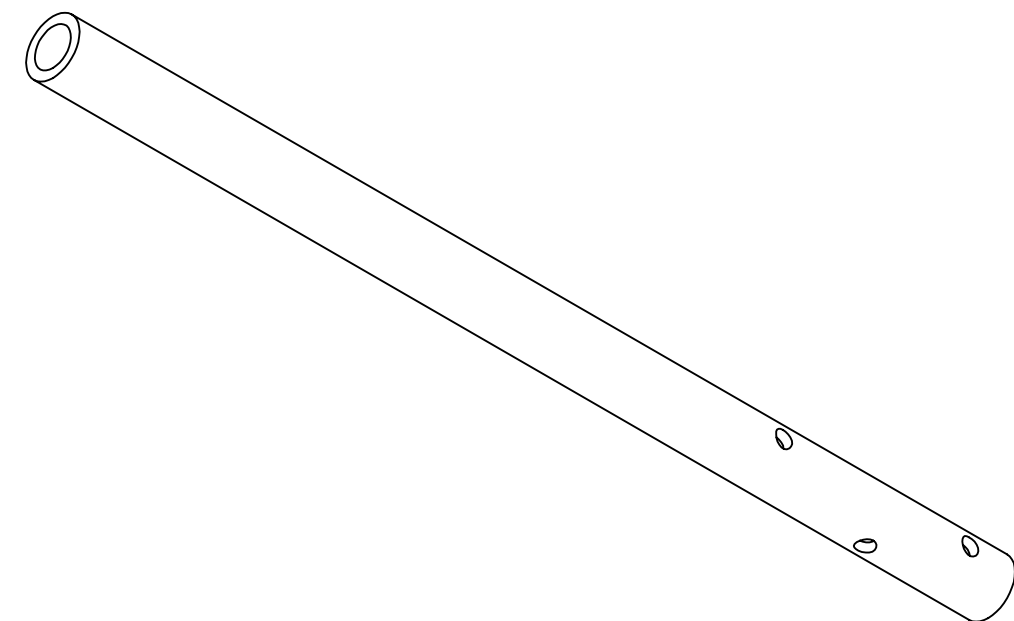
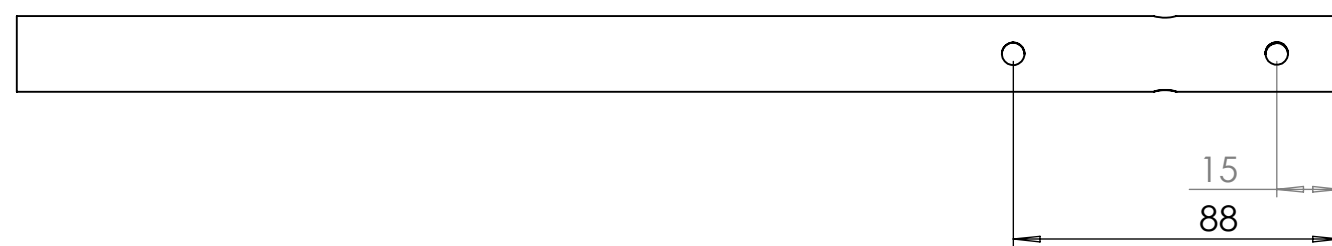
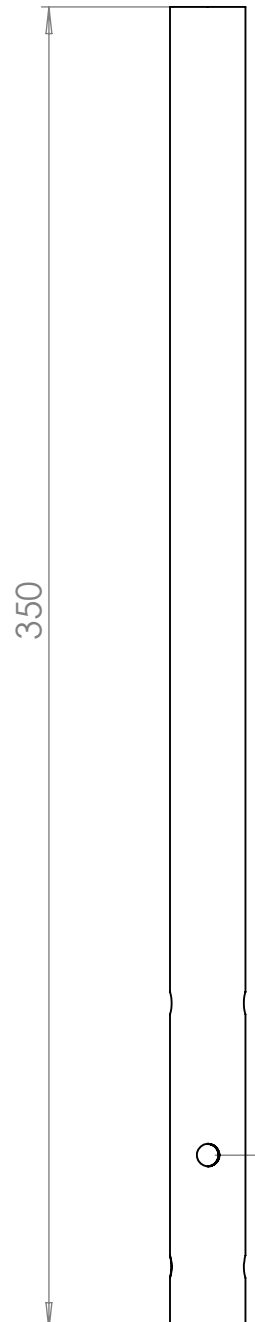
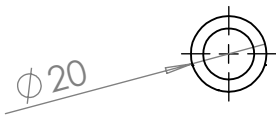


M22 thread

UNLESS OTHERWISE SPECIFIED:		NAME	DATE	QUANTITY: 4	
DIMENSIONS ARE IN MM		DRAWN		TITLE: SUPPORT ROD- BOTTOM	
TOLERANCES:		CHECKED			
FRACTIONAL \pm		ENG APPR.			
ANGULAR: MACH \pm BEND \pm		MFG APPR.			
TWO PLACE DECIMAL \pm		Q.A.		MATERIAL: MILD STEEL	
THREE PLACE DECIMAL \pm		COMMENTS:		SIZE	DWG. NO.
INTERPRET GEOMETRIC TOLERANCING PER:				A	10
MATERIAL					REV
FINISH					
DO NOT SCALE DRAWING				SCALE: 1:10	WEIGHT:
					SHEET 1 OF 1



UNLESS OTHERWISE SPECIFIED:		NAME	DATE	QUANTITY: 4			
DIMENSIONS ARE IN MM		DRAWN		TITLE: SUPPORT ROD-TOP			
TOLERANCES:		CHECKED					
FRACTIONAL ±		ENG APPR.					
ANGULAR: MACH ± BEND ±		MFG APPR.					
TWO PLACE DECIMAL ±		Q.A.		MATERIAL:			
THREE PLACE DECIMAL ±		COMMENTS:		MATERIAL: MILD STEEL			
INTERPRET GEOMETRIC TOLERANCING PER:				SIZE	DWG. NO.	REV	
MATERIAL				A	11		
FINISH				SCALE: 1:10		WEIGHT:	SHEET 1 OF 1
DO NOT SCALE DRAWING							



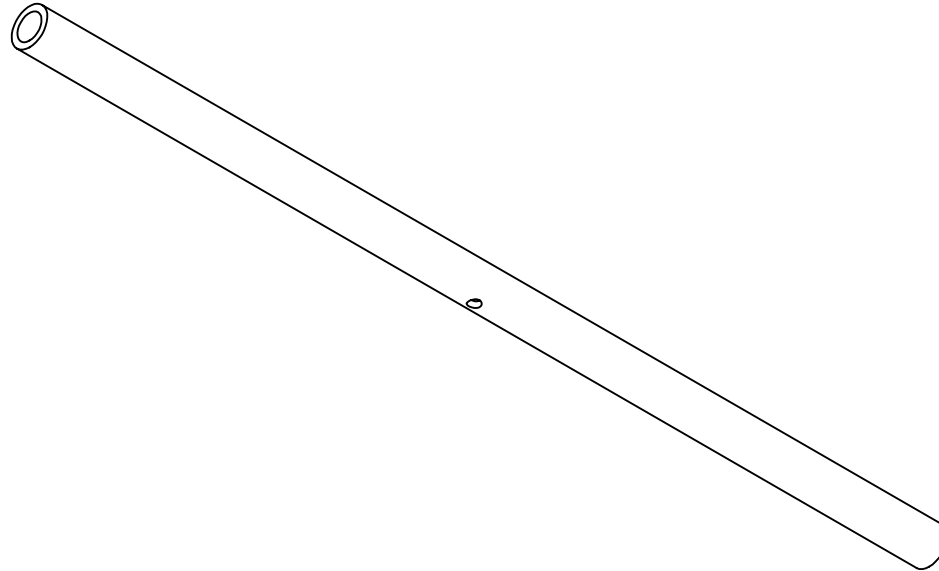
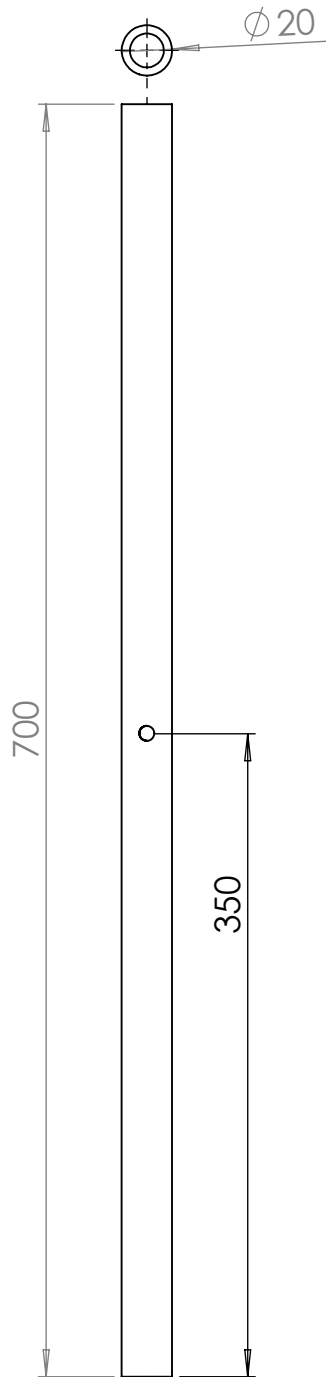
350

35

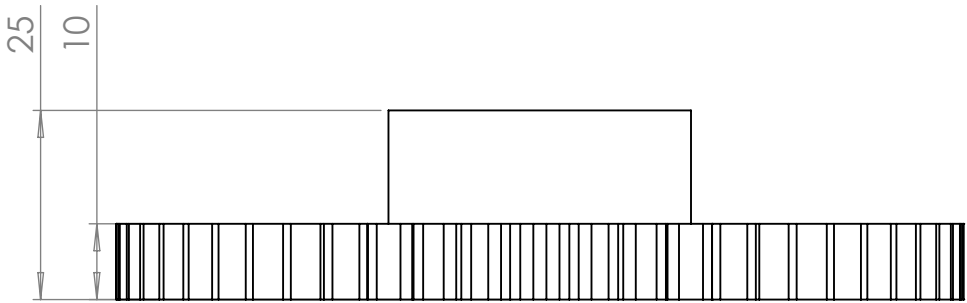
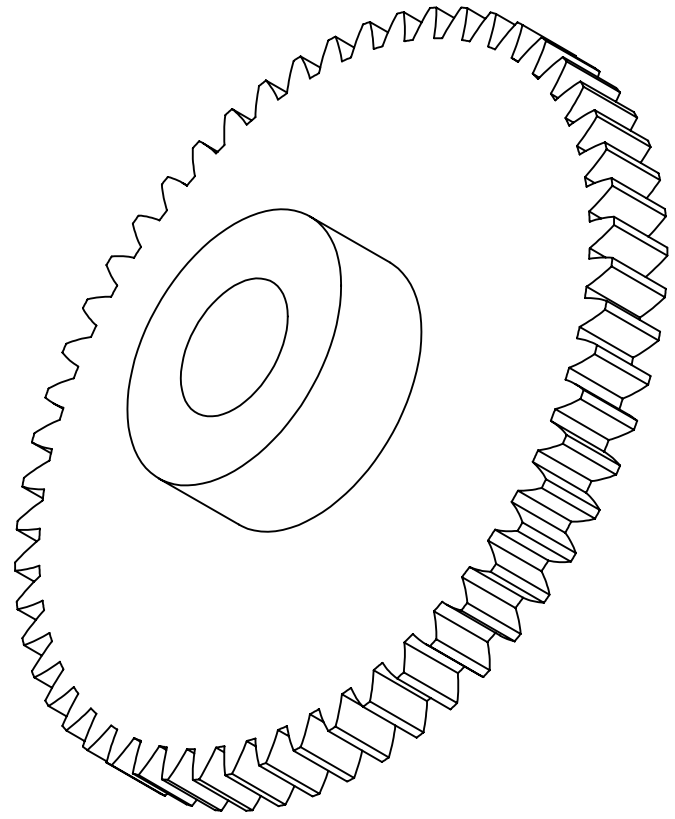
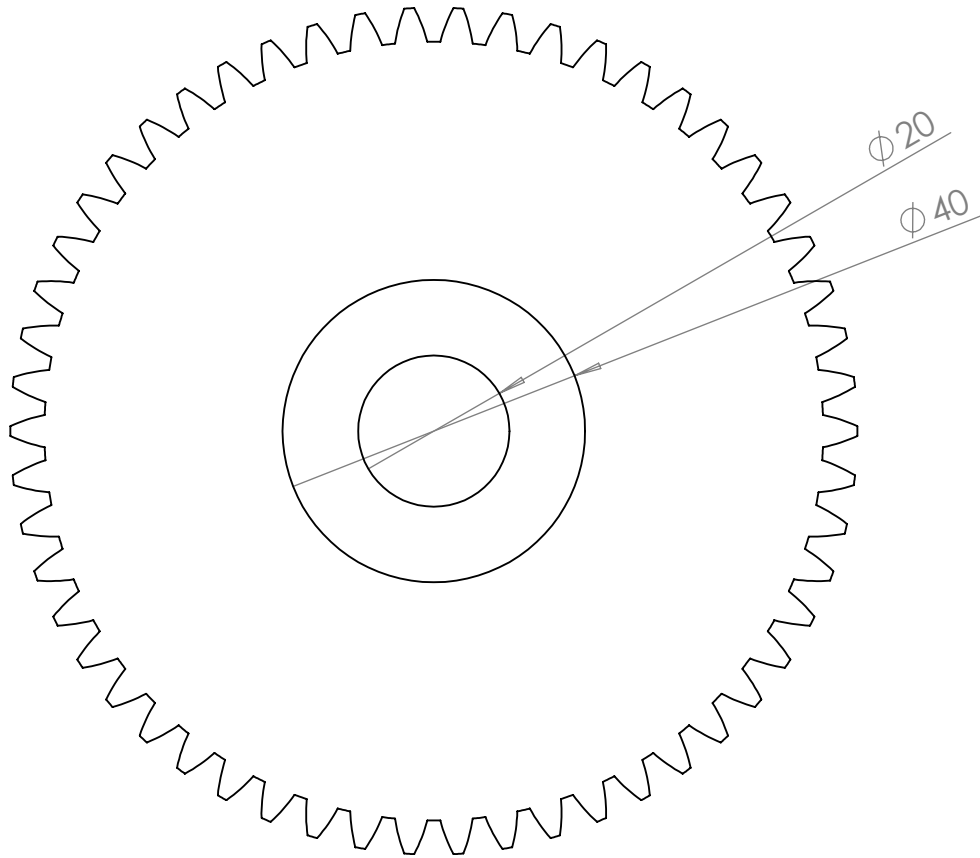
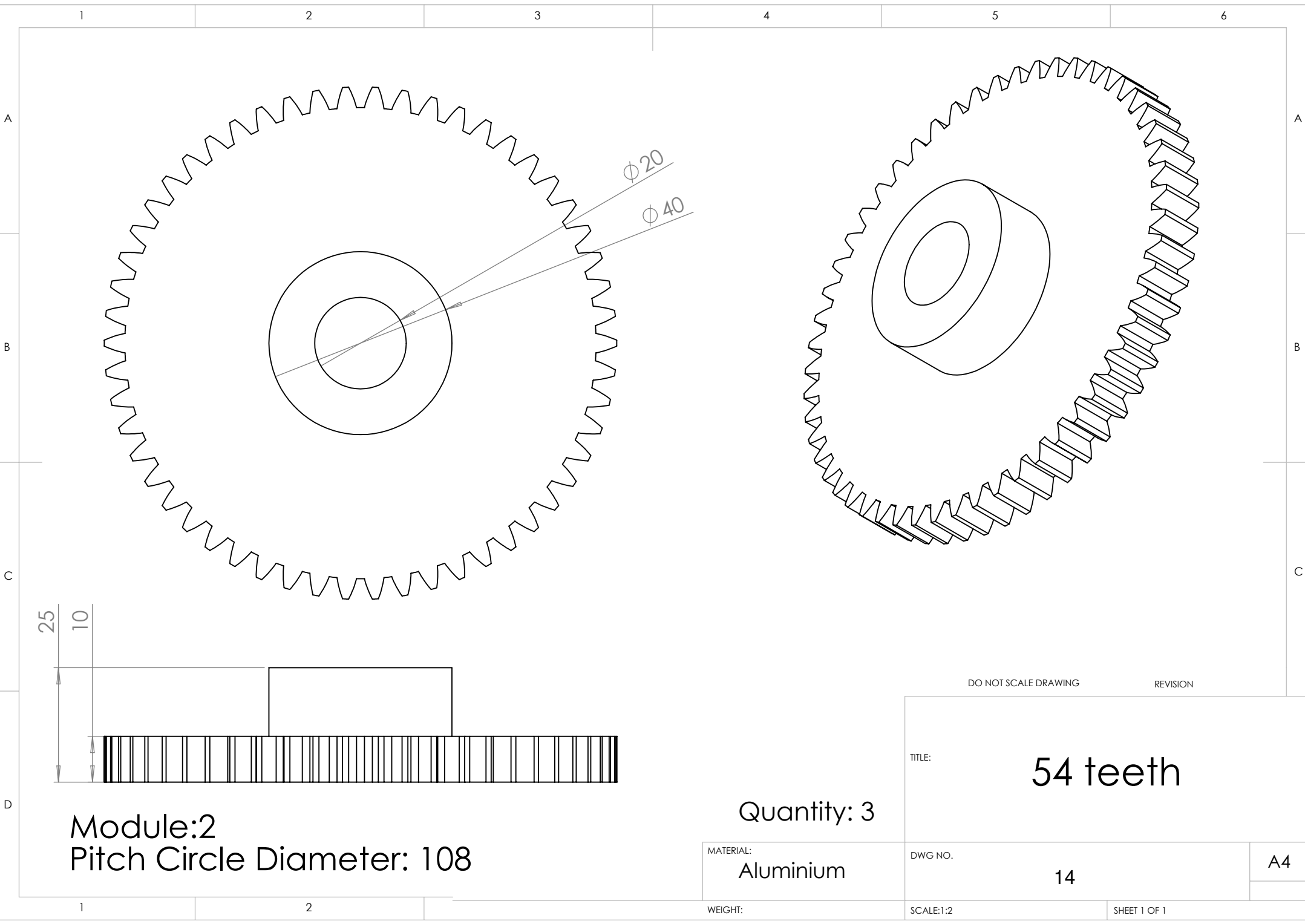
15

88

UNLESS OTHERWISE SPECIFIED:		NAME	DATE	QUANTITY: 1							
DIMENSIONS ARE IN MM		DRAWN		TITLE: GENERATOR SHAFT							
TOLERANCES:		CHECKED									
FRACTIONAL ±		ENG APPR.									
ANGULAR: MACH ± BEND ±		MFG APPR.									
TWO PLACE DECIMAL ±		Q.A.		MATERIAL: MILD STEEL							
THREE PLACE DECIMAL ±		COMMENTS:		<table border="1" style="width: 100%;"> <tr> <td>SIZE</td> <td>DWG. NO.</td> <td>REV</td> </tr> <tr> <td style="text-align: center;">A</td> <td style="text-align: center;">12</td> <td></td> </tr> </table>		SIZE	DWG. NO.	REV	A	12	
SIZE	DWG. NO.	REV									
A	12										
INTERPRET GEOMETRIC TOLERANCING PER:											
MATERIAL											
DO NOT SCALE DRAWING				SCALE: 1:5	WEIGHT:	SHEET 1 OF 1					



UNLESS OTHERWISE SPECIFIED: DIMENSIONS ARE IN MM TOLERANCES: FRACTIONAL ± ANGULAR: MACH ± BEND ± TWO PLACE DECIMAL ± THREE PLACE DECIMAL ± INTERPRET GEOMETRIC TOLERANCING PER: MATERIAL		NAME	DATE	QUANTITY: 1	
	DRAWN				
	CHECKED			MATERIAL: MILD STEEL	
	ENG APPR.				
MFG APPR.			A 13 1		
Q.A.					SCALE: 1:5 WEIGHT: SHEET 1 OF 1
COMMENTS:					
DO NOT SCALE DRAWING					

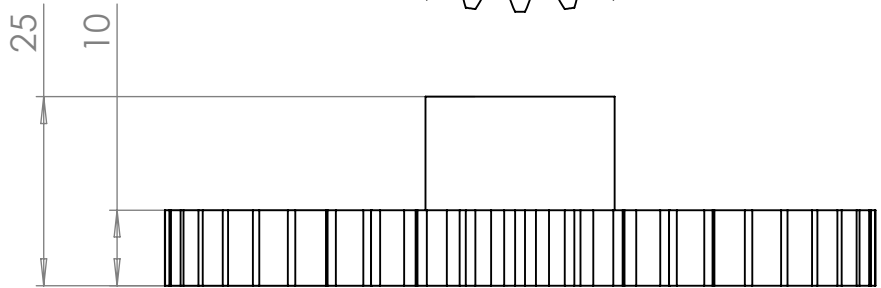
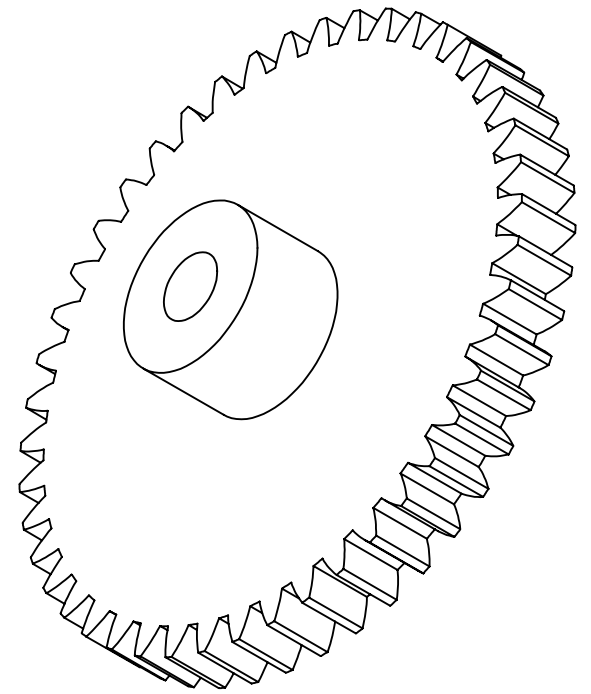
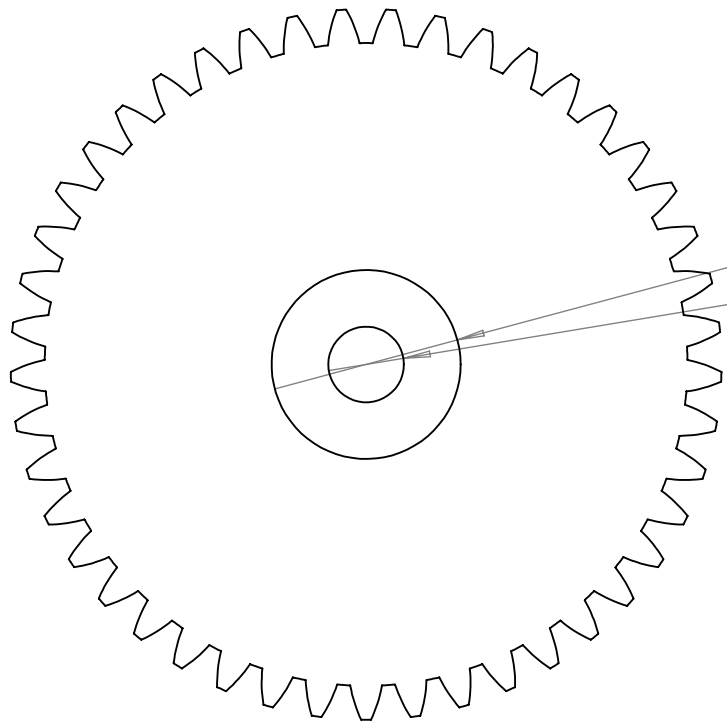


Module:2
Pitch Circle Diameter: 108

Quantity: 3

MATERIAL:
Aluminium

DO NOT SCALE DRAWING		REVISION
TITLE:	54 teeth	
DWG NO.	14	A4
WEIGHT:	SCALE:1:2	SHEET 1 OF 1



Module: 2
Pitch Circle Diameter: 90

Quantity: 1

MATERIAL:
Aluminium

DO NOT SCALE DRAWING REVISION

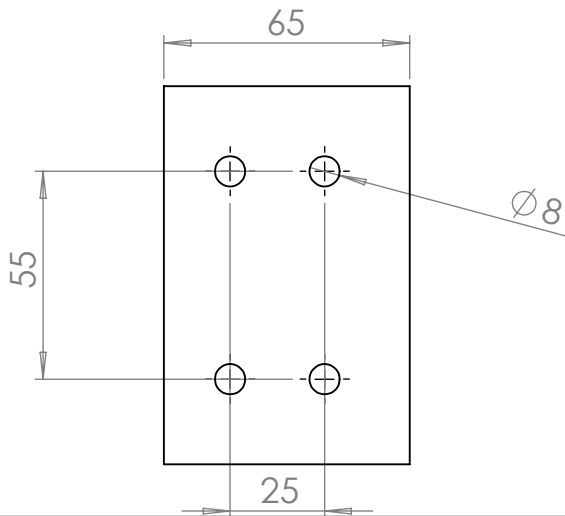
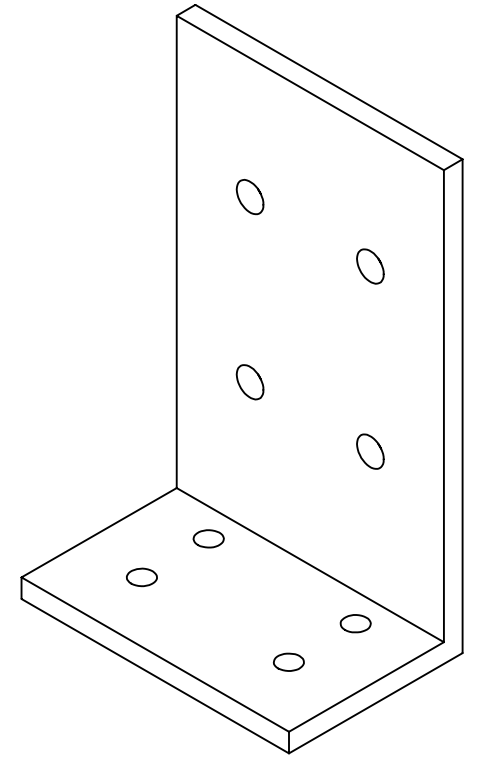
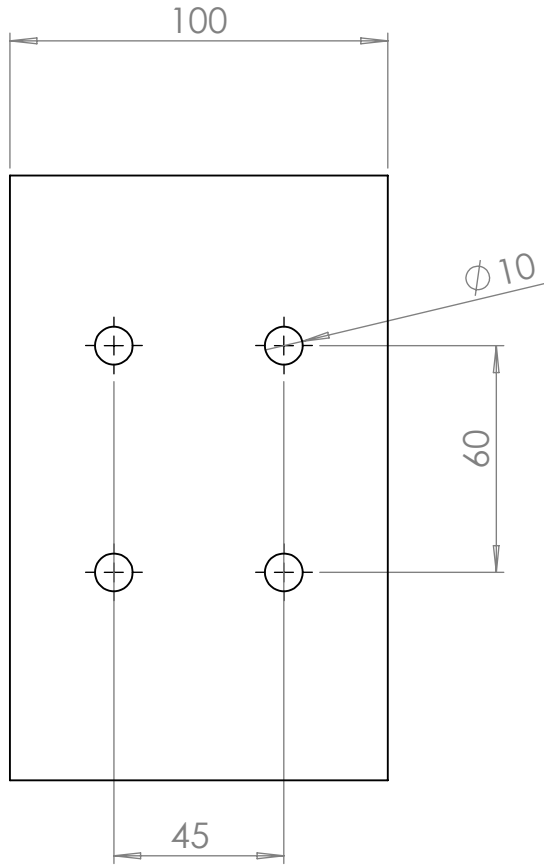
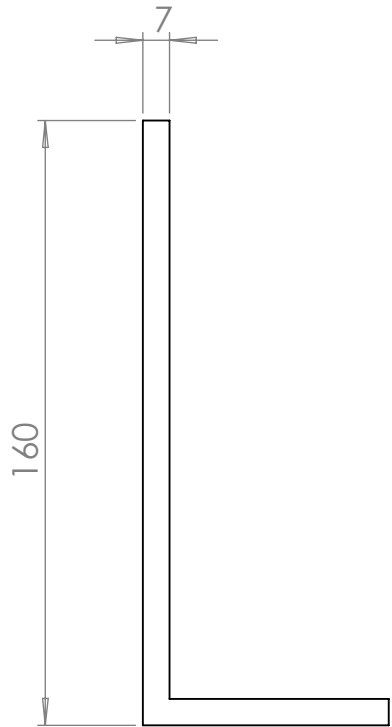
TITLE: 45 teeth

DWG NO. 15

A4

WEIGHT: SCALE:1:2

SHEET 1 OF 1



UNLESS OTHERWISE SPECIFIED:

DIMENSIONS ARE IN MM
 TOLERANCES:
 FRACTIONAL ±
 ANGULAR: MACH ± BEND ±
 TWO PLACE DECIMAL ±
 THREE PLACE DECIMAL ±

INTERPRET GEOMETRIC
 TOLERANCING PER:
 MATERIAL

DO NOT SCALE DRAWING

	NAME	DATE
DRAWN		
CHECKED		
ENG APPR.		
MFG APPR.		
Q.A.		

COMMENTS:

QUANTITY: 1		
TITLE: GENERATOR SUPPORT		
MATERIAL: PLYWOOD		
SIZE	DWG. NO.	REV
A	16	
SCALE: 1:50	WEIGHT:	SHEET 1 OF 1